INSTITUTO TECNOLÓGICO Y DE ESTUDIOS SUPERIORES DE MONTERREY

CAMPUS MONTERREY

DIVISIÓN DE INGENIERÍA Y ARQUITECTURA

TECNOLÓGICO
DE MONTERREY®

PROGRAMA DE GRADUADOS EN INGENIERÍA

THE EFFECTS OF ROLLER BURNISHING PARAMETERS UPON SURFACE PROPERTIES OF AISI 52100 BEARING STEEL (60 HRC)
- A Finite Element Analysis -

TESIS

PRESENTADA COMO REQUISITO PARCIAL PARA
OBTENER EL GRADO ACADÉMICO DE
MAESTRO EN CIENCIAS
CON ESPECIALIDAD EN SISTEMAS DE MANUFACTURA

FRANCISCO JASSO LUCIO

DICIEMBRE DEL 2005

INSTITUTO TECNOLÓGICO Y DE ESTUDIOS SUPERIORES DE MONTERREY

DIVISIÓN DE INGENIERÍA Y ARQUITECTURA
PROGRAMA DE GRADUADOS EN INGENIERÍA

Los miembros del Comité de Tesis recomendamos que la presente Tesis del Ing. Francisco Jasso Lucio sea aceptada como requisito parcial para obtener el grado académico de Maestro en Ciencias con especialidad en:

SISTEMAS DE MANUFACTURA

COMITÉ DE TESIS

Ciro A. Rodríguez González, Ph. D.
ASESOR

Alex Elías Zúñiga, Ph. D.
SINODAL

Jorge A. Cortés Ramírez, D. in Eng.
SINODAL

APROBADO

Federico Viramontes Brown, Ph. D.
Director del Programa de Graduados en Ingeniería

Diciembre del 2005

DEDICATION

This work is dedicated to my beloved parents
Rebeca and Francisco and to my sister Alejandra.

ACKNOGLEDGEMENTS

I would like to express my gratitude to my adviser, Dr. Ciro A. Rodríguez for his trust, guidance and support throughout my research. I also appreciate the suggestions and comments of my thesis committee: Dr. Alex Elías and Dr. Jorge A. Cortés.

I offer my deepest gratitude to the Research Chair in Mechatronics (http://cidyt.mty.itesm.mx/cimec) for giving me the opportunity to conduct my research in collaboration with the Engineering Research Center for Net Shape Manufacturing (ERC/NSM) at The Ohio State University.

I would like to thank the Mechanical Engineering Department (Dr. Alex Elías) and the Center for Innovation in Design and Technology for their support during my graduate studies.

Sincere thanks are extended to Dr. Taylan Altan, for giving me the opportunity to be part of the ERC/NSM during my research. I would like to thank all the students and visiting scholars from OSU for their friendship, help and support. Especial thanks go to Partchapol Sartkulvanich and the members of the machining group.

I am grateful to my parents, my grand mother Lucía and my uncle Emmanuel for their support on every moment in my life.

I would like to thank to my colleagues and friends from the engineering graduate program for their friendship during our studies: Francisco Araya, Eva Delgadillo, Victor Flores, Alejandro Martínez, Reyes Toledo, Esteban Suárez, David Reyes and Milton Esteva.

Finally, I would like to thank all my friends for their continuous support and especially for their patience during my graduate studies.

SUMMARY

This thesis is based on the technical report HPM/ERC/NSM-05-R39 which was written in collaboration with the Engineering Research Center for Net Shape Manufacturing (ERC/NSM) [Jasso et. al, 2005a]. The author of this thesis spent some time on a research stance working at The Ohio State University in a roller burnishing project. Most part of the work presented in this document was conducted during that time.

Hard roller burnishing is a cost effective surface finishing/enhancement process where a hard ball rolls on the machined surface under a high pressure and flattens the roughness peaks. Particularly when combined with hard turning, this process is able to provide a good alternative to abrasion-based finishing methods such as grinding operations.

In this study, two main tasks were conducted, including 1) modifications of FEM modeling of roller burnishing from Yen's model [Yen, 2004] and 2) FEM simulations to analyze the effect of roller burnishing parameters by using real process conditions selected from experiments previously conducted by the ERC/NSM) [Sartkulvanich, 2004b]. Specifically, the contents of each chapter of this thesis can be summarized as follows.

Chapter 1 provides an introduction, which includes the description of roller burnishing process, advantages and challenges encountered in the use of roller burnishing to replace grinding. Overall and specific objectives are discussed in Chapter 2.

Chapter 3 provides a literature review on roller burnishing research. It is mainly divided into three major topics, i.e. experimental study on the surface improvement by roller burnishing process, experimental study on the effect of burnishing process parameters, and modeling of roller burnishing.

Chapter 4 summarizes the details of hard turning and roller burnishing experiments, conducted by the ERC/NSM. Information of experimental procedure and experimental data are given in this chapter. In addition to the data presented in [Sartkulvanich, 2004b], data from experimental measurements of residual stresses on hard turned and burnished AISI 52100 surfaces (obtained by X-ray diffraction technique) are also provided in this chapter.

Chapter 5 presents the modifications made for the previously developed FEM model of roller burnishing in [Yen, 2004]. These include consideration of flow stress models from ball indentation tests, consideration of pressure loss during roller burnishing operation, selection of a workpiece size for the FEM model, determination of maximum ball penetration depth during roller burnishing, and evaluation of tool movement control in the 2D FEM model proposed by [Yen, 2004].

Chapter 6 discusses the FEM predicted results on the effects of the burnishing feeds and burnishing pressures upon surface properties. The predictions of surface finish and residual stresses are the focus of this analysis. FEM results were also compared with experimental data for validation. In summary, hard roller burnishing shows two main improvements on burnished workpieces: surface roughness reduction, and increase in compressive residual stresses beneath the surface. The effect of burnishing pressure is the most significant. Higher burnishing pressure produced smoother surface and more compressive residuals stress. Smaller burnishing feed provides similar surface improvements but to a less degree. Quantitatively, FEM results match well with the experiments for the residual stresses but not with the surface roughness parameters.

Chapter 7 presents the author's personal contributions, the findings of this study, some suggestions for further research on hard turning and roller burnishing as well as the application perspectives for this processes' combination by the Mexican Industry.

TABLE OF CONTENTS

LIST OF FIGURES

LIST OF TABLES

LIST OF SYMBOLS

Symbol	*Unit*	*Definition*
σ	[MPa]	Plastic stress
σ_a	[MPa]	Axial residual stress
σ_t	[MPa]	Tangential residual stress
σ_y	[MPa]	Material yield stress
d_b	[mm]	Ball diameter
D	[mm]	Maximum ball penetration on workpiece
f_b	[mm/rev]	Burnishing feed rate
F_b	[N]	Burnishing force
$F_{b.FEM}$	[N]	Burnishing force used in FEM simulations
f_c	[mm/rev]	Cutting feed rate
HRC	[-]	Rockwell hardness (C-scale)
HU	[MPa]	Universal hardness
n	[-]	Strain hardening exponent
P_b	[MPa]	Burnishing pressure
R_a	[μm]	Mean surface roughness
r_t or r_b	[mm]	Radius of the burnishing tool
R_z	[μm]	Roughness depth
V_b	[m/min]	Burnishing speed
V_c	[m/min]	Cutting speed

CHAPTER 1
INTRODUCTION

The integrity of an engineered surface is normally characterized in terms of surface finish, state of residual stress, microstructural phase transformation and microhardness. These properties are very important on the performance of functional component since they are strongly related to wear resistance, fatigue life and corrosion resistance of manufactured surfaces [Némat, 2000].

The development of advanced PCBN tool materials made machining of hardened steels (with hardness values greater than 55 HRC) possible. This new technology, known as *hard turning*, can replace some rough grinding operations. Hard turning has some advantages over grinding operations such as: 1) low capital investment cost and risks, 2) ease of adding complex geometric features after the workpiece is hardened, 3) environmental friendly (dry cutting conditions), 4) ease of setup, 5) low energy consumption and 6) better quality of surface produced [Yen, 2004].

However, applications of hard turning technology are still limited by tool wear [Klocke, 1998]. Turning with a worn tool can lead to large tensile residual stresses in the surface and poor surface finish. In order to increase hard turning capabilities as a finishing process, it is necessary to employ an additional operation which is able to improve the surface finish after hard turning so that a certain amount of tool wear could be allowed [Klocke, 1998].

Roller burnishing is a chipless surface finish/enhancement process which is illustrated in Figure 1-1. In this process, a smooth free-rolling ball (2-25 mm diameter) is rolled over a machined surface under a normal force which is strong enough to plastically deform (flatten) the surface peaks of the workpiece and to create a compressive residual stress near the surface. The ball is supported in a

hydrostatic bearing with sufficient pressure to lift the ball off the retaining spherical socket. The ball is free to roll on the surface with a very low friction due to the presence of the fluid (emulsion with 3-5% oil component) [Klocke, 1998]. The tool feed is along the workpiece axis in a similar way to turning feed. The process generally provides smooth surface finish and increases compressive residual stresses near the surface.

In order to implement a reliable and cost-effective hard roller burnishing operation, the effect of process parameters (i.e. ball diameter, feed rate, speed, pressure, etc.) upon surface finish integrity (i.e. surface roughness and residual stresses) must be understood. Most of research on roller burnishing has been focused on experimental studies and analytical simplified approaches. The development of a FEM-based predictive model for roller burnishing has been the objective of some researches; however, FEM predicted results for roller burnishing are still not very accurate due to lack of reliable material surface properties (i.e. constitutive equations). The goal of this research is to improve an FEM roller burnishing model previously developed at the ERC/NSM in [Yen, 2004] and to be able to use it for a study on the effect of process parameters upon surface qualities (i.e. surface finish and residual stress) after burnishing. A series of FEM roller burnishing simulations are conducted and validated with the experiments that were previously reported in [Sartkulvanich, 2004b].

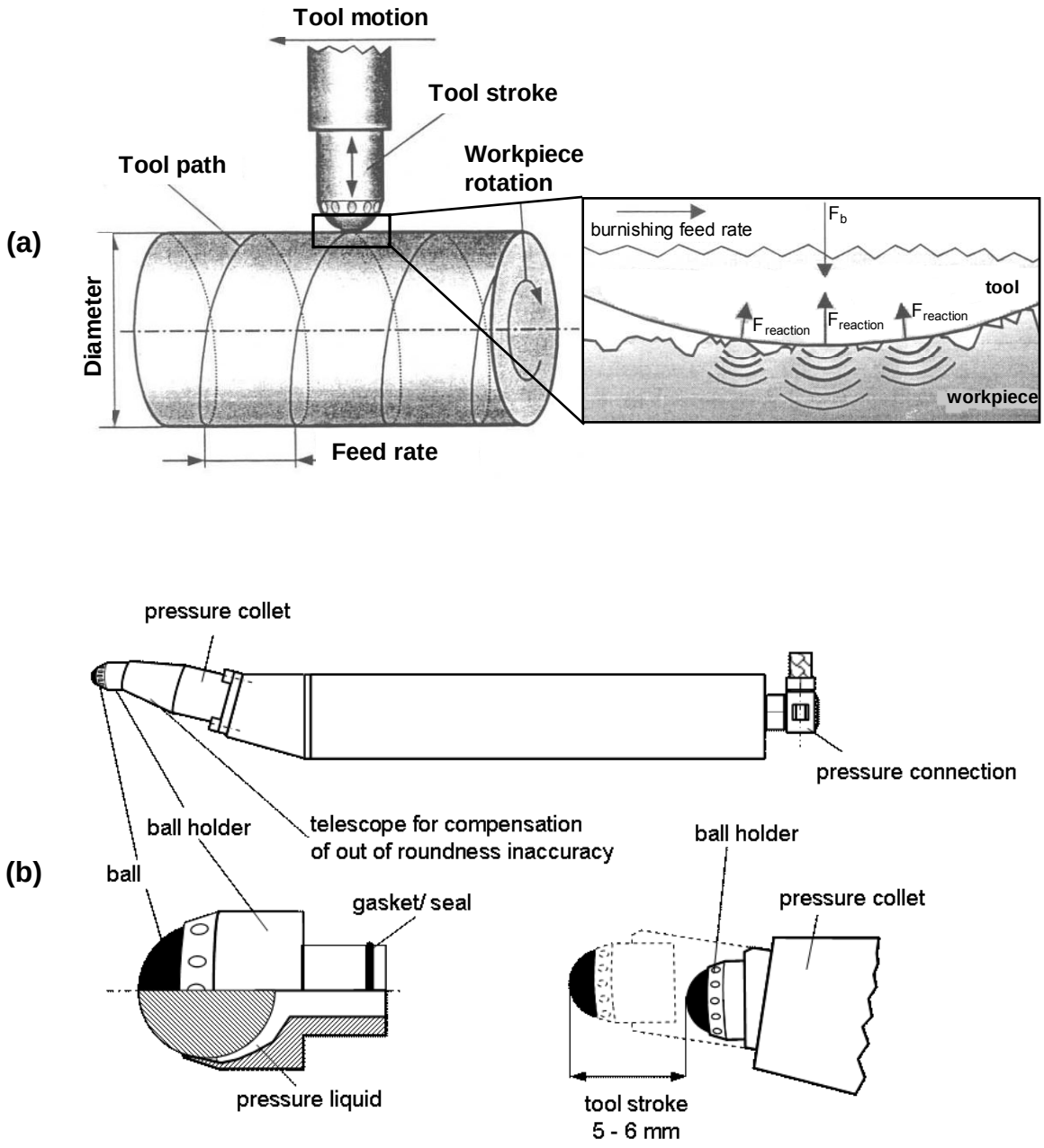

Figure 1-1: (a) Ball burnishing process [Röttger, 2002]; **(b)** A typical roller burnishing tool [Klocke, 1998].

CHAPTER 2
RESEARCH OBJECTIVES

The overall objective of this study is to improve an existing FEM-based model for roller burnishing simulations previously developed at the ERC/NSM [Yen, 2004] so it can be used to predict the effect of process parameters (burnishing feed and pressure) upon surface properties (surface roughness and residual stresses). The specific objectives of this study are to:

- Conduct a literature review to understand roller burnishing process and modeling.

- Further improve the existing 2D FEM model of roller burnishing in [Yen, 2004] in order to predict roller burnishing results more accurately for a given set of process parameters and initial surface properties.

- Analyze the predicted surface roughness and residual stresses by comparing with the results from hard turning and roller burnishing experiments presented in [Sartkulvanich, 2004b].

- Use the FEM roller burnishing model to conduct a study on the effect of process parameters (i.e. burnishing pressure and feed) upon surface qualities (i.e. surface roughness and residual stresses).

CHAPTER 3
LITERATURE REVIEW ON ROLLER BURNISHING

Roller burnishing operations are used to improve surface finish, enhance mechanical properties of surface layer or a combination of both. If roller burnishing is performed on a workpiece that has a surface hardness level greater than 45 HRC then it is known as *hard roller burnishing.* According to the objectives of this research, the literature review was divided in three subjects:

- Study of roller burnishing capabilities for surface finish/enhancement.
- Experimental studies, related to the effect of roller burnishing parameters upon surface qualities. Study of existing predictive models for roller burnishing processes using experimental, analytical or FEM approaches.

3.1 Improvements of Surface Properties by Hard Roller Burnishing

Hard turning conditions (i.e. cutting feed, tool geometry, tool wear, etc.) strongly affect the properties of machined surfaces, especially surface roughness and residual stresses. Some researchers have focused their efforts in understanding the effect of those process parameters upon surface properties during hard turning of AISI 52100 bearing steel [Dahlman, 2004; Liu, 2004; Röttger, 2002 and Klocke, 1998].

Klocke and Röttger used tools with different flank wear widths to show the effect of tool wear upon residual stresses and surface roughness in hard turning of 100Cr6 (or AISI 52100) steel workpieces [Klocke, 1998 and Röttger, 2002]. The different amounts of tool wear produced a big variation on residual stress distributions; however, surface roughness profiles did not change significantly under these cutting conditions (see Figure 3-1). In these studies it was found that

as cutting tool flank wear increases, residual stresses on surface layer become more tensile while residual stresses beneath the machined surface layer at deeper positions become more compressive (Figure 3-1(a)). An increase in tensile residual stresses is due to the increasing thermal effect during cutting with high flank wear.

Klocke and Röttger used hard roller burnishing to finish the hard-turned surfaces. Hard roller burnishing not only improved the surface roughness of turned surfaces but also allowed tool life of cutting tools to increase from 20 to 60 minutes of cutting for obtaining a surface finish (R_a) of 0.17 μm (see Figure 3-2). For the residual stresses, it was observed that hard roller burnishing can generate compressive residual stresses throughout the workpiece's surface layers, although tensile stresses were produced earlier by hard turning with highly worn cutting tools (see Figure 3-3).

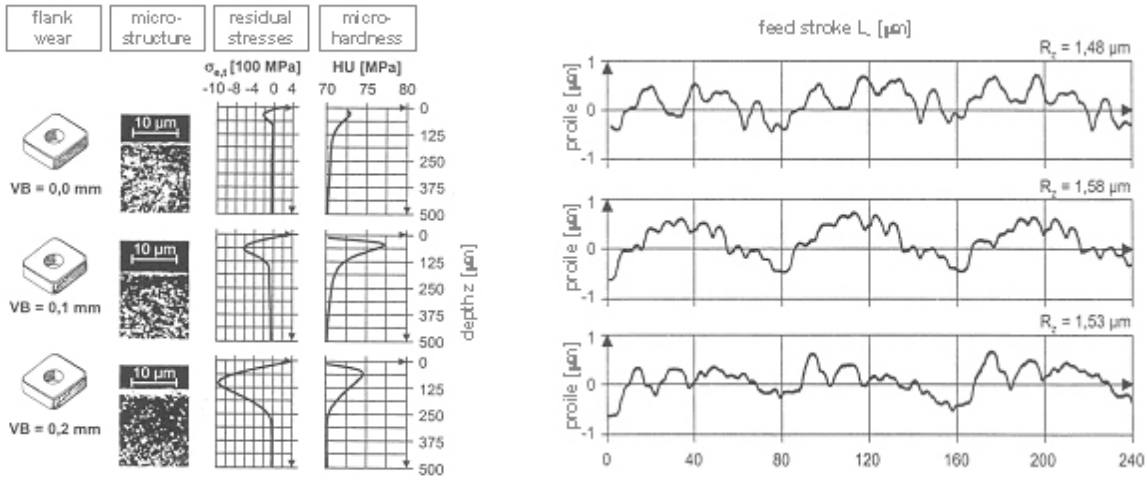

(a) **(b)**

Figure 3-1: Surface layer of hard turned AISI 52100 steel (61.5 HRC) obtained using CBN tools with different flank wear widths. **(a)** Microstructure, residual stresses and micro hardness. **(b)** Surface roughness profile. [Röttger, 2002].

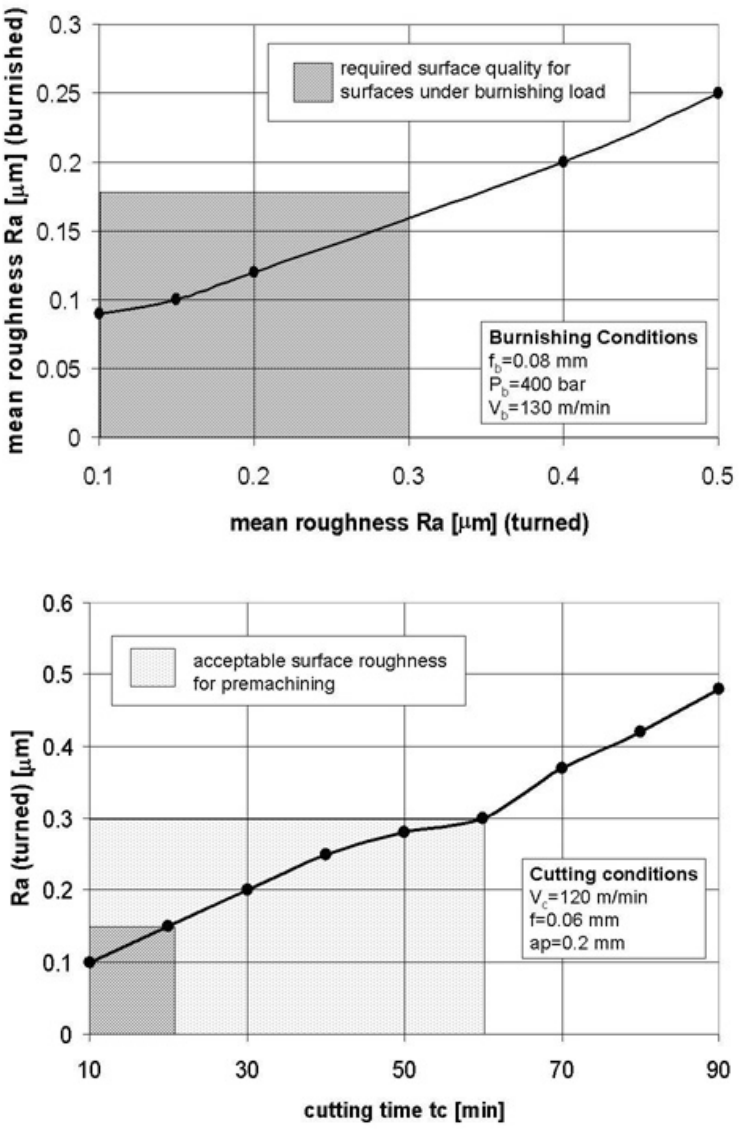

Figure 3-2: Surface quality obtained using hard roller burnishing. Tool life of cutting tools can be increased for hard turning operations when combining both hard turning and hard roller burnishing [Klocke, 1998].

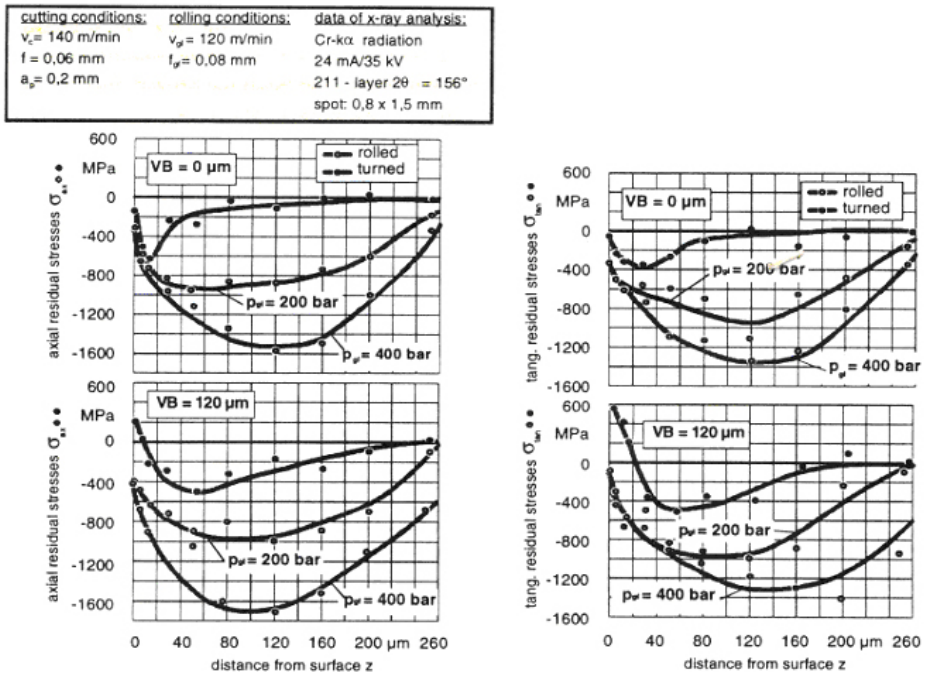

Figure 3-3: Residual stress distribution obtained on a machined workpiece tools with different flank wear widths and after hard roller burnishing [Klocke, 1998].

A roller burnishing equipment supplier, Ecoroll (Germany), summarized experimental studies on the surface improvements by hard roller burnishing [Ecoroll, 2001]. For surface finish, Figure 3-4 obviously illustrates that roller burnishing converts the machined surface profile into a surface with lower roughness. The spike peaks are flattened by the applied burnishing force, forcing the material at the peak to flow into the valleys. As a result, the bearing ratio (i.e. the ratio that indicates the contact size at the certain depth of the surface profile) increases significantly. Higher bearing ratio implies more uniform contact between functional components and thus better performance during operation. For surface hardness improvement, initial hardness of the machined surface and burnishing pressure has a significant influence on an increase in hardness by roller burnishing [Emmer, 1992]. In Figure 3-5, at higher burnishing pressure the hardness increase of a 64 HRC sample is only +3% while it is +20% for a 48 HRC sample.

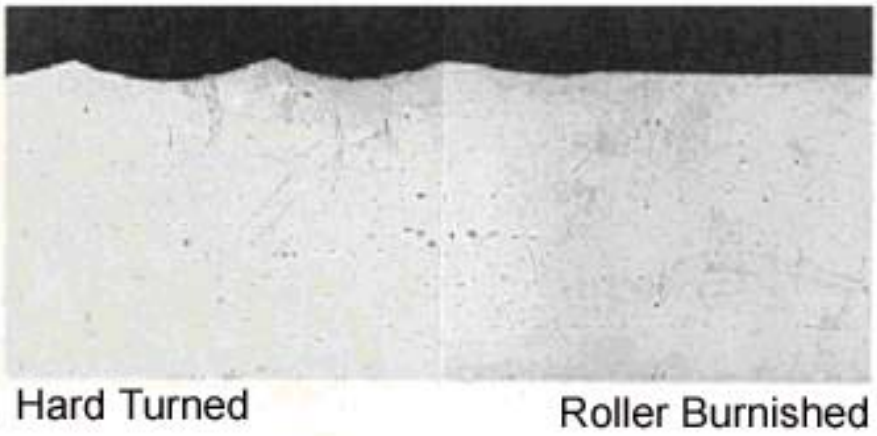

Figure 3-4: Comparison between the surface profiles between hard-turned surface and roller-burnished surfaces [Ecoroll, 2001].

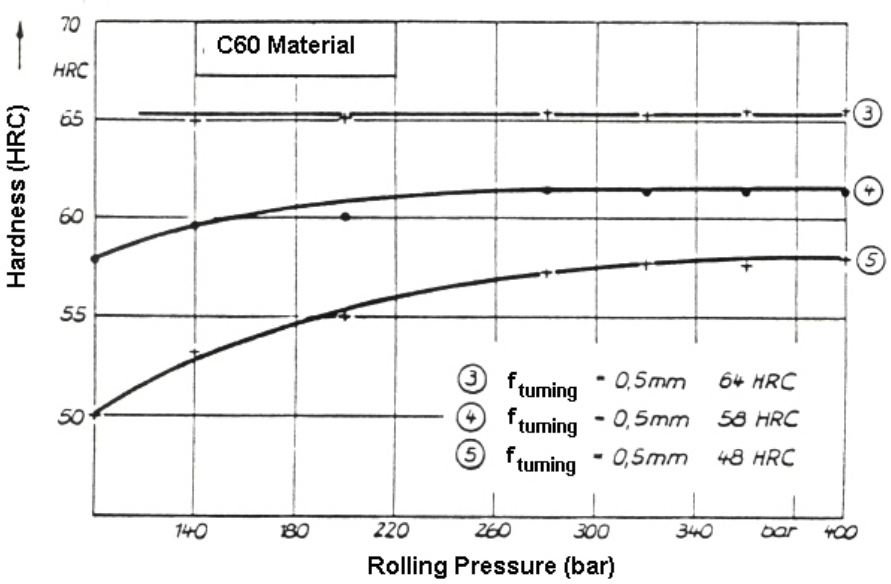

Figure 3-5: Hardness obtained after roller burnishing using different hydraulic pressures and different initial surface hardness levels [Emmer, 1992].

3.2 Experimental Research on the Effects of Roller Burnishing Parameters upon Surface Properties

Roller burnishing process parameters are 1) burnishing speed (V_b), 2) burnishing feed rate (f_b), 3) burnishing pressure (P_b), 4) burnishing force (F_b), 5) burnishing ball diameter (d_b) and 6) number of tool passes (n). Through recent years, most of the research on roller burnishing has been focused on experimental studies on the effects of these process parameters upon surface properties such as surface roughness, surface microhardness and residual stresses. Table 3-1 summarizes some of the experimental research conducted on the effects of roller burnishing parameters.

According to experimental studies listed in Table 3-1, the influence of roller burnishing process parameters upon surface properties can be summarized as follows:

- In general, surface roughness decreases when increasing burnishing speed; however, if burnishing speed is increased beyond a certain limit then surface roughness increases due to machine/tool chatter produced at high speeds (see Figure 3-6(a)) [Némat, 2000; Hassan, 2000 and El-Axir, 2000]. In the case of burnishing 100Cr6 (AISI 52100) steel (61.5 HRC), the effect of burnishing speed was observed to be nearly negligible within a wide burnishing speed range (50 to 450 m/min) [Röttger, 2002]. The increase in surface roughness when using burnishing speeds greater than 450 m/min was also due to excessive machine/tool vibration and dynamic effects.

- Figure 3-6(b) shows the effects of burnishing speed on surface microhardness. As the burnishing speed increases, the surface hardness also increases up to a certain limit.

- There is an optimum burnishing feed for which the obtained surface roughness is minimum (Figure 3-6(c)). Feed values higher than this optimum value increase the surface roughness and decrease surface

microhardness (Figure 3-6(d)). This is due to the fact that distance between two successive ball traces is increased with feed and thus the ball has less chance to flatten the surface peaks. However, if a very low feed value is used, then surface roughness increases due to an excessive amount of cold work repetitively applied on the workpiece surface. Furthermore, surface fatigue, mostly observed in soft materials [Némat, 2000 and Hassan, 2000], may occur.

- The surface roughness decreases with an increase in the burnishing force (or pressure); however, further increase in force could deteriorate surface roughness, especially for soft materials (Figure 3-6(e)) [Némat, 2000 and Emmer, 1992]. In these cases, the bulge of metal in front of the tool becomes very large and the region of the plastic deformation becomes widened which damages the burnished surface.

- An increase in burnishing force/pressure increases surface hardness. This is due to an increase in metal flow that leads to an increase in the amount of plastic deformation and to strain hardening. This also leads to an increase in the compressive residual stresses and therefore an increase in surface hardness (Figure 3-6(f)) [Némat, 2000].

- Roller burnishing produces compressive residual stresses beneath the surface layer. These residual stresses are insensitive to the initial state of residual stresses produced by machining [Röttger, 2002]. Figure 3-7 shows that the residual stresses produced by different worn tools did not affect the final residual stress distribution after hard roller burnishing.

- A large ball diameter is more effective for obtaining low surface roughness, while a small diameter ball is more effective to increase surface hardness and residual stresses [Hassan, 2000].

Author	Parameters studied	Material (Condition)	Tool
[Bouzid, 2004]	Feed (f_b), force (F_b)	AISI 1042 steel (soft)	Spring-loaded
[El-Axir, 2000]	Speed (V_b), force (F_b), feed (f_b), number of tool passes (n)	St-37 steel (soft)	Spring-loaded
[El-Khabeery, 2001]	Speed (V_b), number of tool passes (n)	Aluminum 6061-T6 (soft & flat surface)	Spring-loaded
[Hassan, 1998]	Force (F_b), number of tool passes (n)	Brass (soft)	Spring-loaded
[Hassan, 1996]	Speed (V_b), force (F_b), feed (f_b), number of tool passes (n), ball diameter (d_b)	Non ferrous metals (soft)	Spring-loaded
[Klocke, 1998]	Feed (f_b), speed (V_b), pressure (P_b)	100Cr6 (AISI 52100) Steel (Hardened)	Hydrostatic
[Luca, 2005]	Pressure (P_b), feed (f_b)	Steel (Hardened)	Hydrostatic
[Némat, 2000]	Number of tool passes (n), feed (f_b), force (F_b), burnishing speed (V_b)	Mild Steel and Aluminum (soft)	Spring-loaded
[Röttger, 2002]	Ball diameter (d_b), pressure (P_b), feed (f_b), speed (V_b)	100Cr6 (AISI 52100) Steel (Hardened)	Hydrostatic

Table 3-1: Summary of various experimental studies on the effect of burnishing process parameters.

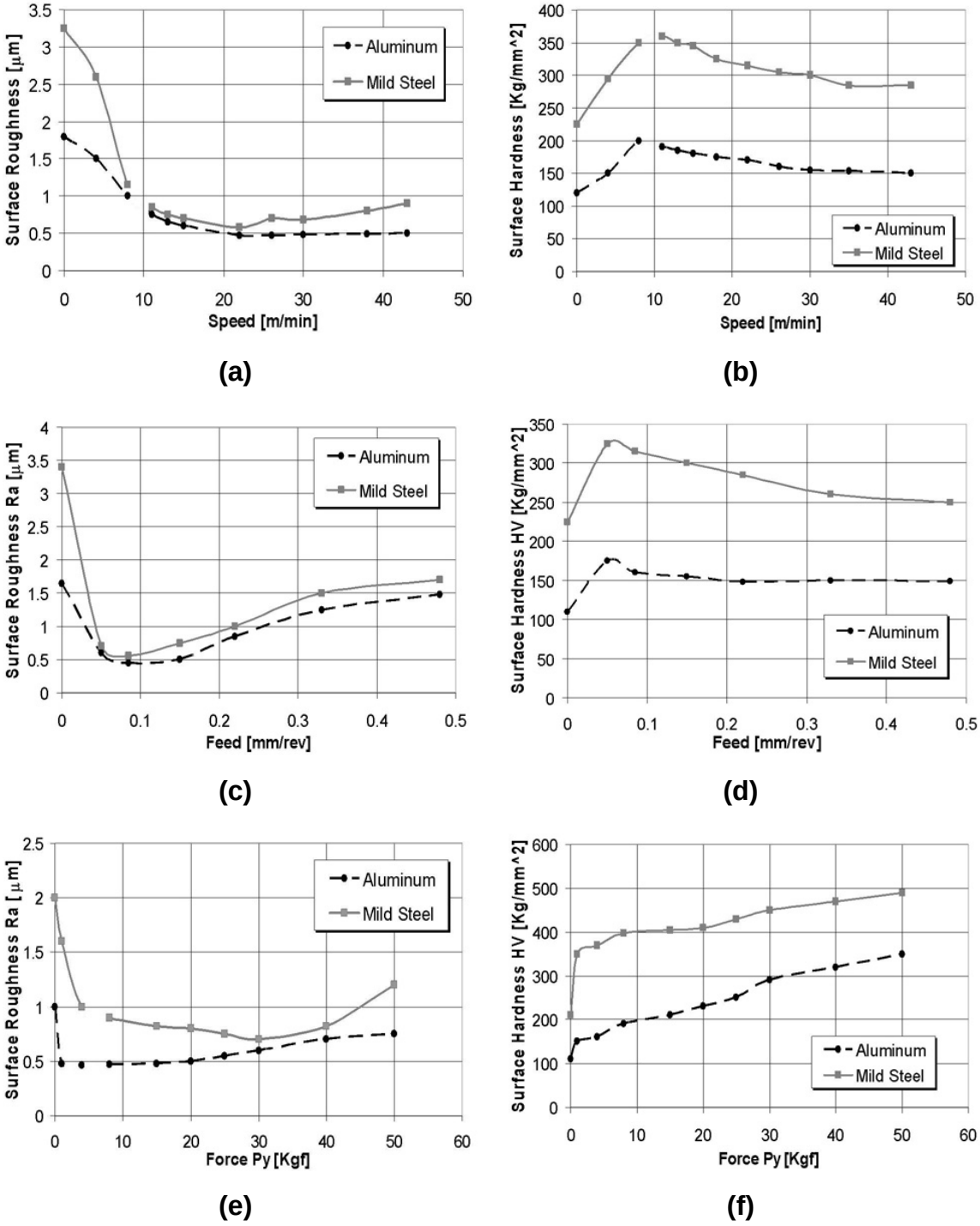

Figure 3-6: Effects of burnishing feed, speed and force on surface roughness and micro hardness during roller burnishing of mild steel and aluminum [Némat, 2000].

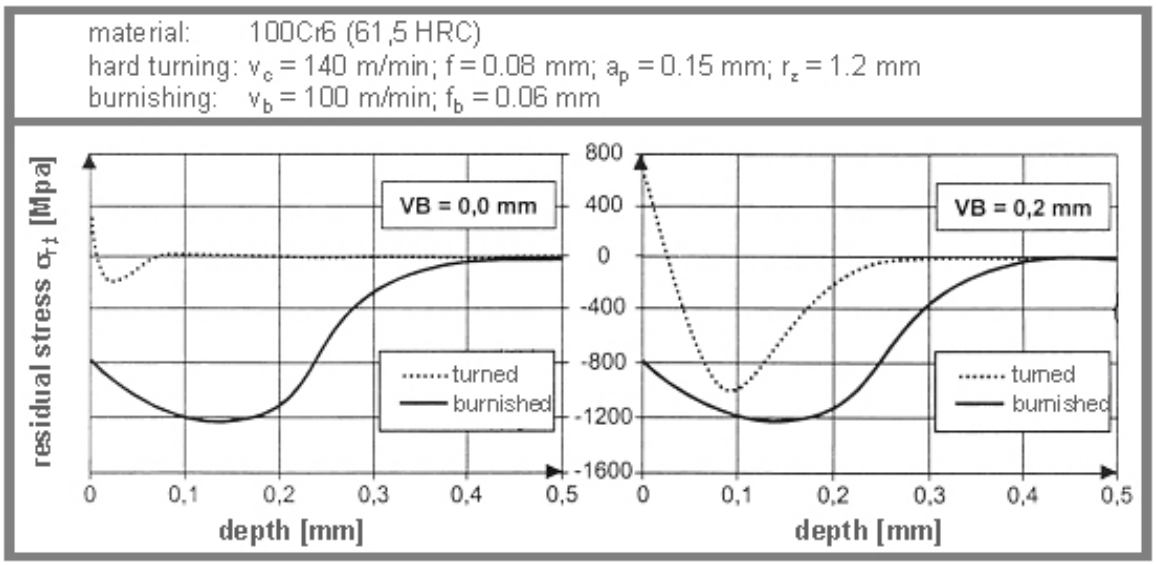

Figure 3-7: Effect of roller burnishing on tangential residual stresses for workpieces with different initial residual stress distributions [Röttger, 2002].

3.3 Modeling of Roller Burnishing

A number of predictive models have been developed in order to estimate surface properties for a given set of roller burnishing conditions (parameters). Table 3-2 shows a list of different roller burnishing predictive models, which were classified in three different categories, i.e. analytical, statistical and FEM models. In addition, in the same table the inputs and outputs for each predictive model are provided.

3.3.1 Statistical Modeling

Hassan developed a statistical model to correlate roller burnishing force and number of tool passes with the mean surface roughness, R_a [Hassan, 1998]. Roller burnishing experiments were conducted on brass workpieces using a spring-loaded tool as shown in Figure 3-8(a). Hassan used the response surface method (RSM) to fit a second-order equation, as shown in Figure 3-9.

(a)

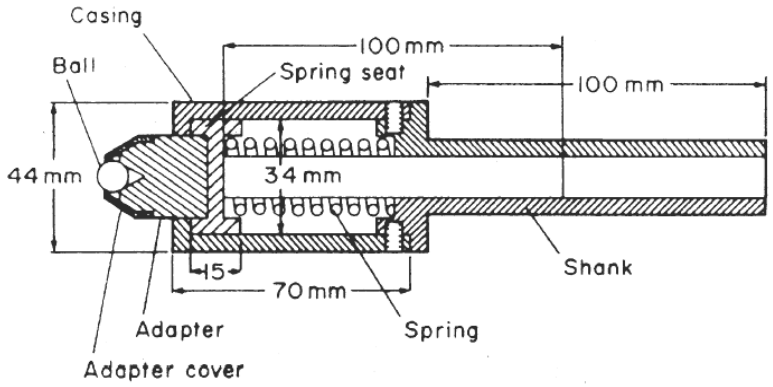

(b)

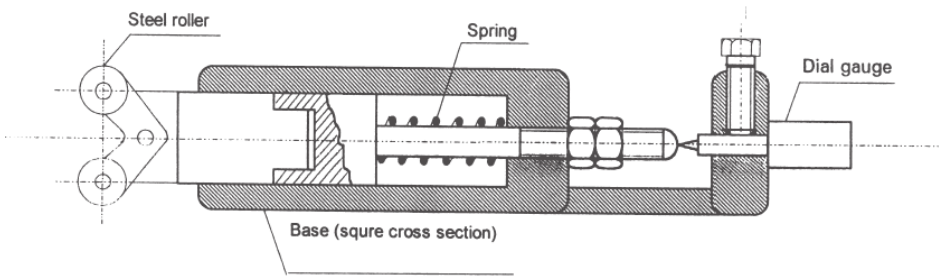

Figure 3-8: Spring-based roller burnishing tools. **(a)** Ball roller [Hassan, 1998]. **(b)** Cylinder rollers [El-Axir, 2000].

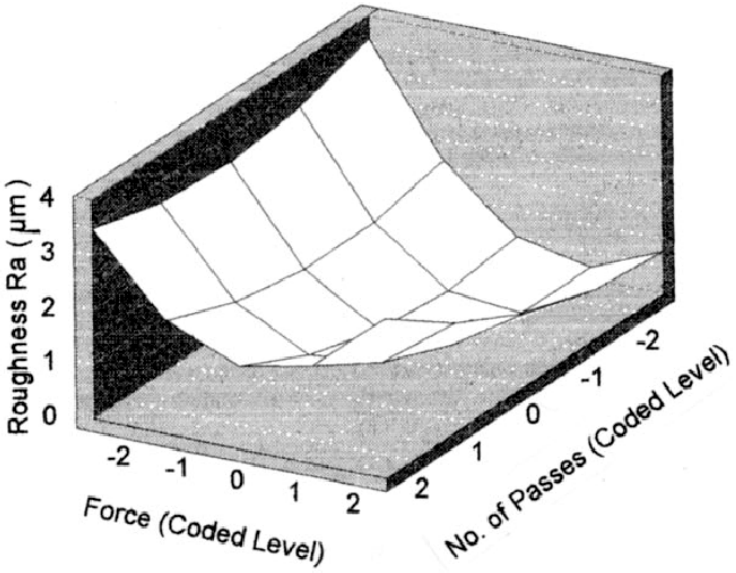

Figure 3-9: Three dimensional plot of the surface roughness vs. burnishing force and number of tool passes based on the mathematical model developed in [Hassan, 1998].

Author	Process Parameters Considered	Model Outputs	Approach
[Black, 1997]	Tool geometry, Burnishing force	Plastic strain, Depth of deformed layer	Analytical
[Bouzid, 2004] & [Bouzid, 2005]	Surface roughness, Burnishing feed, force, Ball diameter, Workpiece diameter	Surface roughness, Ball penetration depth, Residual stresses	Analytical & FEM
[El-Axir, 2000]	Burnishing speed, feed, Burnishing force, Number of tool passes	Surface roughness, Surface microhardness	Statistical
[Hassan, 1998]	Burnishing force, Number of tool passes	Surface roughness	Statistical
[Röttger, 2002]	Burnishing pressure, Feed, Ball diameter, Initial roughness	Surface roughness, Residual stresses	Analytical& FEM
[Skalski, 1995]	Tool radius, Workpiece yield strength	Burnishing force, Penetration depth, Contact radius	FEM
[Yen, 2004]	Burnishing pressure, Feed, Ball diameter, Initial roughness	Surface roughness, Residual stresses	FEM
[Zhuang, 2004]	Burnishing pressure, Feed, Speed, Number of tool passes	Residual stresses	FEM

Table 3-2: Summary of roller burnishing models proposed by various researchers.

El-Axir conducted roller burnishing experiments on St-37 steel workpieces using a spring-loaded tool (see Figure 3-8(b)). He studied the effect of burnishing speed, force, feed and number of passes upon surface roughness and microhardness. El-Axir developed mathematical models to predict the surface roughness and microhardness of the burnished workpieces using design of experiments (DOE) technique.

3.3.2 Analytic Models

Bouzid developed an analytical equation to determine the surface roughness depth (R_z) after burnishing for AISI 1042 steel, as shown in Figure 3-8(a) [Bouzid, 2004]. Low feed values (f_b) and a spring-loaded tool (with F_b=150 N) were used. According to this model, the roughness depth, R_z (or an average peak-to-valley distance of the surface profile, see APPENDIX A for a complete definition of surface roughness parameters) can be calculated using the equation

$$R_z = \begin{cases} R_{zi} - \delta + h & \text{if } \delta \le R_{zi} \\ R_z = h & \text{if } \delta \ge R_{zi} \end{cases} \tag{3.1}$$

where

R_{zi} is the original roughness depth of the machined surface

δ is the tool penetration depth on the workpiece (see Figure 3-10(a))

h is the height of the non burnished material left between two successive ball traces (see Figure 3-10(b)) which is given by

$$h(\mu m) = \frac{125 f_b^2}{R} \tag{3.2}$$

Bouzid used Hertz theory for normal contact of elastic solids (sphere-cylinder contact) to predict tool penetration depth on workpiece (δ) before using Eq. (3.1) to estimate the surface roughness. Good agreement between experimental and

predicted results was obtained although the author recognized the need of using an FEM-based model to accurately predict the ball penetration depth (δ) while considering the elastic-plastic material behavior. However, Bouzid only studied the case for which the ball penetration depth is smaller than the original surface roughness ($\delta \leq R_{zi}$). There is no documented evidence that the second expression in Eq. (3.1) is able to predict the surface roughness for those cases when the penetration depth is greater than the original surface roughness ($\delta \geq R_{zi}$). In addition, the effect of the initial machined surface roughness was neglected when calculating the ball penetration depth (δ).

Black developed equations for determining factors such as the power required to carry out the burnishing process, the depth of the deformed surface layer and the states of stress and strain induced in this layer in terms of the burnishing tool geometry, the applied force, the workpiece material properties and the friction conditions at the tool/workpiece interface [Black, 1997]. The approach was based on the slip-line theory. A simplified 2D plane strain model was established in which a wedge-shaped tool was sliding over the surface as shown in Figure 3-11. A rigid-perfectly plastic material was assumed. Physically, the model represented the pushing of a wave of a plastically deformed material ahead of the wedge.

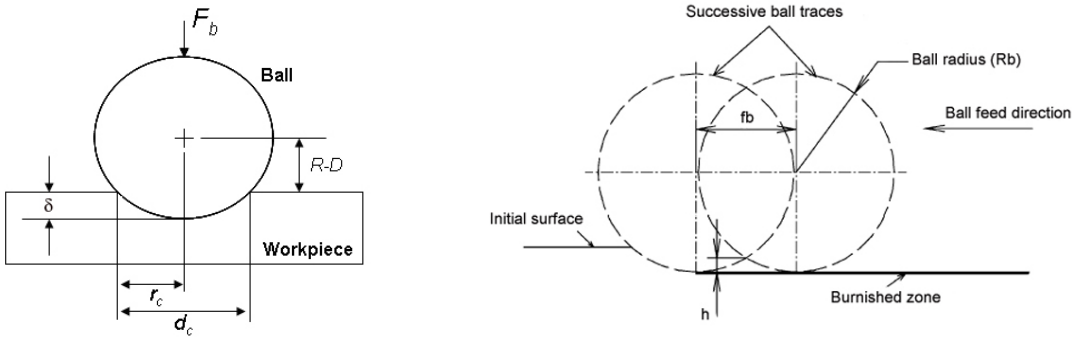

(a) **(b)**

Figure 3-10: (a) Ball penetration depth of tool on workpiece. **(b)** Surface geometry in roller burnishing [Bouzid, 2004].

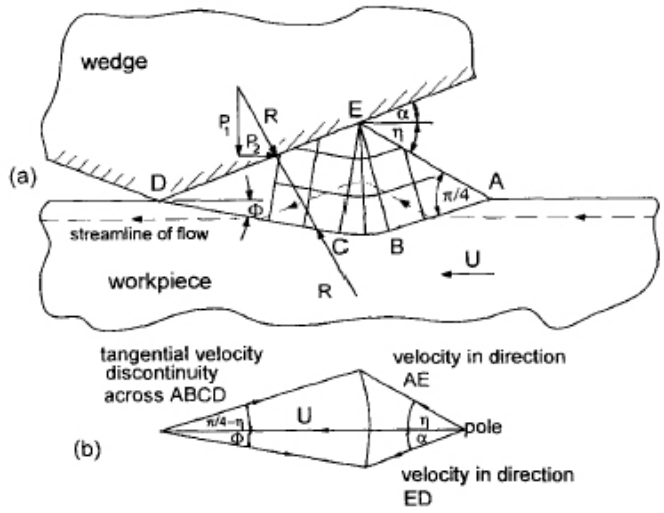

Figure 3-11: Burnishing model. **(a)** Slipline field. **(b)** Hodograph [Black, 1997].

Röttger proposed an analytical model based on Hertz elastic contact theory [Röttger, 2002]. Unlike [Bouzid, 2004], the contact was assumed between two spherical bodies instead of cylinder-sphere bodies. The radius of the circular contact area was calculated using Eq. (3.3)

$$r_c = \sqrt[3]{\frac{3rF_b\left(1-\upsilon^2\right)}{2E}} = \sqrt[3]{\frac{3\pi rP_b r_t^2\left(1-\upsilon^2\right)}{2E}}$$
$$r = \frac{r_w r_t}{r_w + r_t}; E = \frac{2E_w E_t}{E_w E_t}; F_b = \pi r_t^2 P_b \qquad (3.3)$$

where

F_b is the burnishing force

P_b is the burnishing pressure

r_c is the contact area radius

r_w is the workpiece radius

r_t is the tool radius

E_w is the workpiece's modulus of elasticity

E_t is the tool's modulus of elasticity

υ is the Poisson's ratio for the workpiece (ν=0.3)

The state of stress generated in the surface was calculated as a function of Hertz contact pressure (p_0), the contact area (r_c) and the normalized depth (z), as shown in the following equation

$$p_0 = \frac{1}{\pi}\sqrt[3]{\frac{3F_b E^2}{2r^2\left(1-\nu^2\right)^2}} \tag{3.4}$$

For $z/r_c \leq 0.43$

$$\begin{aligned}
\sigma_r &= -\frac{p_0}{1+\left(\frac{z}{r_c}\right)^2} \\
\sigma_t &= -p_0 \cdot \left(\frac{1+2\cdot\left(\frac{z}{r_c}\right)^2}{\sqrt{1+\left(\frac{z}{r_c}\right)^2}} - 2\cdot\left(\frac{z}{r_c}\right) \right) \\
\sigma_a &= -p_0 \cdot 2 \cdot \upsilon \cdot \left(\sqrt{1+\left(\frac{z}{r_c}\right)^2} - \left(\frac{z}{r_c}\right) \right)
\end{aligned} \tag{3.5}$$

For $z/r_c \geq 0.43$

$$\begin{aligned}
\sigma_r &= -\frac{p_0}{1+\left(\frac{z}{r_c}\right)^2} \\
\sigma_t &= -p_0 \cdot 2 \cdot \upsilon \cdot \left(\sqrt{1+\left(\frac{z}{r_c}\right)^2} - \left(\frac{z}{r_c}\right) \right) \\
\sigma_a &= -p_0 \cdot \left(\frac{1+2\cdot\left(\frac{z}{r_c}\right)^2}{\sqrt{1+\left(\frac{z}{r_c}\right)^2}} - 2\cdot\left(\frac{z}{r_c}\right) \right)
\end{aligned} \tag{3.6}$$

where

z is the depth, measured from the contact point

σ_r is the radial stress

σ_t is the tangential stress

σ_a is the axial stress

Using elastic components of stress calculated by Eq. (3.5) and Eq. (3.6), Röttger calculated the effective stress (Von Mises) to estimate the size of the plastic deformation zone and stress distribution under different loading conditions.

3.3.3 Finite Element Models

Skalski developed a 2D quasi-static burnishing model to numerically analyze the relations between the tool force, penetration depth, radius of the contact area, and depth of plastic deformation under different tool radii and workpiece yield strengths [Skalski, 1995]. The model used axisymmetric formulation and assumed that the tool was rigid and the workpiece was an elastic-plastic body with strain hardening. Along the tool-workpiece contact zone, Coulomb's friction was used. The effects of speed and time were neglected. Simulation assumed isothermal condition. Figure 3-12 shows the corresponding finite element model.

The results from Skalski's study showed that the force acting on the tool was more influenced by the tool radius rather than the yield strength of the material. In addition, a nearly linear relationship exists between the width and the depth of the plastic deformation zone.

Bouzid developed an FEM-based model to consider the elastic-plastic behavior of the workpiece material when calculating the ball penetration depth δ (see Figure 3-13); however, Eq. (3.1) and Eq. (3.2) were still used to determine the roughness depth R_z [Bouzid, 2005]. The use of this approach enhanced the initial

analytical model proposed by [Bouzid, 2004] because it was possible to calculate the residual stresses related to the macroscopic contact geometry. Bouzid observed a good agreement between the model predictions and experimental results; however, the model did not consider initial surface roughness and the effect of burnishing feed.

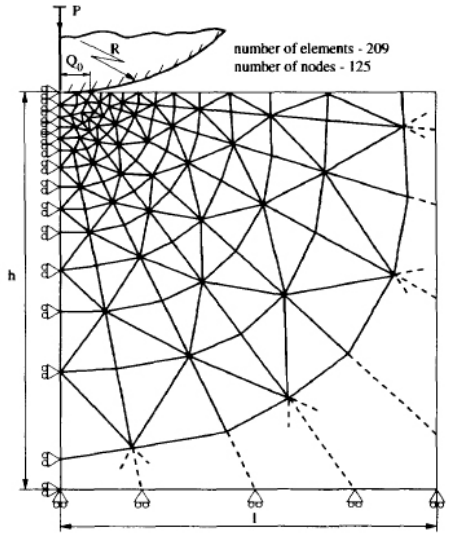

Figure 3-12: Discretization of a deformed workpiece object in FEM simulation [Skalski, 1995].

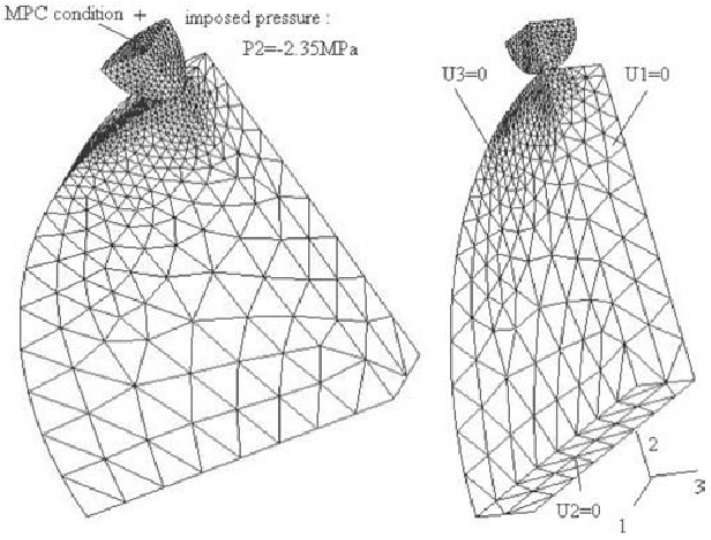

Figure 3-13: 3-D FEM model used to determine the tool penetration depth (δ) on the workpiece [Bouzid, 2005].

Röttger developed a 2D FEM simulation model for roller burnishing using an implicit Lagrangian FEM package named DEFORM^{TM}-2D [Röttger, 2002]. A cylindrical workpiece could be divided into two different cross sections for analysis, as shown in Figure 3-14. Cross-section B made possible the analysis of the effects of initial surface roughness and the burnishing feed. Plane strain condition was assumed for the tangential direction of the workpiece.

In Röttger's simulation, ball is considered as a rigid object and workpiece as an elastic-plastic object. During a simulation cycle, the tool is pressed down the workpiece surface until the burnishing force (F_b) is reached. Subsequently, the ball is lifted up and shifted horizontally by a distance equal to the burnishing feed (f_b). This process is repeated for four cycles in order to complete one roller burnishing simulation, as shown in Figure 3-15. Simulation results for surface roughness (R_z) and residual stresses were in good agreement with experimental results. However, force prediction from plane strain simulation is based on the fixed width of 1 mm (in tangential direction), while diameter of contact area is in the range of 0.5 mm (calculated using elastic contact theory). The author did not mention whether the width of 1 mm for the contact area was realistic.

Yen proposed some modifications to Röttger's 2D FEM model in order to increase its accuracy while using the same FEM code (DEFORM^{TM}-2D) [Yen, 2004]. The major modifications to the model are shown in Table 3-3. On the other hand, a 3D model was also developed using DEFORM^{TM}-3D (see Figure 3-16). In this model, the ball translates toward the workpiece while rotating with a tangential velocity at the contact point equal to the burnishing speed. The maximum ball penetration depth was iteratively adjusted in order to maintain and match the known burnishing force [Yen, 2004].

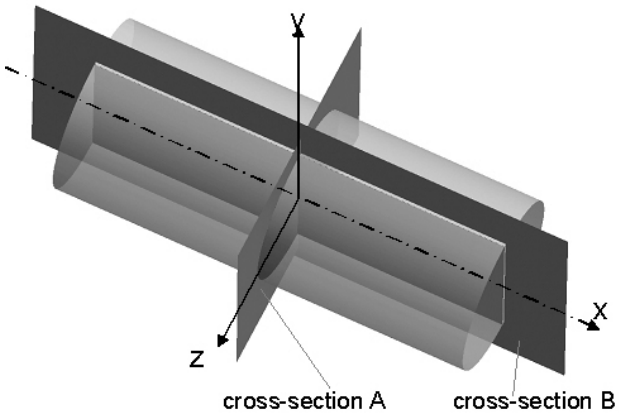

Figure 3-14: Two orthogonal 2D cross-sections that can be considered as simulation planes for 2D roller burnishing model.

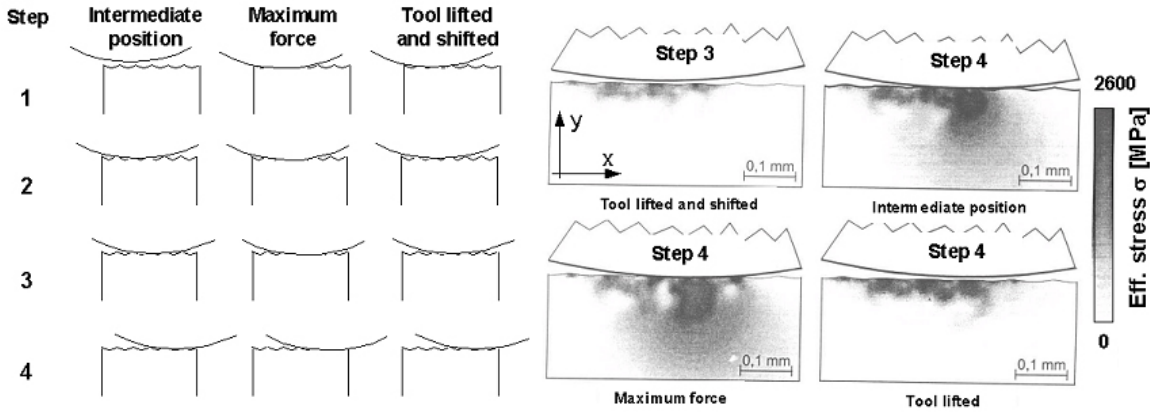

Figure 3-15: Simulation sequences for the 2D FEM model of roller burnishing (left) and the predicted effective stress (right) [Röttger, 2002].

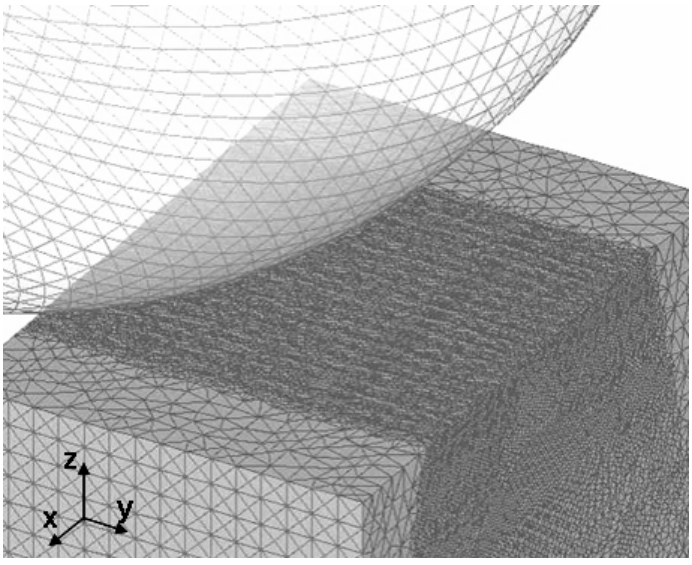

Figure 3-16: 3D FEM model for roller burnishing proposed in [Yen, 2004].

Features	Röttger's Model (2002)	Yen's Model (2004)
# simulation cycles / length	4 cycles / 0.18 mm	> 6-10 cycles / 0.6 mm
Control method for tool movement	Force control	Force control / Displacement control
Duration of one cycle	2 seconds	~ 0.0003 second
Shape of loading curve	Linear	Second-order polynomial
Workpiece dimensions	1.95mm × 2.3mm	2mm × 4 mm
Bulk material model for the workpiece	[Röttger, 2002]	[Röttger, 2002] [Poulachon, 2001] & [ATP, 2002]
Variation of surface layer properties (initial strain)	Not considered (homogeneous)	Evaluated (heterogeneous)
Residual stress by cutting	Not considered	Evaluated
# elements between two roughness peaks	12 – 14	15 - 17
Surface geometry (p-p width, p-v height)	(0.18mm, 0.011mm)	(0.18mm, 0.011mm)
FEM code used	DEFORM™-2D (v7.0)	DEFORM™-2D (v7.2)

Table 3-3: Comparison of simulation settings for Röttger's original model [Röttger, 2002] and modifications proposed by Yen [Yen, 2004].

Zhuang developed a three-dimensional finite element model for roller burnishing simulations by using ABAQUS/Standard [Zhuang, 2004]. In this model, workpiece is considered as an elastic-plastic object and tool as a rigid object. Additionally, a hemispherical rigid surface houses the upper half of the burnishing ball (simulating the tool's ball holder shown in Figure 1-1(b)) without friction in order to model the ball floating in the pressured burnishing fluid. During FEM simulations, the burnishing ball is pressed by the rigid surface against a flat workpiece and moved forward. Similarly to Yen's model (shown in Figure 3-16), contact at the tool/workpiece interface is considered to be frictionless because the burnishing fluid is acting as coolant/lubricant.

Zhuang used the simulation model described above to evaluate the effects of some process parameters (i.e., burnishing pressure, ball diameter, burnishing feed and number of tool passes) on residual stresses. Results predicted by Zhuang's simulations were in good agreement with experimental residual stresses measured by X-ray diffraction technique [Zhuang, 2004].

CHAPTER 4
ROLLER BURNISHING ON HARD TURNED SURFACES OF AISI 52100 (60 HRC)

Hard turning and hard roller burnishing experiments were conducted by the ERC/NSM. Surface roughness and hardness measured data were reported in [Sartkulvanich, 2004b]. In this chapter, additional data related to measured residual stresses on machined/burnished surfaces is presented.

4.1 Workpiece Material and Geometry

Workpiece samples used for hard turning and burnishing experiments were cylindrical bars, made of AISI 52100 bearing steel (see Table 4-1 for details). Samples were heat treated to obtain a surface hardness of 60 HRC prior to hard turning.

Workpiece Material	Workpiece Geometry	Dimensions		Number of samples
		Diameter	Length	
AISI 52100 steel (hardened to 60 HRC)	Cylindrical bar	2 inches (50.8 mm)	6 inches (150 mm)	16

Table 4-1: Information on the workpiece used for hard turning and roller burnishing experiments [Sartkulvanich, 2004b].

4.2 Specifications of Machine and Tools for Hard Turning and Hard Roller Burnishing Experiments

A Hardinge CNC lathe "Quest Model" was used for both hard turning and hard burnishing experiments. Technical information of CNC machine capabilities and cutting tools used in hard turning experiments are shown in Table 4-2 [Sartkulvanich, 2004b].

Ecoroll equipment was used for hard roller burnishing experiments. It consists of a hydraulic pump, connecting hose, an electric panel and a fluid container (tank). Technical information about the hydraulic pump and burnishing tools used for roller burnishing experiments are shown in Table 4-3.

Machine Tool		• CNC Hardinge Lathe, "Quest" Model. • Use of Hydrostatic Linear Guideway. • Maximum Spindle Speed = 15,000 rpm
Cutting Tool	**Tool Holder**	Kennametal (AISI MDJNL 124B) • Side Rake Angle = -5° • Back Rake Angles = -5° • Lead Angle = -32° • Included Angle = 55°
	Cutting Insert	Kennametal (DNGA432T0820, Grade: K090) • A Composite (Black) Ceramic, composed of Alumina and 30% TiC • Included Angle = 55°

Table 4-2: Specifications of the machine and cutting tools used for hard turning experiments.

Hydraulic Pump Ecoroll HGP 4.3	Maximum Pressure	400 bar (or 40 MPa)
	Electricity Requirement	400 V, 50 Hz
NC Control and Tank	Custom made by PMMC at University of Toledo	
Hard Roller Burnishing Tools Ecoroll HG 6	Ceramic tool ball	6 mm diameter
	Tool holder	15° contact angle

Table 4-3: Specifications of hydraulic pump and burnishing tools for hard roller burnishing experiments.

4.3 Experimental Procedures and Process Conditions

4.3.1 Experimental Procedures

Experimental procedure is summarized as follows:

1) All 16 samples were heat treated to get a surface hardness of 60 HRC.
2) Samples were machined to obtain hard turned surfaces with a length of 130 mm (see Step 1 on Figure 4-1). Workpiece was supported in both sides by the lathe's chuck and a tailstock in order to have enough stiffness during machining (and subsequent burnishing) to avoid as possible excessive deflections of the workpiece when acting as a cantilever beam.
3) The hydrostatic burnishing tool was fixed with a contact angle of 15° (see Figure 4-2). Burnishing tool was pressurized first and then loaded on the workpiece before the lathe's spindle was rotated. Burnishing pressure (P_b) was controlled during experiments using the hydraulic unit described in Table 4-3.
4) Burnishing tests were conducted on the machined surface at three different locations so that each sample would contain a non-machined surface, a hard turned surface and three burnished surfaces (see Step 2

in Figure 4-1). The burnishing feed was set in the same direction as cutting feed (see Figure 4-2).

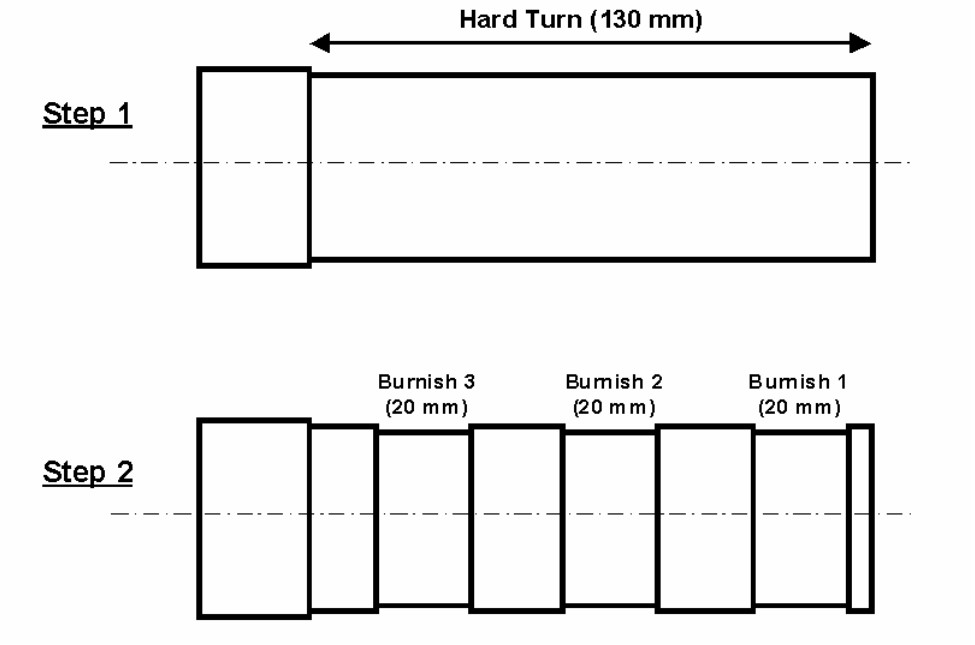

Figure 4-1: Sequences of hard turning and hard roller burnishing experiments [Sartkulvanich, 2004b].

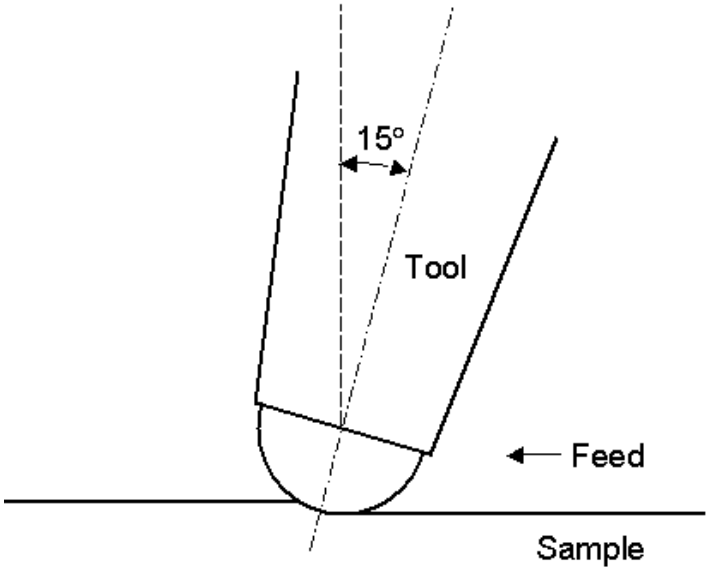

Figure 4-2: Contact between a roller burnishing tool and a workpiece sample [Sartkulvanich, 2004b].

4.3.2 Process Conditions

Hard turning tests were conducted using a cutting condition for which an equivalent machined surface roughness could be generated. The cutting condition selected corresponds to some cutting conditions for the same workpiece material, which are documented in literature [Dahlman, 2004; Poulachon, 2004; Thiele, 1999 and Röttger, 2002]. For hard roller burnishing tests, process parameters used are shown in Table 4-4 (burnishing pressures, feeds and speeds). The ranges of burnishing process parameters were suggested by Ecoroll Company.

Process Conditions for Hard Turning Experiments	
Cutting Speed [m/min]	122
Cutting Feed Rate [mm/rev]	0.1
Depth of cut (mm)	0.127
Process Conditions for Hard Roller Burnishing Experiments	
Burnishing Pressure [MPa]	28, 32, 36,40
Burnishing Feed [mm/rev]	0.02, 0.05, 0.08, 0.11
Burnishing Speed [mm/min]	150, 300, 450

Table 4-4: Process conditions for hard turning and hard roller burnishing experiments [Sartkulvanich, 2004b].

4.4 Measurement of Surface Properties

4.4.1 Surface Roughness

Roughness parameters, namely roughness depth (R_z) and mean roughness (R_a) were measured by using a “Stylus” surface analyzer (see details in Table 4-5). Roughness parameters were measured according to DIN 4768 and 4762 standards. A detailed definition of those standards is provided in APPENDIX A.

All measured surface roughness parameters of the tested samples are given in [Sartkulvanich, 2004b].

4.4.2 Residual Stresses

Residual stresses were measured in axial (σ_a) and tangential (σ_t) directions (see Figure 4-3) using the X-ray diffraction technique. Figure 4-4 and Figure 4-5 show the residual stress distribution (in both directions) along the workpiece depth beneath the surface for hard turned and roller burnished samples respectively. The conditions used for X-ray diffraction measurements are shown in Table 4-6.

Surface Roughness Measurements	
Machine Name	Federal Surface Analyzer
Specifications	- Provides total profile, as well as roughness and multi parameter measurement capability . - Software: ProfileView 3.1 - Graphical display or profile, waviness, roughness, bearing area curve, amplitude density function and power spectral density. - Zoom capabilities for all computed curves - Switching between ANSI, ISO, DIN and JIS standards. - Gaussian, 2RC and RC Phase Correct Filters. - Vertical resolution is from 0.002 to 0.010 μm (based on assigned length of measurement).

Table 4-5: Technical information for surface roughness measurements.

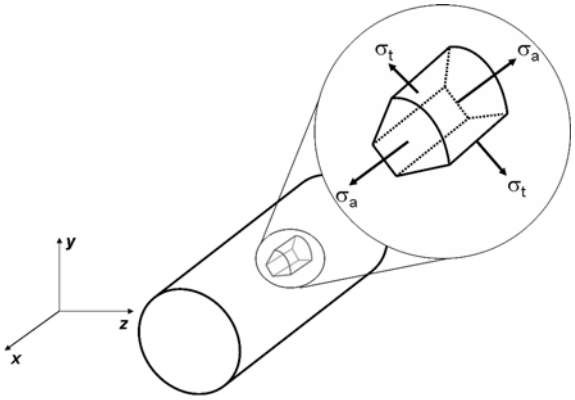

Figure 4-3: Direction of the residual stresses measured on hard turned and hard burnished surfaces.

X-ray diffraction conditions	
Characteristic X-ray	Cr Kα
Diffraction Plane	{2 1 1}
Tube Voltage	35 kV
Tube Current	1.5 mA
psi tilt angles	0°, 18.4°, 26.6°, 33.2°, 39.2° and 45°
Stress Constant	Carbon steel stress

Table 4-6: Conditions used for X-ray diffraction to determine residual stresses of the hard-turned and burnished surfaces.

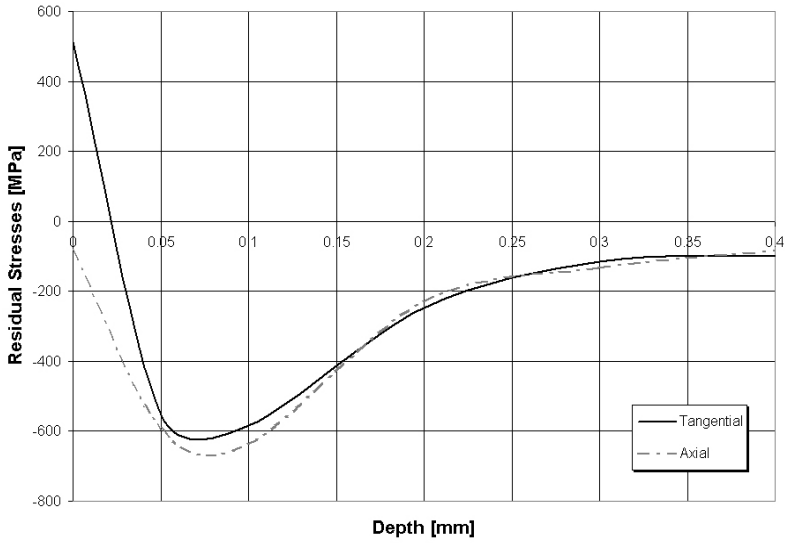

Figure 4-4: X-ray measured residual stresses for a hard turned sample (see Figure 4-1). Cutting conditions are those shown in Table 4-4.

(a)

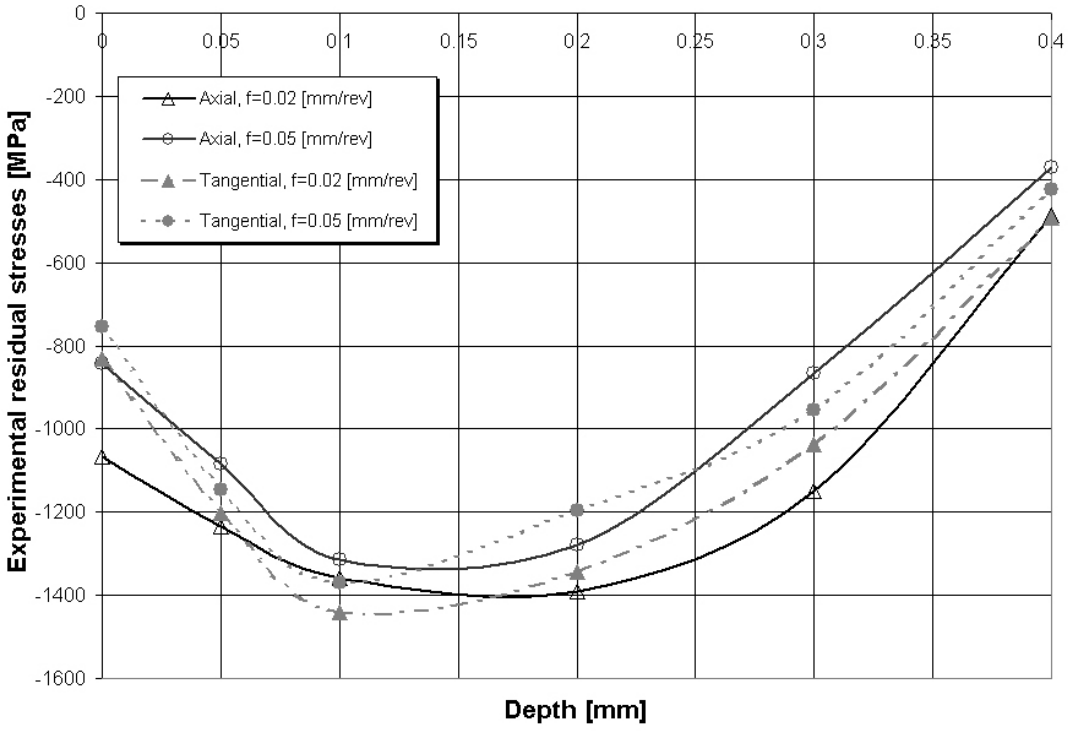

(b)

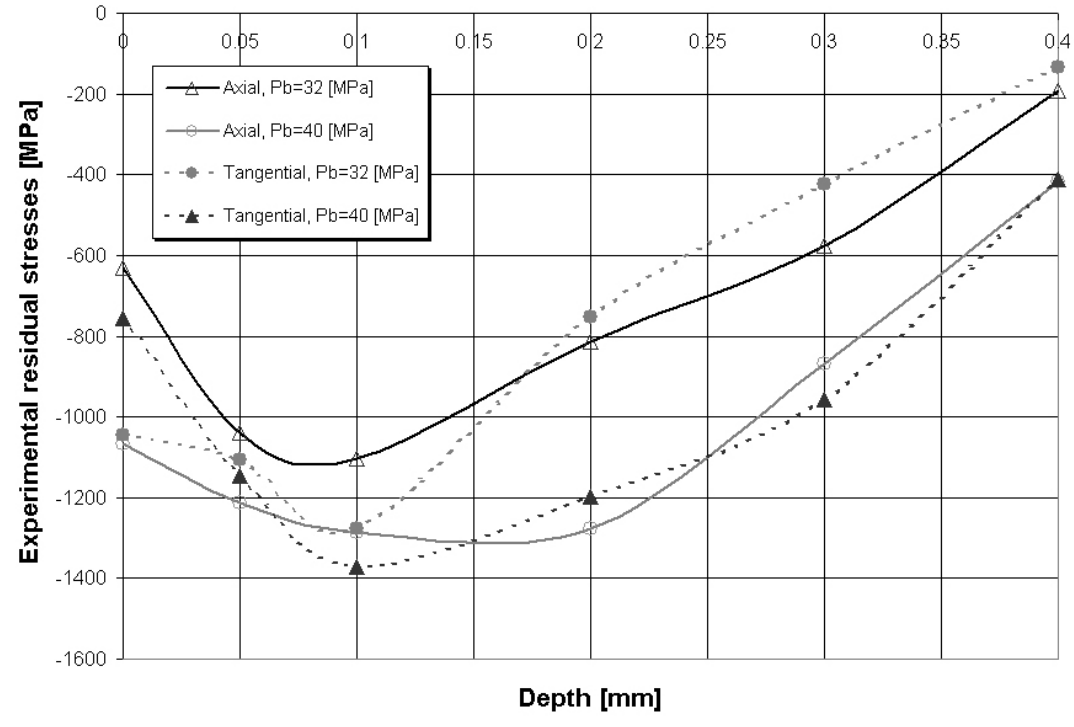

Figure 4-5: X-ray measured residual stresses for the selected burnished surfaces. **(a)** P_b=40 MPa and different burnishing feeds (f_b). **(b)** f_b=0.05 mm/rev and different burnishing pressures (P_b). See Table 4-4 for the complete set of roller burnishing parameters.

CHAPTER 5
ESTABLISHMENT OF FINITE ELEMENT SIMULATION MODEL FOR ROLLER BURNISHING

In order to study the effect of burnishing feed and pressure on surface roughness and residual stresses, it was necessary to modify the 2D FEM roller burnishing model previously developed in [Yen, 2004]. This chapter describes the changes implemented on Yen's model so that the effect of process parameters on surface properties can be simulated.

5.1 Flow Stress Models of AISI 52100 Steel Previously Used for FEM Roller Burnishing Simulations

The use of the finite element method (FEM) to conduct numerical simulations on metal forming/cutting operations requires a reasonable knowledge of the workpiece's material properties, especially the flow stress properties [Morris, 2005]. Röttger proposed a flow stress equation for bulk 100Cr6 (or AISI 52100) bearing steel, as given by

$$\bar{\sigma} = C\bar{\varepsilon}_p^{\,n}\dot{\bar{\varepsilon}}_p^{\,m} + \sigma_y \tag{5.1}$$

where C=300 MPa, n=0.3, m=0.1,and $\bar{\sigma}_y = 2500$ MPa. In that equation, $\bar{\sigma}$ is the flow stress, $\bar{\varepsilon}_p$ is the plastic strain, and $\dot{\bar{\varepsilon}}_p$ is the plastic strain rate [Röttger, 2002].

Röttger found a good agreement between his FEM predicted results using the flow stress model given in Eq. (5.1) and experimental effective residual stress. However, no further information was provided in [Röttger, 2002] on how to obtain

Eq. (5.1) and how to determine the experimental effective residual stress (where the residual stress can be measured only in axial and tangential directions in practice, but not the shear stress).

In Yen's study, the effects of the variations of material behavior at different surface depths were studied by considering residual stress/strain information extracted from experimental measurements in [Röttger, 2002]. Simulations were conducted using the same flow stress model for bulk material given by Eq. (5.1). Residual stresses predicted by this modified model (with including variations of initial stress/strain from machining) were very similar to those obtained without initial stress/strain data. Additionally, the predicted residual stresses fairly agreed with experimental data published by [Röttger, 2002].

The flow stress at the machined surface of the workpiece (before roller burnishing) may differ from the bulk properties due to large plastic deformations and possible phase transformations generated during machining [Ramesh, 2004 and Morris, 2005]. Finite Element inverse analysis and ball indentation tests are useful to provide the material properties for the manufactured (hard turned) surfaces, which could be more reliable than other tests that are conducted on bulk workpiece samples. New material flow stress property from ball indentation tests was included in the present FEM model of roller burnishing.

In this work, there are five major modifications and tasks conducted additionally to the FEM model done by Yen [Yen, 2004], as listed below.

(1) The flow stress properties for roller burnishing simulations were obtained from an FEM inverse analysis and instrumented ball indentation tests (Section 5.2).
(2) Force calculation considered the pressure loss during actual operation. This was implemented by calibration of the experimental force measurements respect to the applied burnishing pressure (Section 5.3.1).
(3) The initial machined surface roughness for the workpiece model was obtained from experimental measurement instead of theoretical

calculation that was determined from nose radius and turning feed (Section 5.3.2).

(4) The effects of displacement boundary conditions of the workpiece model were studied in order to select the reasonable size for the workpiece model in roller burnishing simulation (Section 5.3.3).

(5) Analyses of the contact by using several approaches (e.g. elastic contact theory, FEM elastic-plastic ball indentation) were performed to determine the maximum penetration depths where the ball tool engages into the workpiece surface (Section 5.3.4).

5.2 Determination of Flow Stress Properties of an AISI 52100 (60 HRC) Hard Turned Surface

The flow stress properties at the machined surface can be determined by using instrumented ball indentation experiments and FEM inverse analysis [Morris, 2005]. The flow stress data can be represented as in the following equation (see also in Figure 5-1)

$$\sigma = \begin{cases} E\varepsilon & \text{if} \quad \varepsilon \le \varepsilon_y \\ R\varepsilon^n & \text{if} \quad \varepsilon \ge \varepsilon_y \end{cases} \tag{5.2}$$

where

σ is the true stress

ε is the true total strain

ε_y is the yield strain

R is the strength coefficient

n is the strain-hardening exponent

The equation shown above was converted into a flow stress equation for plastic deformation, which is in function of plastic strain (as shown in Eq. (5.2)). This was done by considering the fact that the true stresses from elastic and plastic

regimes are equal at the same yield strain (ε_y) so that the flow stress is given by the equation:

$$\sigma = \sigma_y \left(1 + \frac{E}{\sigma_y} \varepsilon_p \right)^n \tag{5.3}$$

where

- σ is the true stress
- ε_p is the plastic strain
- E is the modulus of elasticity (constant E=210 GPa for steel)
- n is the strain hardening exponent

Morris determined the values of σ and n in Eq. (5.3) for the AISI 52100 hard turned surface [Morris, 2005]. The strategy to determine these values can be summarized as follows:

1. Instrumented ball indentation tests were conducted on an AISI 52100 workpiece at three different locations over the hard-turned surfaces. Indentation tests were similar to hardness tests with the difference that the indentation depth was recorded simultaneously with the applied load during the indentation, which allows to plot a load-stroke curve as that shown in Figure 5-2.

2. An FEM model for ball indentation was established using DEFORM^{TM}-2D, with 2D-axisymmetric formulation (see Figure 5-3). In this model, a ball indenter was pushed in the normal direction to the flat workpiece surface.

3. The FEM inverse analysis was performed by conducting a series of ball indentation simulations with different sets of flow stress data, for the different values of σ_y and n of the Eq. (5.3). The flow stress was obtained at which the load-stroke curves from FEM simulations match the experimental curves (see Figure 5-4).

4. Values for σ_y and n were averaged from the three different machined surfaces. The obtained flow stress equation has σ_y=1765 MPa and n=0.157 (see Table 5-1), which give the flow stress equation for a hard turned AISI 52100 surface as in the following equation (in MPa).

$$\sigma = 1765\left(1+\frac{210000}{1765}\varepsilon_p\right)^{0.157} \tag{5.4}$$

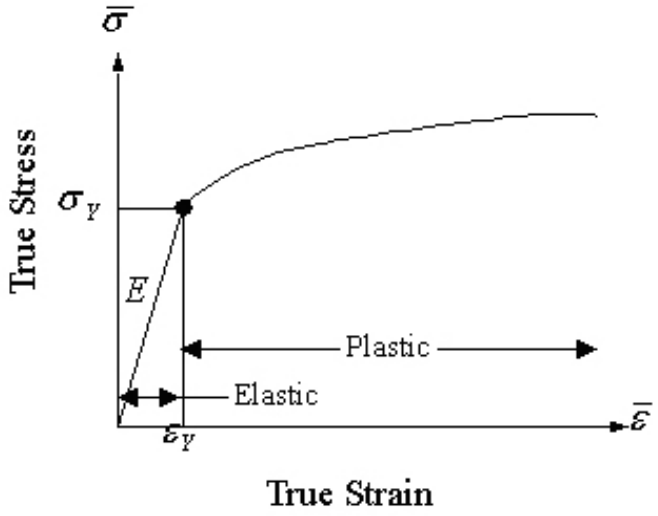

Figure 5-1: Graphical representation of the flow stress equation used in roller burnishing simulations.

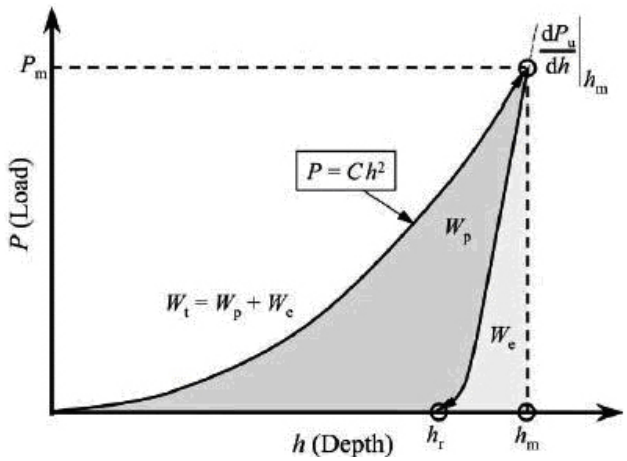

Figure 5-2: A typical load-stroke curve from instrumented ball indentation tests [Morris, 2005].

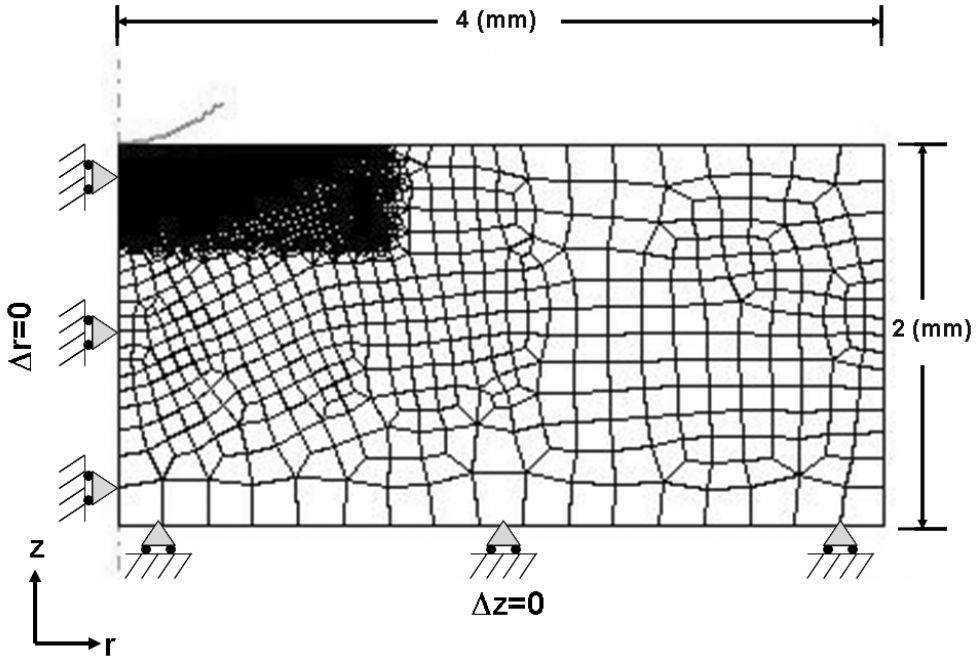

Figure 5-3: Finite element model setup for ball indentation simulations using DEFORM^{TM}-2D [Morris, 2005].

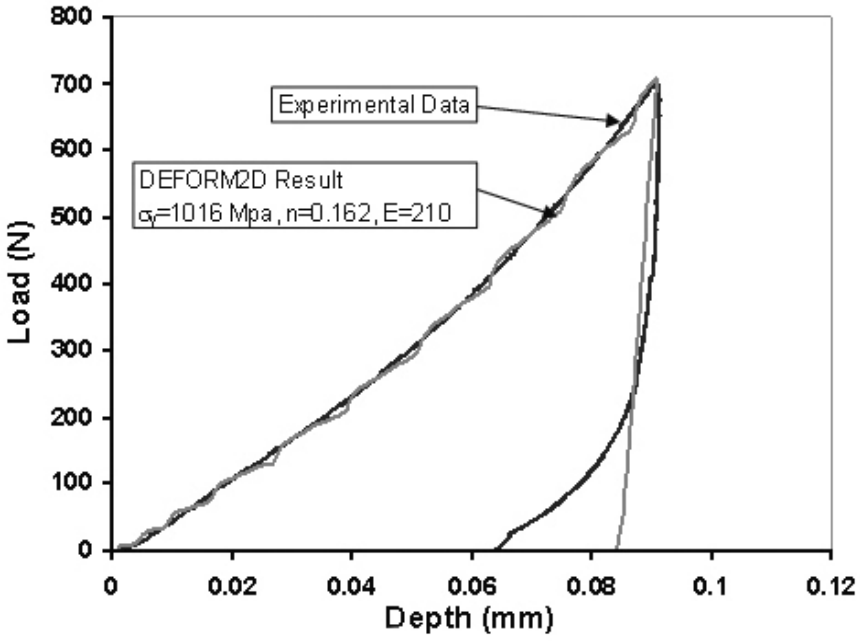

Figure 5-4: Comparison of load-stroke curves from experimental indentation tests and FEM simulation for AISI 52100 steel [Morris, 2005].

Test	FEM Inverse Analysis	
	σ_y [MPa]	n
A1	1667	0.179
A2	1665	0.178
A3	1860	0.128
Average	**1765**	**0.157**
St. Dev.	115	0.025

Table 5-1: Values for σ_y and n that define the flow stress of AISI 52100 machined surfaces. Results were obtained from FEM inverse analysis and instrumented ball indentation tests [Morris, 2005].

The difference between Eq. (5.1) and Eq. (5.4) is that Morris' model (Eq.(5.4)) does not consider strain-rate dependence as in Röttger's equation (Eq. (5.1)). This means that the effect of burnishing speed cannot be considered in FEM simulations with Morris' flow stress model. However, as discussed in Section 3.2, several experimental studies showed that the effect of burnishing speed was negligible for a wide range of burnishing speeds (50 to 450 m/min) [Röttger, 2002]. In addition, surface finish and hardness measurements from roller burnishing experiments conducted by the ERC/NSM also showed similar observations [Sartkulvanich, 2004b] for the speed range of 150 to 450 m/min. Thus, the use of Eq. (5.4) for FEM roller burnishing simulations is reasonable.

5.3 Modeling of Roller Burnishing with a 2D Simplified Model

Although, roller burnishing is a three-dimensional process in nature, the use of 3D FEM model (described in Section 3.3.3) to analyze the effect of various process parameters upon surface properties is limited, due to extremely high computational time required to run the simulation (~200,000 elements for the workpiece model and ~4 days to complete one single path). For these reasons, the use of a 2D FEM model for burnishing simulations is important because the computational time could be significantly reduced and the effects of various process parameters on surface qualities could be studied.

Simulation procedures are similar to those developed Yen and Röttger, [Yen, 2004 and Röttger, 2002]. Steps of 2D simulation can be described in Figure 5-5.

Step-1: The ball moves down at a constant velocity to press on the workpiece. The burnishing fluid is considered to act as lubricant/coolant all the time. For this reason, process is modeled as frictionless and isothermal according to information available in [Klocke, 1998; Röttger, 2002 and Zhuang, 2004].

Step-2: The ball stops at a certain maximum penetration depth.

Step-3: The ball unloads from the workpiece and return to its original position and shifts in the right direct for the distance of burnishing feed.

Step-4: The processes of loading/unloading/shift are repeated for 11 cycles.

There are a number of modifications and considerations to the existing 2D FEM model. These include the consideration of pressure loss (Section 5.3.1), determination for the effective size of the workpiece model (Section 5.3.3), determination of maximum ball penetration depth (Section 5.3.4) and evaluation of different ball movement controls (Section 5.3.5).

5.3.1 Pressure Loss in Hydrostatic Burnishing Tools and Burnishing Force

Burnishing force (F_b) can be estimated analytically from the burnishing pressure (P_b) that hydrostatically applies to the ball tool (see Figure 1-1). The burnishing force is given by the equation

$$F_b = \frac{\pi}{4} d_b^2 P_b \tag{5.5}$$

where d_b is the tool's ball diameter.

Röttger measured the forces that the workpiece reacted to the overall burnishing tool holder by using a dynamometer on the tool holder fixture. Measurements were conducted during roller burnishing on AISI 52100 hardened surfaces using different ball diameters and burnishing pressures [Röttger, 2002]. The experimental burnishing forces were compared with the theoretical forces calculated using Eq. (5.5). Evidence showed that the theoretical forces are about 11% to 12% higher than the experimental forces (see Figure 5-6 and Table 5-2). The differences between these two forces are due to small fluid pressure loss during burnishing operation, which generally occurs along the gap between the ball and the socket [Röttger, 2002]. According to these force differences, percentages of pressure loss can be considered to be approximately 11% to 12%. This percentage of pressure loss was taken into account in the 2D FEM model.

Burnishing pressure [MPa]	Theoretical force [N]	Experimental force [N]	% Difference
20	565	499	+12%
30	848	748	+11%
40	1131	1006	+11%

Table 5-2: Comparison of the forces obtained from theoretical calculations and experimental measurements [Röttger, 2002].

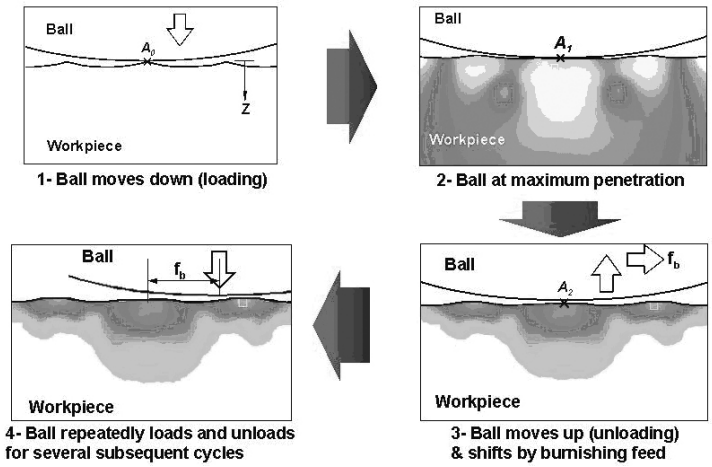

Figure 5-5: Simulation steps used in a 2D FEM roller burnishing model.

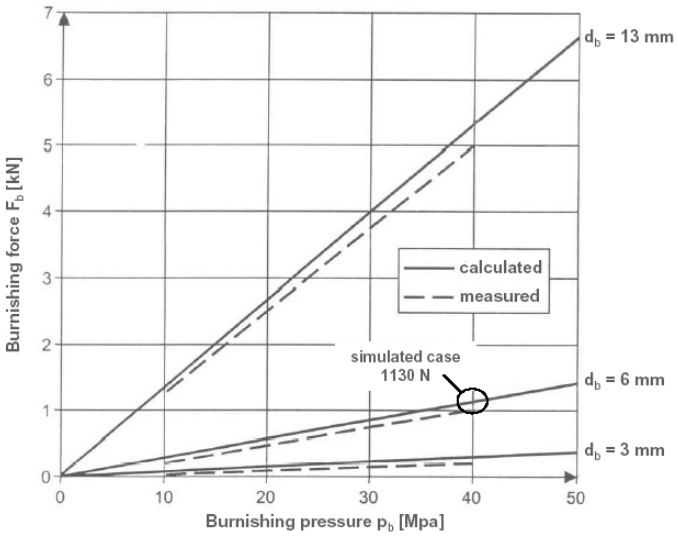

Figure 5-6: Comparison between the calculated and measured burnishing forces for different ball diameters [Röttger, 2002].

Burnishing pressure loss and experimental setup for 15° contact angle (between the ball tool and the workpiece), described in Section 4.3.1, were considered for calculating the burnishing force to be used in 2D roller burnishing simulations. Therefore, the calculated burnishing forces ($F_{b,FEM}$) can be given by

$$F_{b,FEM} = 0.89 F_b \cos(15°) \tag{5.6}$$

where F_b is the analytical burnishing force calculated by using Eq. (5.5).

5.3.2 Modeling of Tool/Workpiece Objects in the 2D FEM Model of Roller Burnishing

Since the flow stress model for the AISI 52100 hard turned surface given by Eq. (5.4) is not strain rate dependant, the 2D FEM model cannot analyze the effect of burnishing speeds. However, the effects of burnishing speeds can be considered as insignificant, according to many experimental studies. As mentioned earlier in Section 3.3.3, cross-section 'B' of Figure 3-14, which contains the hard turned surface profile, was used to conduct 2D roller burnishing simulations. In this simulation model, the tool loading on workpiece surface was represented as an indentation for each burnishing path [Yen, 2004]. The ball was considered a rigid object and the workpiece was considered as an elastic-plastic object. Because pressurized fluid acts as coolant and lubricant in the process, the FEM model can assume isothermal condition and friction coefficient of zero. The displacement boundary constraints that were applied on the left, right and bottom boundaries of the workpiece are shown in Figure 5-7.

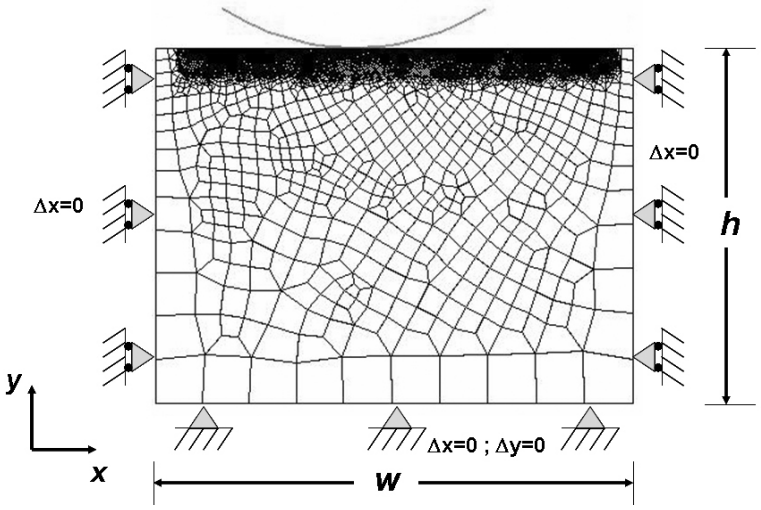

Figure 5-7: 2D FEM plane strain model for roller burnishing simulations used to evaluate the effect of process parameters upon surface properties. Model represents cross-section 'B' of Figure 3-14.

5.3.3 Determination of a Workpiece Size for Roller Burnishing Simulations

It was necessary to conduct a sensitivity analysis in order to determine the workpiece's optimum dimensions, i.e. the width (*w*) and the height (*h*) in Figure 5-7. 2D roller burnishing simulations were performed for only one indentation cycle (no feed effect) using different workpiece dimensions shown in

Table 5-3. The objective was to analyze the effect of boundary constraints on the predicted roughness and residual stresses from different sizes of the workpiece models. Starting from a 3x2 mm^2 workpiece, the dimensions were increased until the predicted results did not vary significantly from one simulation to another. The criteria selected to achieve this goal was based on the observation of the effective stress distributions when applying the maximum burnishing force (F_b) on the contact surface during the indentation.
Observation was made such that the lines of the effective stress contour should not get in contact with the workpiece boundaries during the maximum tool penetration (when the maximum burnishing force has been applied). Figure 5-8 shows the effective stress distributions of two different workpieces (3x2 mm^2 and 5x4.5 mm^2). Both workpieces were subjected to the maximum load used on roller burnishing experiments (P_b=40 MPa) while considering the pressure loss by using the approach discussed in Section 5.3.1. The boundary effect can be observed in Figure 5-8(a) and Figure 5-9(a), where the stress distributions were distorted by boundary displacement constraints.

The size of the workpiece strongly influences the predicted results for both residual stress and surface roughness. However, the results do not change dramatically when the workpiece size are increased beyond an optimum workpiece size. Figure 5-10(a) shows the evolution of surface roughness prediction. It can be observed that surface roughness does not change dramatically for workpiece sizes equal to and greater than 5x4.5 mm^2. The effective stress contour is in contact with the 3x2 mm^2 workpiece boundaries during the maximum load and thus causes the difference in the predicted surface

roughness. The effective residual stress predictions are shown in Figure 5-10(b). It can be observed in this figure that residual stresses are also affected by the displacement boundary constraints when the workpiece size is smaller than 5x4.5 mm^2.

The observation of the effective stress contour (obtained during the maximum load) as a criterion to select a workpiece size for 2D roller burnishing simulations is simple and useful. The workpiece height *h* mainly influences the predicted results. Simulations showed that workpiece dimensions *w* and *h* should be at least 5 and 4.5 mm respectively. However, the width dimension *w* needs to be increased in order to consider the effect of the burnishing feed (f_b) in the simulations, as will be discussed later in Section 5.3.5.

Sample	Width *w* [mm]	Height *h* [mm]
1	3	2
2	5	3.5
3	5	4.5
4	7	6

Table 5-3: Workpiece dimensions used to study the size effects in 2D roller burnishing simulations.

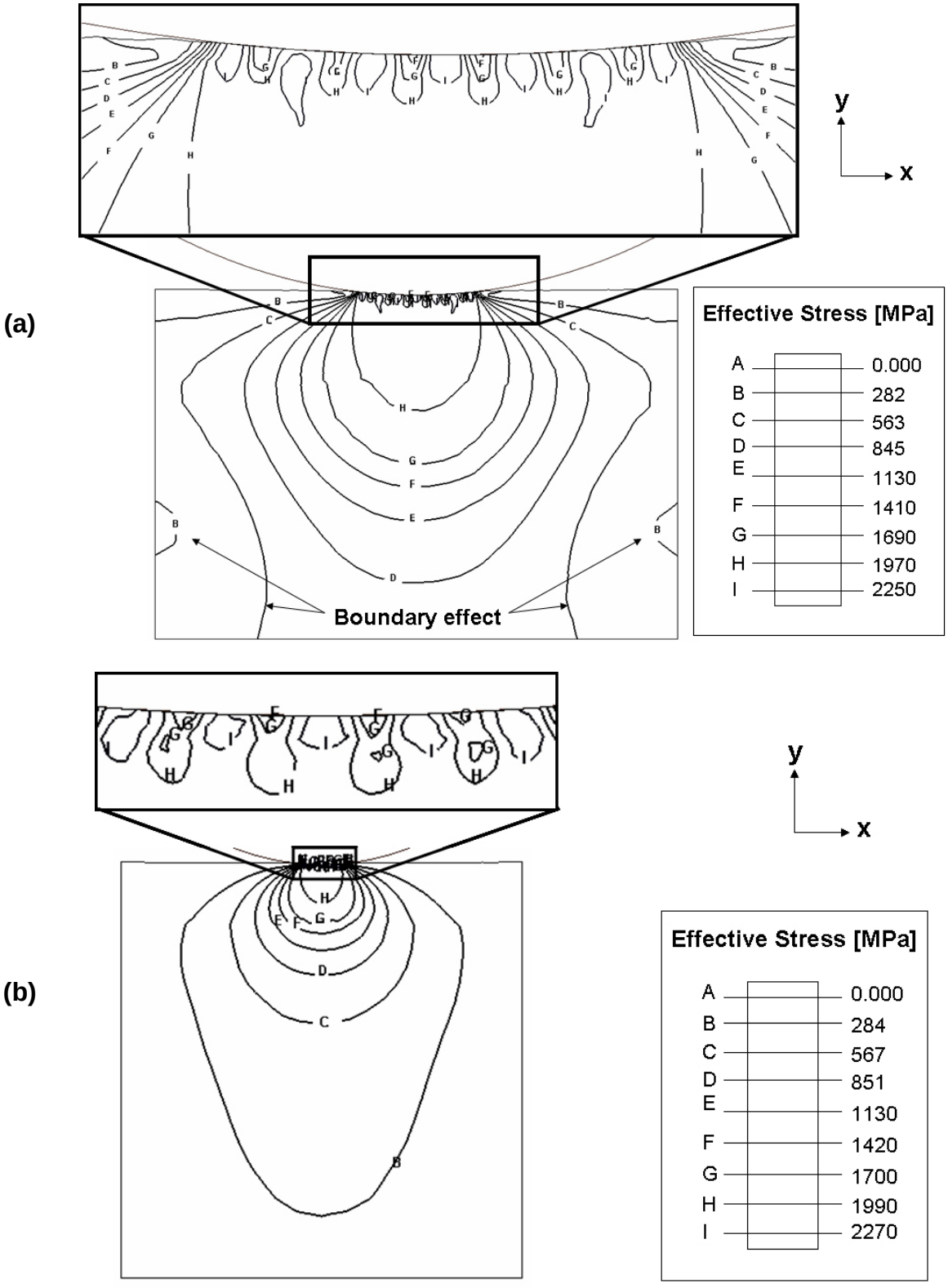

Figure 5-8: Effective stress line contour from 2D roller burnishing simulations during maximum load for two different workpiece sizes. **(a)** 3x2 mm, **(b)** 5x4.5 mm. Ball diameter is 6 mm. Stress unit are in MPa.

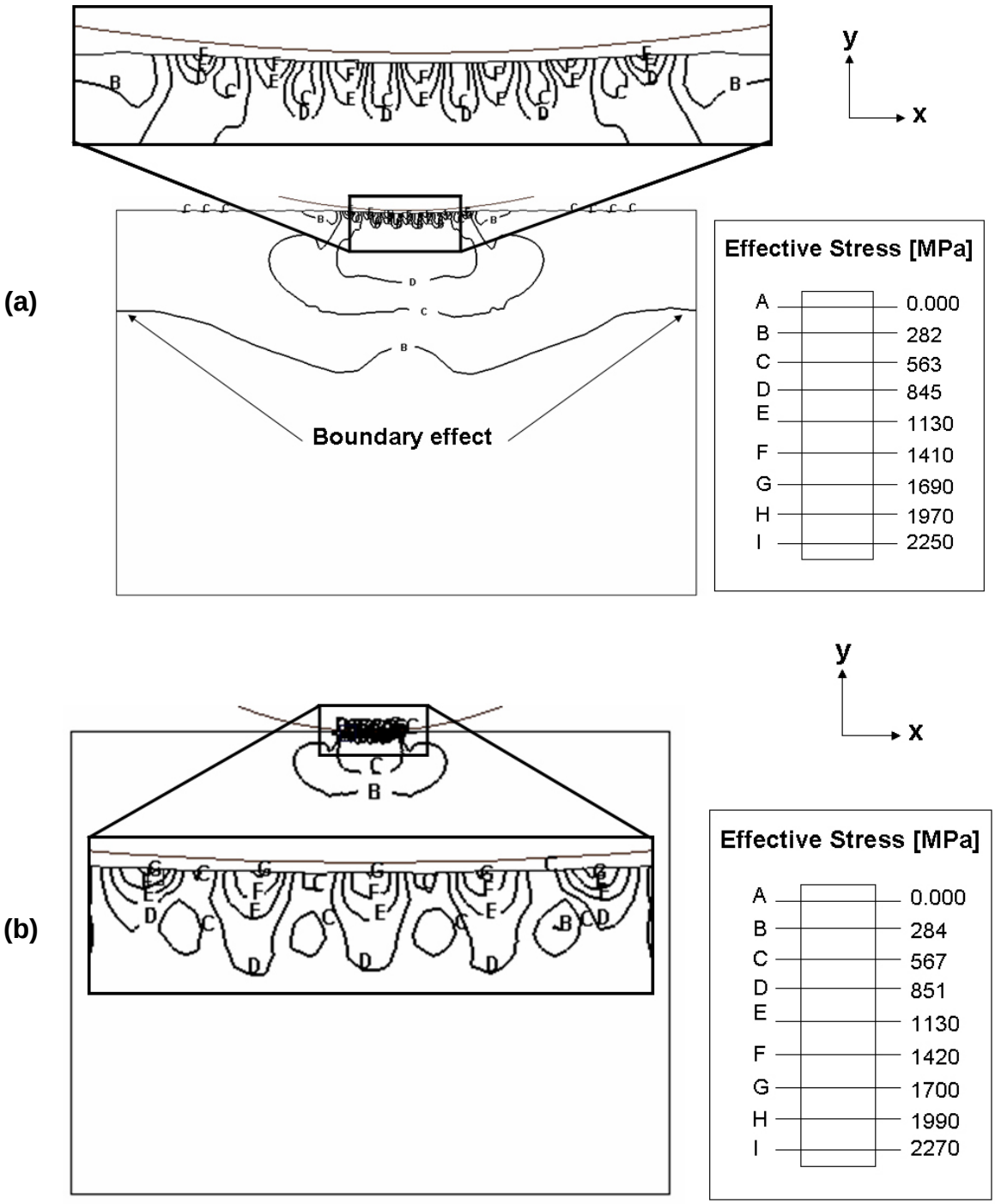

Figure 5-9: Effective stress line contour diagrams from 2D roller burnishing simulations after unloading the ball tool for two different workpiece sizes. **(a)** 3x2 mm, **(b)** 5x4.5 mm. Ball diameter is 6 mm. Stress unit are in MPa.

(a)

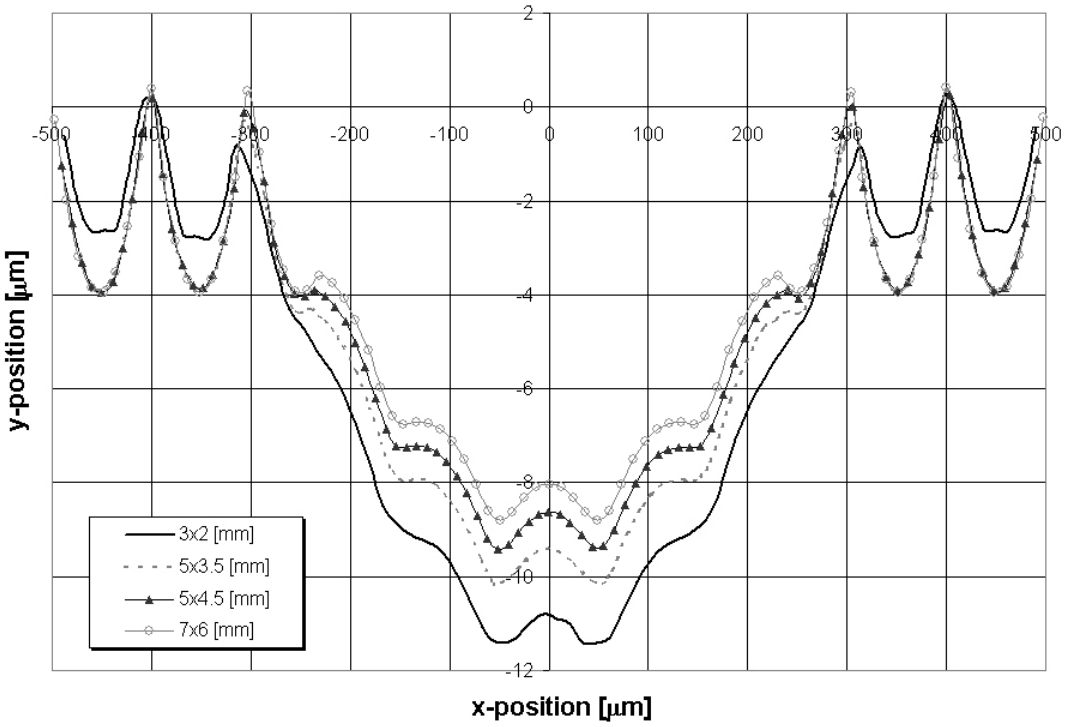

(b)

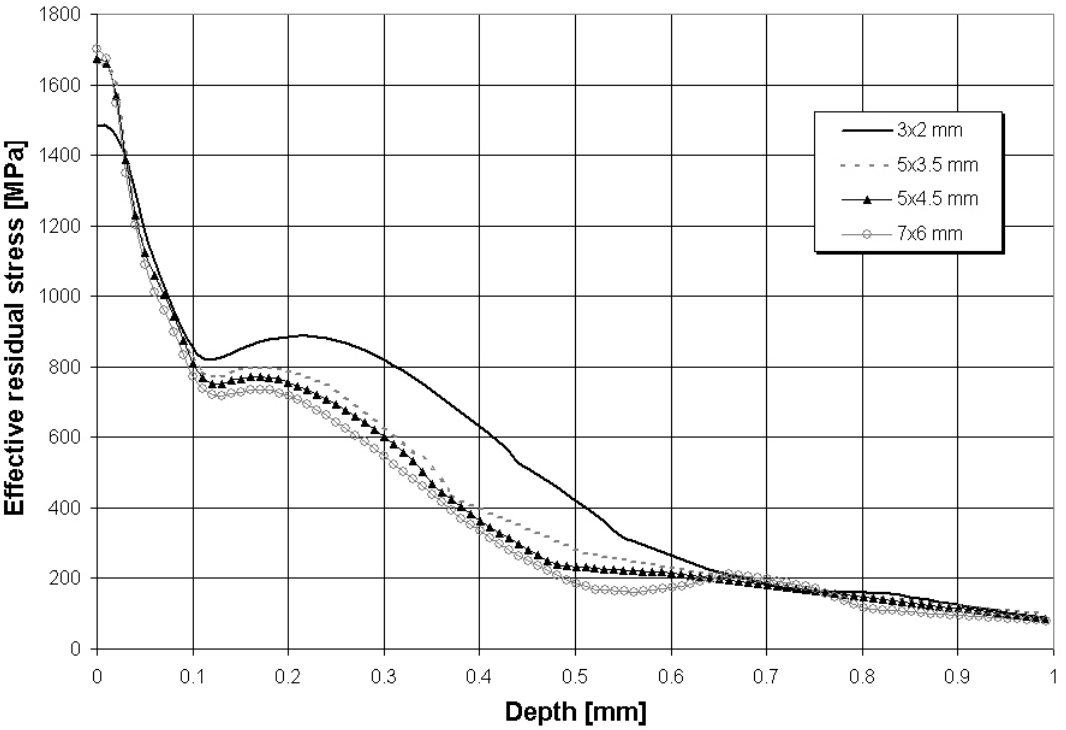

Figure 5-10: Sensitivity of the surface qualities to the workpiece sizes in FEM model. **(a)** Surface roughness. **(b)** Effective residual stresses.

5.3.4 Determination of Maximum Ball Penetration Depth from 3D Roller Burnishing Model and Comparison with Other Approaches

In the established 2D model, the ball movement is controlled by displacement. For every indentation cycle, the ball moves toward the workpiece until reaching the same maximum penetration depth and then unloads from the workpiece. This maximum ball penetration was considered from the results of 3D roller burnishing simulations of one single path. DEFORM^{TM}-3D was used for modeling roller burnishing. Mesh density of the workpiece and the ball in 3D FEM model is shown in Figure 5-11. In the 3D model, the ball tool moves in the y-direction and rotates around its x-axis. Other settings and assumptions used for this 3D model are shown in Table 5-4.

The maximum penetration depth was obtained by conducting three 3D simulations at three different penetration depths to construct the predicted load vs. ball penetration depth curve, as shown in Figure 5-12. For the given burnishing pressure, burnishing force can be calculated by using Eq. (5.6). The corresponding maximum ball penetration depth at the given burnishing force can be found from Figure 5-12. An example on how to obtain maximum ball penetration depth from the given burnishing pressure of 40 MPa is presented in the same figure, where the obtained maximum penetration depth is 0.028 mm.

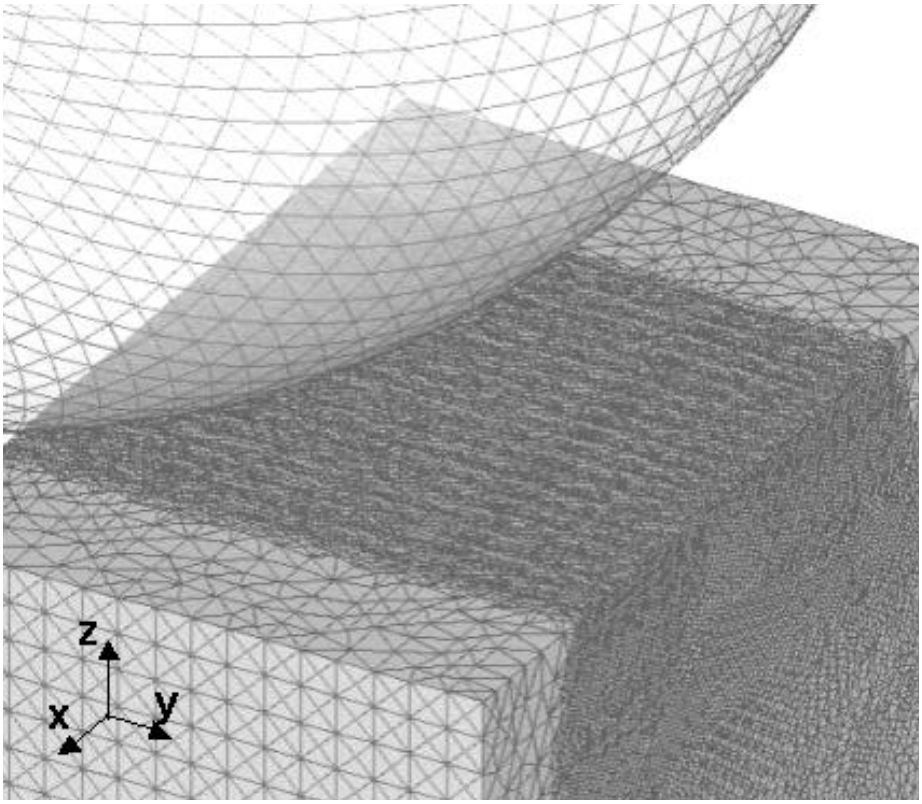

Figure 5-11: Mesh definition of a 3D FEM roller burnishing model.

Object type	Elastic-plastic workpiece, Rigid tool
Friction	μ = 0 (rolling + lubricant)
Thermal condition	Isothermal (coolant) [Klocke, 1998; Röttger, 2002 and Zhuang, 2004].
Initial roughness	Mean roughness depth, R_z, measured from stylus profiler
Tool Movement	Tool moves toward the workpiece and rotates at the same tangential speed.
Burnishing force (F_b)	Controlled by the fluid pressure and calculated by "pressure x projecting area" and consideration of 11% pressure loss (calibrated with experiment)

Table 5-4: Setup of the 3D FEM roller burnishing model.

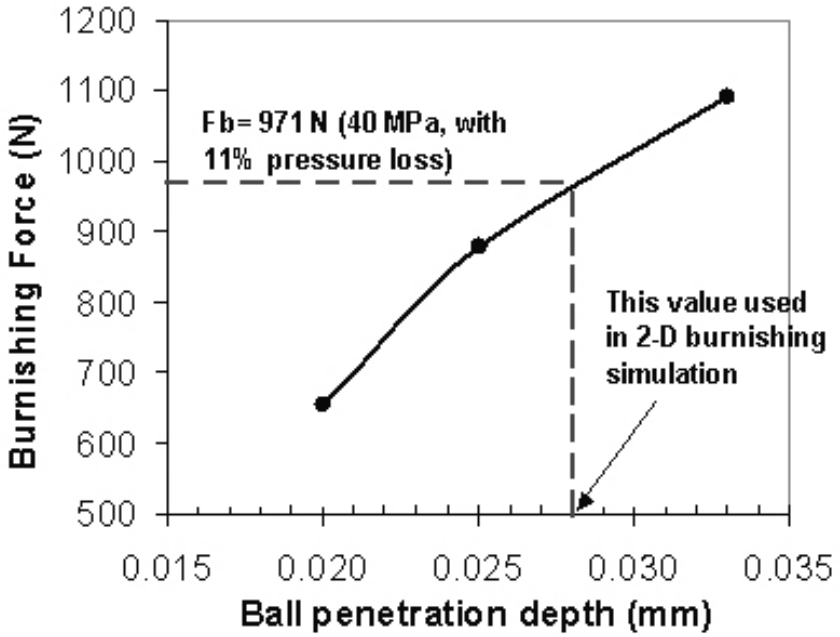

Figure 5-12: Burnishing Force vs. maximum ball penetration depth curve obtained from 3D roller burnishing simulation.

The 3D FEM solution for maximum penetration depth is however based on the assumption that all simulation settings are correct and the DEFORM^{TM}-3D package provides reliable results. Therefore, other approaches to obtain the maximum penetration depth were also conducted and compared with the 3D FEM solutions. Overall, there are five approaches as listed below.

(1) Elastic theory for a ball-to-cylindrical contact (ball indentation).
(2) 2D elastic axis-symmetric simulation (ball indentation).
(3) 2D elastic-plastic axis-symmetric simulation (ball indentation).
(4) Simplified 2D roller burnishing simulation (plane strain assumption).
(5) 3D Roller burnishing simulation (discussed previously).

The maximum penetration depths were determined using the force value considered the pressure loss and the material flow stress properties described in Section 5.2. All analyses were conducted for the burnishing pressure of 40 MPa (maximum pressure value used in the experiments). Methods (1) to (3) are based

on ball indentation solutions and the assumption of flat workpiece surface (with no roughness profile).

Method (1) employs Hertz's contact theory, described in [Bouzid, 2004]. Tool and workpiece are considered as elastic objects. Calculations for the maximum penetration depth and contact diameter are shown in APPENDIX B.1. Method (2) assumes a rigid ball tool and a flat elastic workpiece in a 2D axis-symmetric simulation (modeled with DEFORM^{TM}-2D). Method (3) was established similar to Method (2), except that the workpiece was assumed as elastic-plastic object with the flow stress properties given in Eq. (5.4). Method (4) used 2D FEM plane strain roller burnishing model and determined the depth by matching the predicted force with the applied burnishing force. Since force calculated in 2D FEM is based on plane strain assumption, the resulted force is for the width of 1 mm (normal to plane direction). For realistic force calculation, the width (W) needs calibration by assuming that the rectangular contact area (in 2D plane strain model) is equivalent to the circular contact area defined by the contact diameter (d_c), as can be seen in Figure 5-13. Method (5) used the results of 3D FEM roller burnishing simulation, as discussed previously.

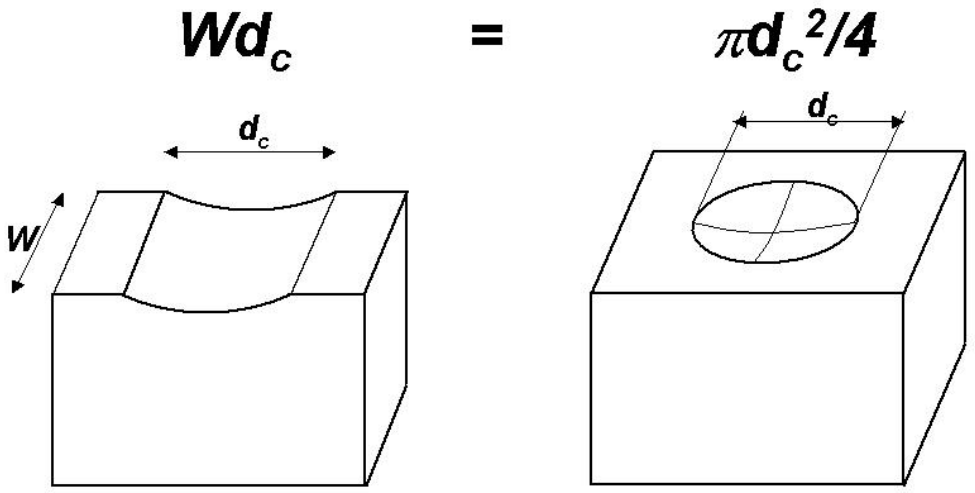

Figure 5-13: Equivalent contact area assumption used to estimate the width of plane strain contact for the simplified 2D FEM model (Method (4)).

Table 5-5 summarizes the maximum penetration depths determined from all five different methods. Method (2) (Elastic axis-symmetric simulation) provided the smallest value of maximum penetration depth that could be determined; however, it was obviously larger than the initial machined surface roughness (peak to valley) of 4 micron. When comparing between Methods (2) and (3) (or Elastic vs. Elastic-plastic axis-symmetric simulation), the simulation results showed strong elastic deformation during unloading of the ball. Both Methods (2) and (3) however might provide smaller maximum penetration depths than what could be expected from roller burnishing. In roller burnishing, the ball rolls and contacts with the workpiece mostly ahead of rolling direction and leaning toward feed direction, not in an exact circular contact like ball indentation. Therefore, its area of contact is much smaller than that of ball indentation solution. With the same applied burnishing force, the maximum penetration depth in roller burnishing must be larger than those obtained from ball indentation models.

Method / Model	**Max. Penetration Depth (μm)**
(1) Elastic theory of contact	17.6
(2) 2D elastic axis-symmetric simulation	17
(3) 2D elastic-plastic axis-symmetric simulation	20
(4) 2D roller burnishing simulation (plane strain)	29
(5) 3D roller burnishing simulation	28

Table 5-5: Comparison of maximum penetration depth from theoretical calculation and different FE simulation models

2D Roller burnishing simulations were conducted using two maximum penetration depths, determined from Method (3) (elastic-plastic axis-symmetric simulation) and Method (4) (force matching in 2D roller burnishing simulation). This should provide the predictions of surface qualities at the lowest and highest values (20 and 29 μm) possible for the maximum penetration depth determined.

Overall, two 2D burnishing simulations for two different maximum penetration depths were conducted, as summarized below.

- 2D simulation using the maximum penetration depth of 20 μm.
- 2D simulation using the maximum penetration depth of 29 μm

Burnishing feed of 0.05 mm was considered as a distance between consecutive indentation cycles of the ball tool in the simulations. Simulations were conducted for 11 indentation cycles or the corresponding burnished distance of 0.5 mm. The results of surface roughness and residual stresses from these two simulations were compared with experimental data.

Surface roughness profiles from the simulations are shown in Figure 5-14. The values of surface roughness parameters, i.e. roughness depth R_z and mean roughness R_a, are shown in Table 5-6. As can be expected, with more penetration depth D, the entire surface profile was deformed deeper. However, the determined surface roughness parameters (determined using formulae described in APPENDIX A) showed only slight difference (about 0.1 μm) between two maximum penetration depths used. In addition, although lower and upper solutions of the maximum penetration depths (20 and 29 μm) were used, the predicted surface roughness parameters were still much lower than that of the experiment, where R_z are approximately 60% different from the experiment.

On the other hand, the maximum penetration depth (D) showed significant influence on the predicted residual stresses in both axial and tangential directions, as shown in Figure 5-15. For the residual stress at the depth of 0.2 mm from the surface, the maximum penetration depth (D) of 29 μm provided much higher compressive residual stresses than those used the depth of 20 μm (about 45% for axial and 49% for tangential residual stresses). Summary of residual stresses and comparisons with the experiments are given in Table 5-7. The maximum penetration depth of 29 μm (corresponding to the Method (4)) predicted the residual stresses in agreements with the experimental data, while the maximum penetration depth of 20 μm overestimated the residual stress up to

45%. Thus, it is more reasonable to employ either Method (4) or Method (5), which determined the corresponding maximum penetration depth of 29 μm and 28 μm respectively. For the solution of more realistic tool/workpiece contact of roller burnishing process, Method (5) that was previously described, was used in this study because it was based on 3D FEM solutions and reasonably represented 3D nature of practical roller burnishing process.

Process Parameters (P_b= 40 MPa; f_b=0.05 mm)						
	Max. penetration depth D=20 μm, Method (3)		Max. penetration depth D=29 μm, Method (4)		Experimental surface roughness	
Roughness parameters	R_z [μm]	R_a [μm]	R_z [μm]	R_a [μm]	R_z [μm]	R_a [μm]
	0.57	0.29	0.49	0.34	1.5	0.25
Error (%)	-62.13%	-16.13%	-67.47%	-35.95%	[−]	[−]

Table 5-6: Surface roughness parameters obtained from 2D simulations using different ball penetration depths and experimental surface roughness.

Process Parameters (P_b= 40 MPa; f_b=0.05 mm)						
	Max. penetration depth D=20 μm, Method (3)		Max. penetration depth D=29 μm, Method (4)		Experiment, measured at 0.2 mm depth	
Residual stresses	Axial stress σ_a [MPa]	Tangential stress σ_t [MPa]	Axial stress σ_a [MPa]	Tangential stress σ_t [MPa]	Axial stress σ_a [MPa]	Tangential stress σ_t [MPa]
	-703.69	-711.68	-1290.70	-1401.10	-1277.60	-1196.40
% Error	44.92%	40.51%	-1.03%	-17.11%	[−]	[−]

Table 5-7: Residual stresses obtained from 2D simulations using different maximum ball penetration depths and the experimental measurement.

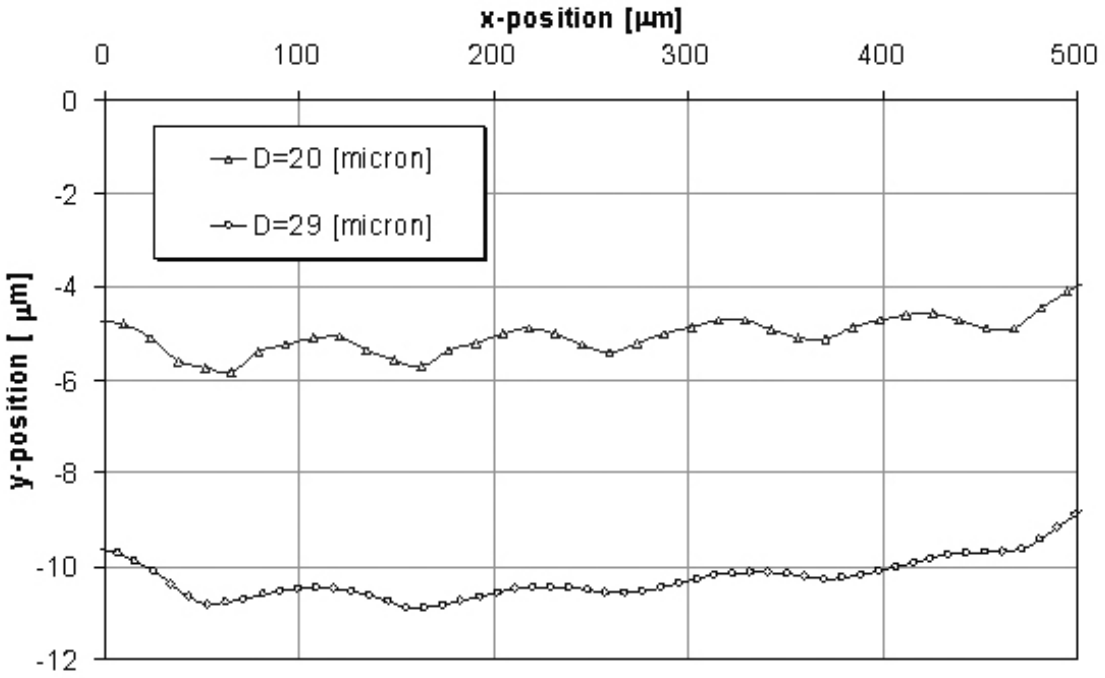

Figure 5-14: Surface roughness profiles predicted for two different maximum ball penetration depths.

(a)

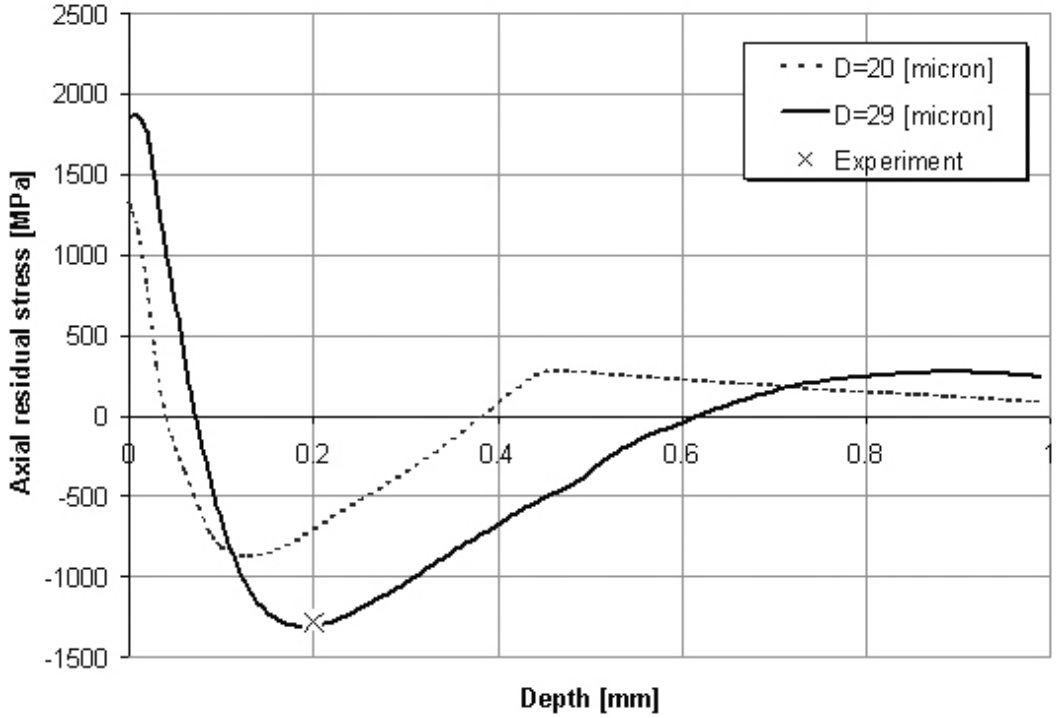

(b)

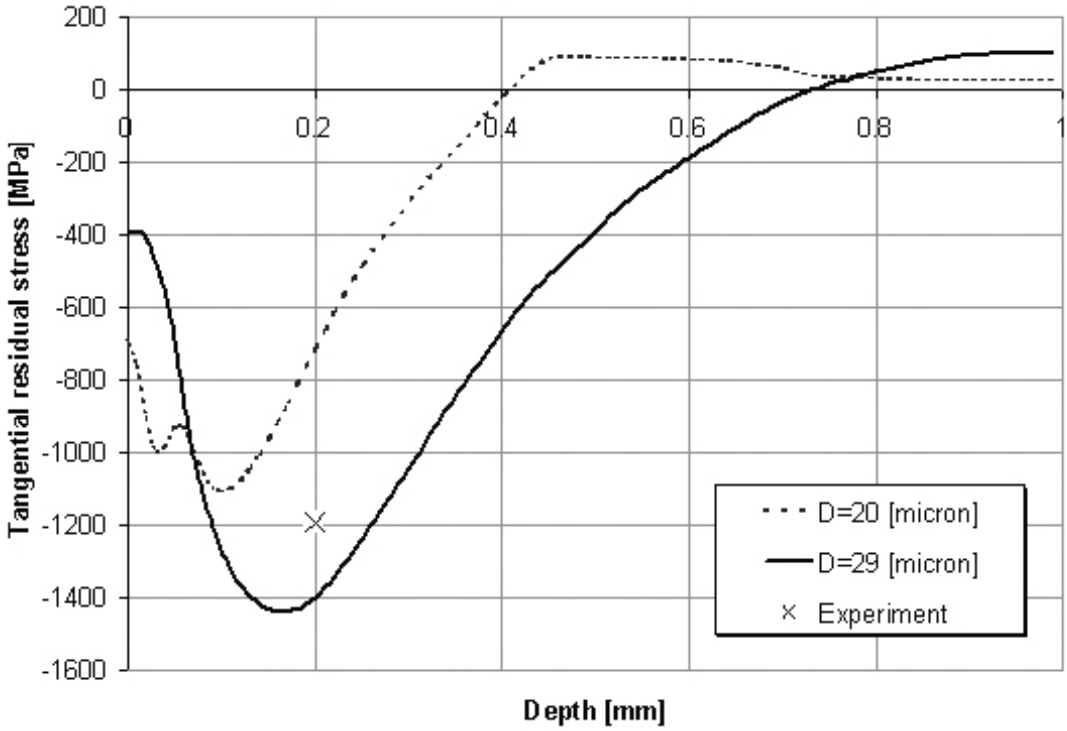

Figure 5-15: Residual stress distributions from the 2D simulations with different maximum penetration depth inputs, in comparison with experimental data. **(a)** Axial stress. **(b)** Tangential stress.

5.3.5 Evaluation of Tool Movement Control

2D roller burnishing simulations with feed effect can be conducted by using two different ball movement controls, i.e. *displacement control* and *force control* [Yen, 2004]. In the *displacement control*, the ball moves down and presses on the workpiece surface until reaching a maximum penetration depth for every indentation cycle. In the *force control*, the ball presses on the workpiece until reaching maximum applied load for every indentation cycle.

Two 2D roller burnishing simulations, using both tool movement control methods, were conducted for 11 indentation cycles (to consider the feed effect) in order to compare their surface finish results. The mesh and the size of the workpiece model are shown in Figure 5-16. A roller burnishing condition considered for these two simulations has P_b=40 MPa, f_b=0.05 mm/rev and d_b=6 mm whereas the initial surface roughness of the workpiece was considered from the experimental roughness measurements of the hard-turned surface.

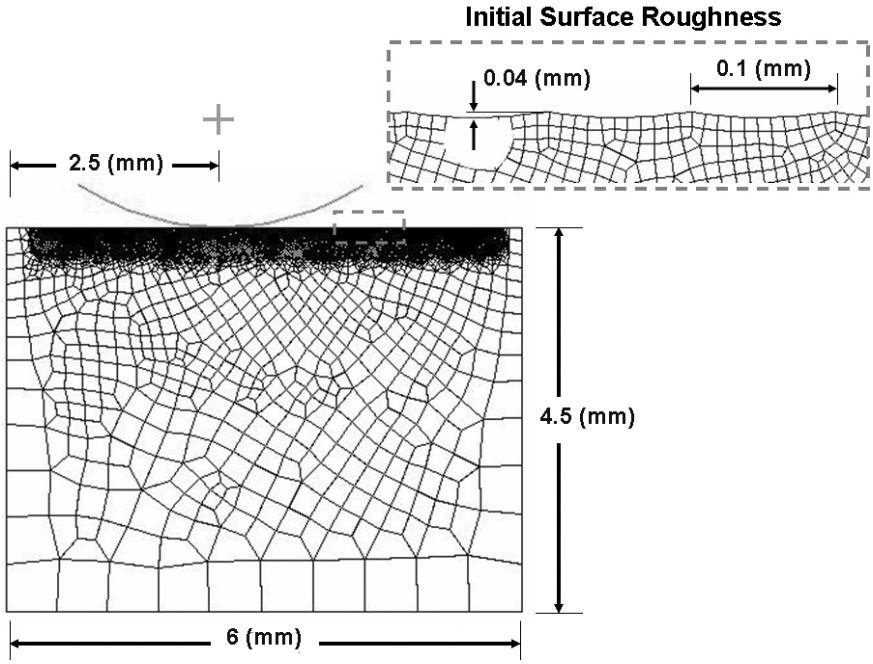

Figure 5-16: 2D FEM model used to conduct roller burnishing simulations with feed effect (ball diameter = 6 mm).

To evaluate and compare the ball movement control methods, both simulations were assumed to have the same first indentation cycle, which has identical maximum penetration depth and maximum load (as can be seen in Figure 5-17). For the next subsequent indentation cycles (the 2^{nd}, 3^{rd}, …. cycles), the ball indented into the workpiece for the same maximum penetration depth as of the first cycle for the *displacement control* while the ball indented to reach the same maximum load as that of the first cycle for the *force control*.

Surface roughness results predicted by both methods are shown in Figure 5-18. Simulation using force control shows more deformation of the workpiece surface than the displacement control. This phenomenon can be explained by the load-stroke curve presented in Figure 5-17. From the load-stroke curves of the force control, the values of the maximum penetration depths increase for the successive cycles, i.e. the 2^{nd}, 3^{rd} and 4^{th} cycles. As the maximum force maintains constant and there is less material to be deformed for the successive indentation cycle (due to material loss during previous indentation, as can be seen in Figure 5-19), the maximum ball penetration depth increases.

If the displacement control is used, the burnishing force decreases for successive simulation cycles (the 2^{nd}, 3^{rd} and 4^{th} cycles), as shown in Figure 5-17. It can be observed in Figure 5-19 that there is a gap between the tool and the workpiece once the first indentation has been completed and the tool starts the second indentation cycle. This means in the second cycle there is a certain distance that the tool travels without touching the workpiece surface. Therefore, the burnishing force decreases.

As previously presented in Section 5.3.4, the simulation results showed that displacement control method (for the input maximum penetration depth of 29 μm) underestimates the surface finish, of about 67% lower than the experiment. However, with force control method, simulation will produce much lower surface roughness compared with those of the experiments and the displacement control method. In addition, as previously mentioned, the predictions of residual stresses are highly sensitive to the maximum penetration depth. This depth value obtained

by using the force control method during successive indentations may exceed the initial depth of the first indentation significantly and underestimate the residual stresses.

Therefore, displacement control was used for 2D roller burnishing simulations to study the effect of process parameters upon surface roughness and residual stresses (in CHAPTER 6).

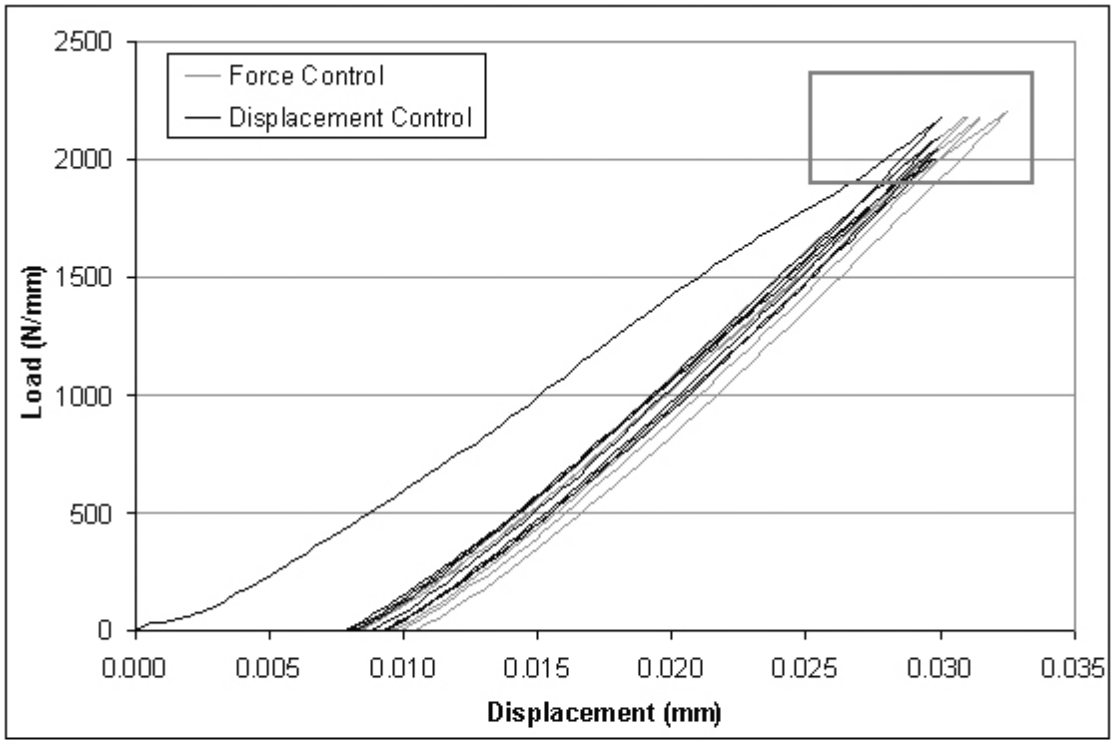

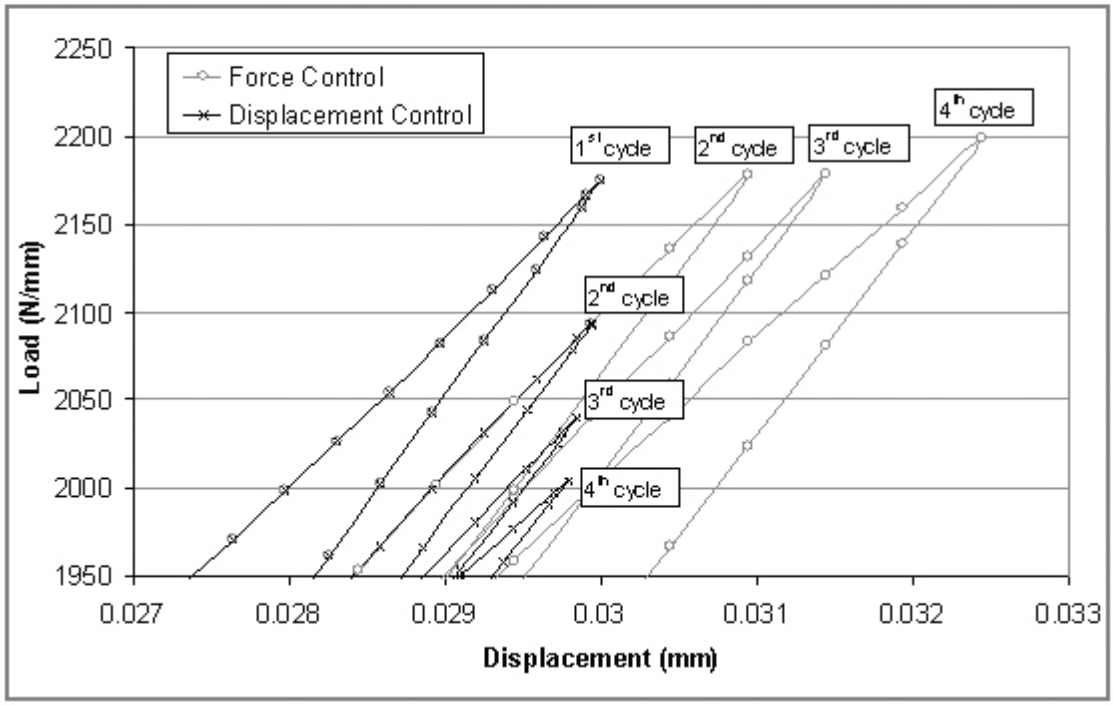

Figure 5-17: Load-displacement curves from 2D roller burnishing simulations using displacement and force control methods.

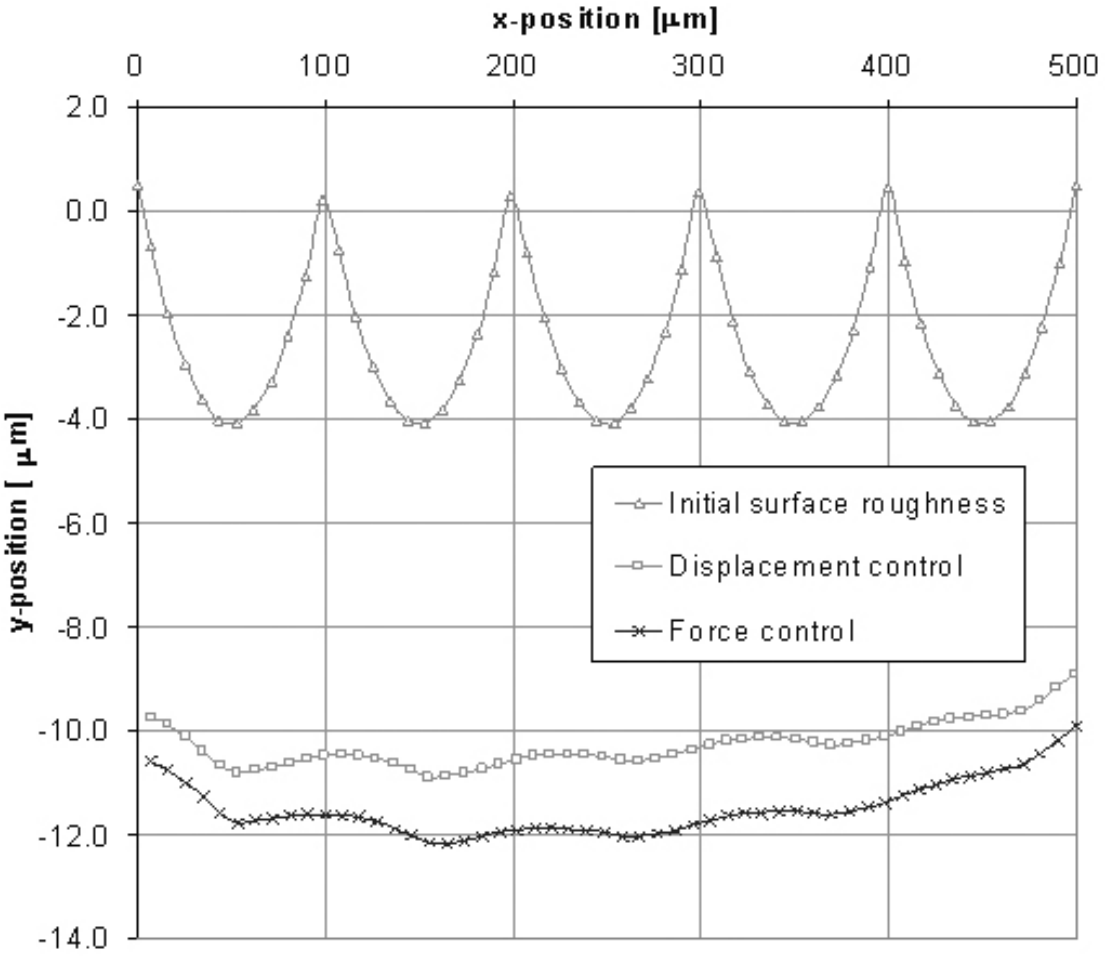

Figure 5-18: Comparison between surface finish predicted by 2D simulations when using displacement and force control.

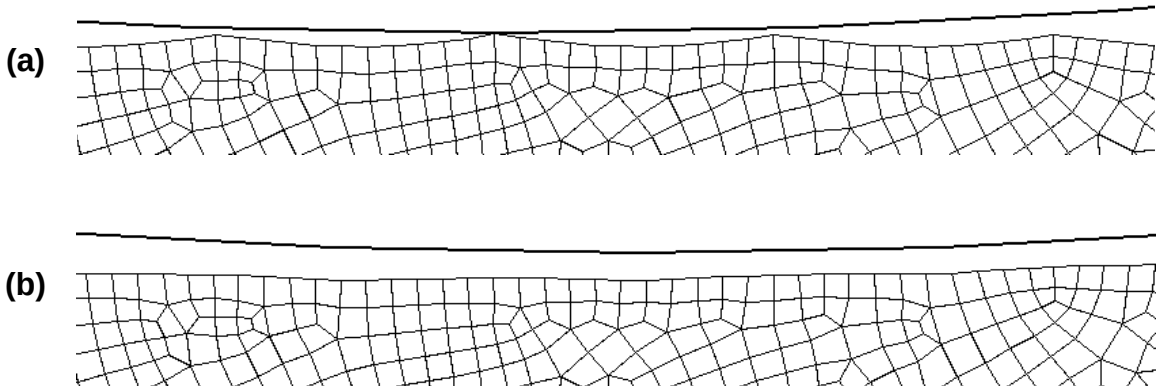

Figure 5-19: Comparison of the surface roughness profiles: **a)** at the start of the 1st indentation cycle (initial roughness) and **b)** at the start of the 2nd indentation cycle.

CHAPTER 6
ESTIMATED EFFECT OF PROCESS PARAMETERS ON BURNISHED SURFACES AND COMPARISON WITH EXPERIMENTAL RESULTS

Process parameters that have the most important influence on surface quality after roller burnishing are burnishing pressure (P_b) and burnishing feed (f_b) [Klocke, 1998; Röttger, 2002 and Luca, 2005]. In this chapter, the effects of these parameters on surface roughness and residual stresses were analyzed by using 2D FEM model of roller burnishing, previously described in CHAPTER 5. A number of burnishing conditions were selected from [Sartkulvanich, 2004b] for the analysis, as shown in Table 6-1. The effect of burnishing feed was simulated by setting the burnishing pressure to 40 MPa (corresponding to the maximum ball penetration depth (D) of 0.028 mm) while changing only the burnishing feeds. These are indicated as Simulation #1 to #4 in Table 6-1. On the other hand, the effects of burnishing pressures were analyzed by setting the burnishing feed to 0.05 mm/rev and changing the burnishing pressures (in Simulation #2, #5 and #6 in Table 6-1).

Run #	**Burnishing conditions considered during FE simulations** **Ball diameter, d_b = 6 (mm), Tool contact angle = 15 degree**		
	Burnishing feed (f_b) [mm/rev]	Burnishing pressure (P_b) [MPa]	Corresponding maximum ball penetration depth (D) [mm]
1	0.02	40	0.028
2	0.05	40	0.028
3	0.08	40	0.028
4	0.11	40	0.028
5	0.05	36	0.025
6	0.05	32	0.022

Table 6-1: Process parameters considered in FEM roller burnishing simulations to study their effects upon surface roughness and residual stresses.

It was discussed in CHAPTER 5 that displacement control method produced more reliable results than the force control method. Therefore, it was used for the 2D FEM simulation. The use of the displacement control method requires the accurate determination of the maximum ball penetration depth (D), which can be calculated by several methods (as discussed in Section 5.3.4). According to the comparison of the predicted surface qualities obtained from different methods and the consideration of the realistic tool/workpiece contact in roller burnishing, it was decided to use 3D roller burnishing model to calculate the maximum ball penetration depth. Figure 5-12 is the burnishing force vs. maximum ball penetration depth curve from 3D roller burnishing simulation. It was used to determine the maximum penetration depths for the given burnishing pressures.

6.1 Extraction of Surface Properties Data from 2D FEM Simulation of Roller Burnishing

6.1.1 Surface Roughness

The deformed workpiece after burnishing can be extracted from simulation database file by using the DEFORM^{TM}-2D pre-processor. Workpiece geometry was exported as a tabulated set of (x,y) coordinates of the boundary nodes. The node coordinates where the surface was indented by the ball tool (hereafter, referred to as the *burnished zone*) were zoomed in and plotted as shown in Figure 6-1. Typical standard parameters used to describe the surface topography are the mean roughness (R_a) and the roughness depth (R_z). Their formulae are shown in APPENDIX A. A MAPLE code was created in order to read node coordinate data and calculate the integration function for the mean roughness (R_a). This code is also presented in APPENDIX A. Roughness depth (R_z) was calculated in MS-EXCEL by taking an average of “maximum y – minimum y” for every interval of 0.1 mm of the burnished surface profile.

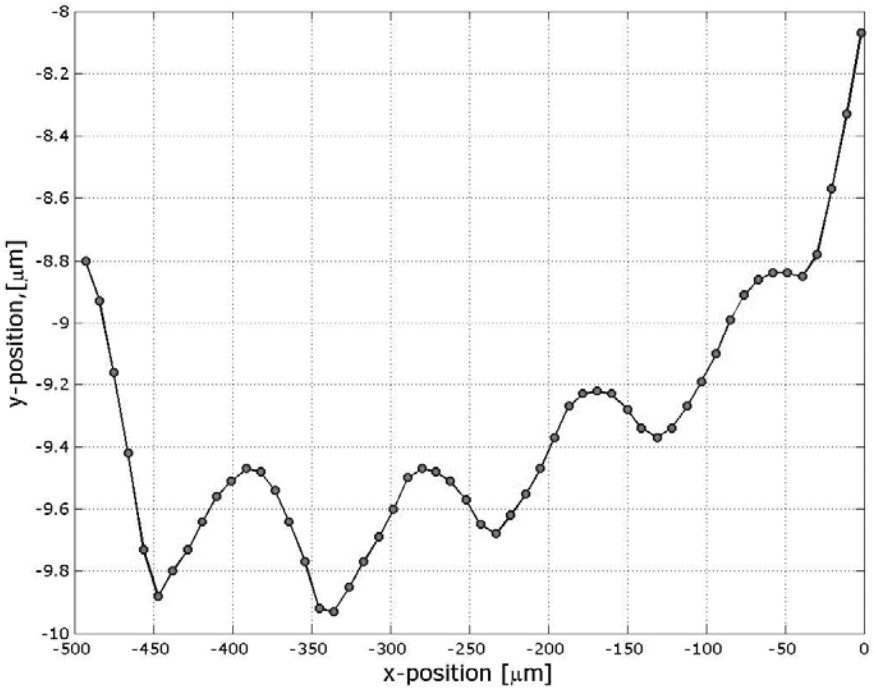

Figure 6-1: Workpiece's surface roughness profile extracted from a simulation database using the DEFORM^{TM}-2D pre-processor. The result shown was obtained for the following combination of process parameters: P_b= 40 MPa; f_b=0.05 mm/rev and d_b=6 mm.

6.1.2 Residual Stresses

The effective stress contour diagram shows that high effective residual stresses predicted by 2D FEM simulations mostly locate in the local areas beneath the roughness peaks (see Figure 6-2). This means that there is a large variation of the stress from the peak to the valley positions of the surface profile. However, it can be observed in Figure 6-2 that the same residual stress pattern is repeatedly present in every peak of the burnished zone. In order to obtain a reasonable representative residual stress distribution from the 2D simulation, the values of residual stresses were obtained by taking an average of residual stresses at the center of the burnished zone from the DEFORM^{TM}-2D simulation database.

Axial and tangential residual stresses can be measured experimentally by using the X-ray diffraction technique (Section 4.4.2). This technique exploits the fact

that when a metal is under stress (applied or residual) the resulting elastic strains cause the atomic planes in the metallic crystal structure to change their spacing [Al-Zkeri, 2005]. The method is based on the emission of X-rays through bombarding target surfaces made of materials such as Copper, Chromium and Molybdenum with electrons, A and D in Figure 6-3. These rays of electrons impact the surface where the residual stresses are being measured at an angle θ and penetrate to a very thin surface layer (typically tens of μms), depending on their frequency. The rays interact with the crystallites on the sample surface and then leave the surface at the same angle θ, FH and BC in Figure 6-3 [Al-Zkeri, 2005]. X-ray diffraction has a spatial resolution of 1-2 mm down to tens of μm and a penetration depth of around 10-30 μm, depending on the material and source.

Since residual stresses measurements with X-ray diffraction were conducted on the burnished surfaces at unknown positions (i.e. peak, valley or between them), the variations of residual stresses from peak to valley in an FEM simulation were considered by taking an average of the residual stresses. As illustrated in Figure 6-2, the residual stress distributions over the depth were obtained for points 1, 2, 3, 4 and 5 of the surface peak at the middle of the burnished zone. The average residual stresses were taken from the stress data of these five points. Stresses in x-direction represent axial stress while stresses in z-direction represent tangential residual stress for the 2D plane strain model used for FEM roller burnishing simulations. Residual stresses in y-direction are small and negligible. The averaged residual stress distributions (i.e. axial and tangential stresses) from 2D FEM simulation are plotted and compared with those of five zones (i.e. at points 1, 2, 3, 4 and 5) in Figure 6-4. Later in Sections 6.2.2 and 6.3.2 of this chapter, experimental measurements of residual stresses will be compared with these average values extracted from 2D roller burnishing simulations.

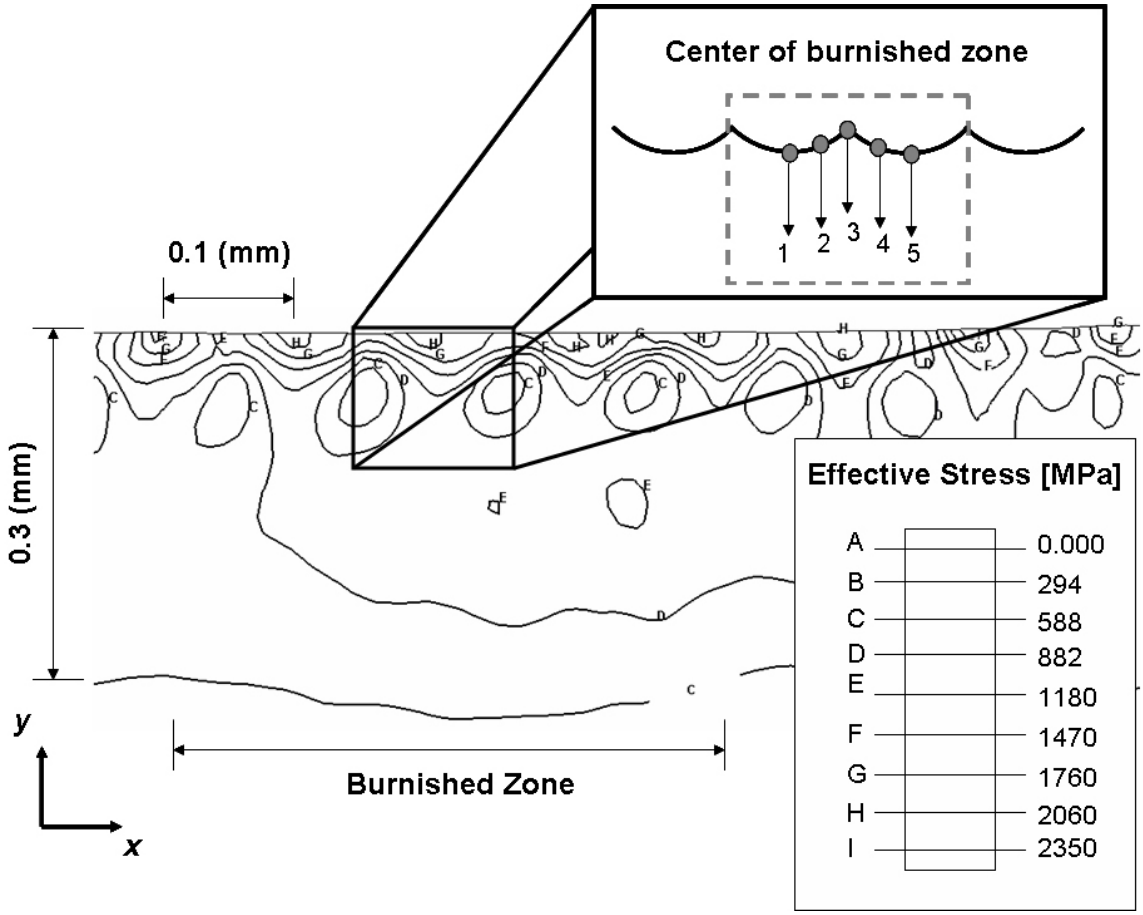

Figure 6-2: Illustration for residual stress data extracted from the 2D FEM roller burnishing simulations. Stress units are in MPa.

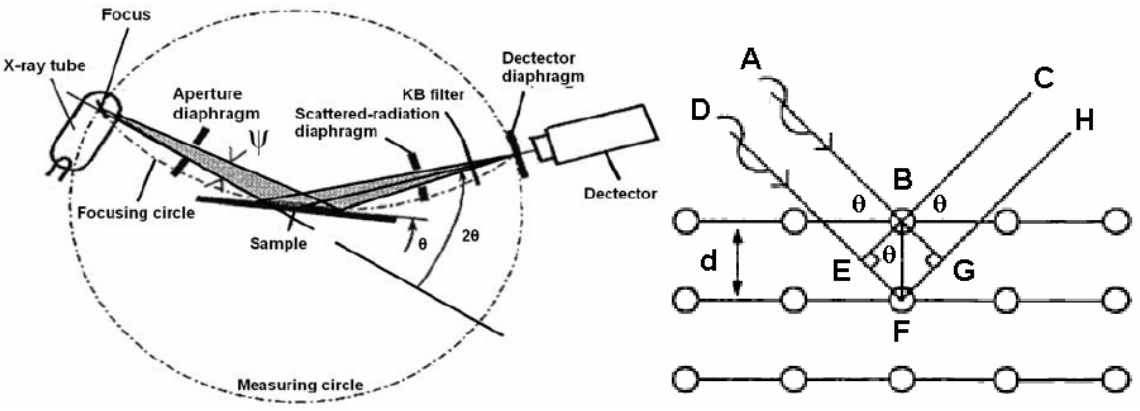

Figure 6-3: Diffraction of X-ray by a crystalline material [Al-Zkeri, 2005].

(a)

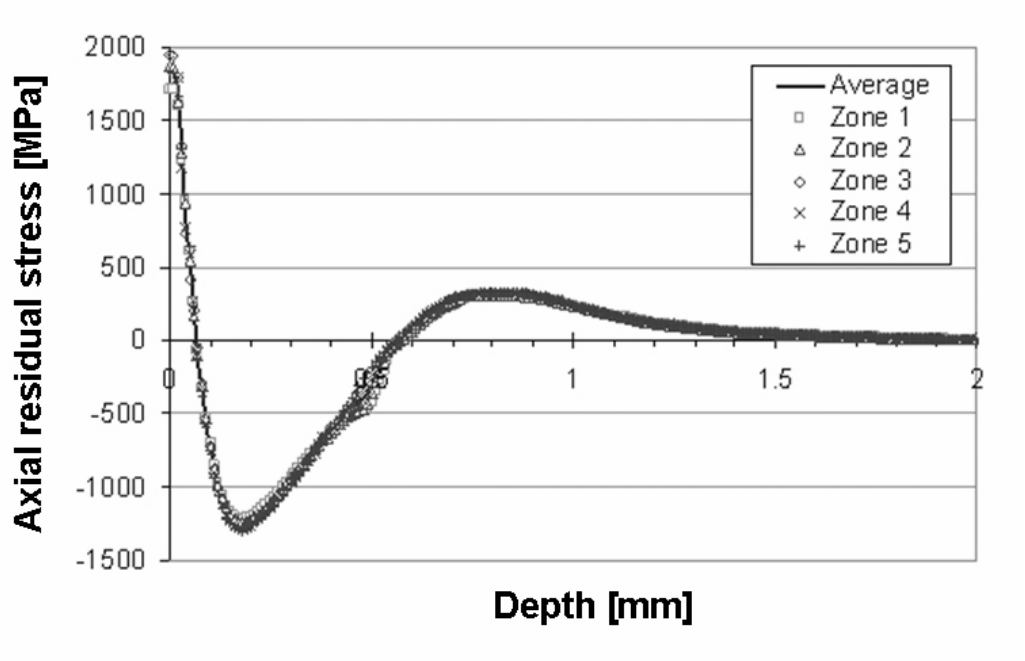

(b)

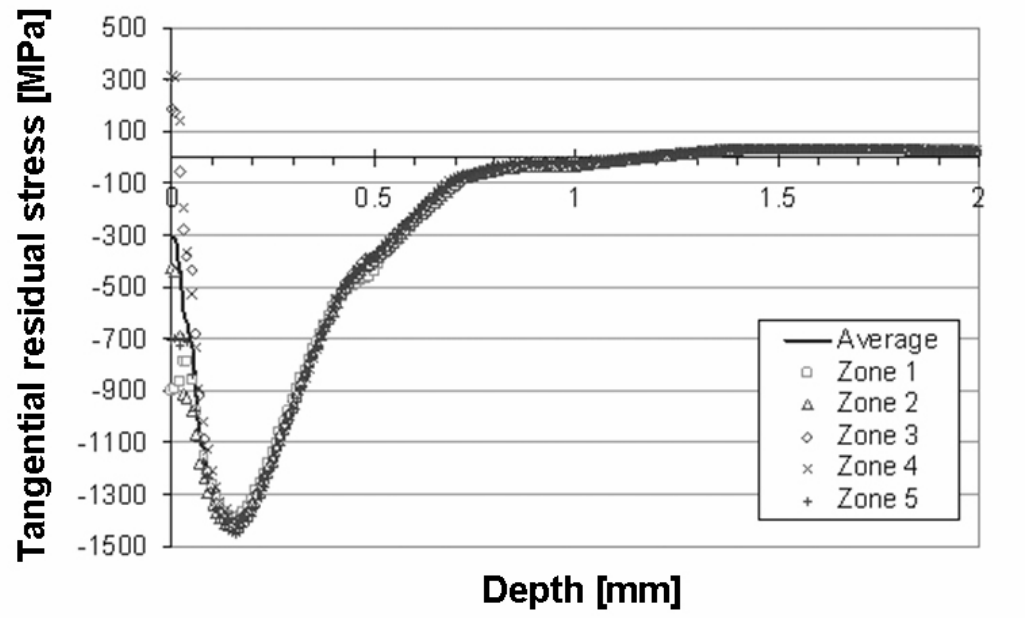

Figure 6-4: Comparison between the residual stress distributions calculated in the different zones defined in Figure 6-2. (a) Axial stress. (b) Tangential stress. The result shown was obtained for the following combination of process parameters: P_b = 40 MPa; f_b = 0.05 mm/rev; d_b = 6 mm.

6.2 Effects of Burnishing Feed (f_b) on Surface Properties

6.2.1 Surface Roughness

Figure 6-5 shows the comparison between the variations of surface roughness parameters R_a and R_z predicted by 2D FEM simulations and experimental results in [Sartkulvanich, 2004b] for different feed values (f_b) but at the same burnishing pressure (P_b = 40 MPa). It should be noticed in this figure that as burnishing feed increases, mean roughness (R_a) also increases. This is due to the fact that the distance between successive burnishing ball traces increases with the burnishing feed and thus there is less chance for the ball to smooth out all the edges of the irregularities [Némat, 2000 and Bouzid, 2004].

The problem of using a burnishing feed of 0.11 mm/rev is that this value is almost equal to the cutting feed (f_c) of 0.1 mm/rev (see Table 4-4). According to roller burnishing experiments presented in [Klocke, 1998], if the same feed rate is used for hard turning and roller burnishing, the tool's rolling motion can be parallel to the feed grooves of the hard turned surface and hence burnishing ball will not be able to flatten the surface ridges [Klocke, 1998]. On the other hand, if a very small burnishing feed is used (i.e., 0.02 mm/rev), the tool has more chances to flatten the surface peaks and to produce a greater amount of plastic deformation on the workpiece surface due to the overlapping of successive ball traces.

The variation of surface roughness parameters (R_z and R_a) provided by 2D FEM simulations showed the same trend as experimental results from [Sartkulvanich, 2004], as shown in Figure 6-5. However, simulation predictions for surface roughness showed reasonable agreement only for the mean roughness (R_a) but significant difference for the roughness depth (R_z). This difference may be due to the combination of several factors, i.e. 1) the numerical error produced during FEM calculations, 2) the plane strain assumption (whereas roller burnishing process is a 3-D process in nature), 3) the fact that FEM cannot consider the influence of stiffness and dynamic of machine tools and workpiece-setups (i.e. chatter can occur in real process and is not being considered), and 4) the smallest element size on the workpiece's meshes was 8 μm (located at the

tool/workpiece contact interface) while the roughness amplitude of the burnished surface was about 1 μm.

For existing computational capability, it is not practical to reduce the element size down to 1 μm since the number of mesh elements will increase considerably and may take several weeks to complete one simulation. 2D FEM simulations provided only qualitative results for the effects on surface roughness parameters, especially for the mean roughness (which is most commonly used). Increasing burnishing feed causes higher surface roughness, which was in agreement with the observation taken by several experimental studies [Klocke, 1998; Némat, 2000; Sartkulvanich, 2004b and Luca, 2005].

6.2.2 Residual stresses

Comparing to grinding or honing operations, roller burnishing is dominant for its ability to produce compressive residual stresses to the machined surface [Klocke, 1998; Némat, 2000; Bouzid, 2004 and Yen, 2004]. In order to predict the residual stresses (stresses in the workpiece after external force has been removed), roller burnishing simulations were conducted considering an elastic-plastic workpiece.

According to FEM simulations results, as shown in Figure 6-6, decrease in burnishing feed raises the magnitude of the compressive residual stresses. This can be explained by the fact that small feed indicates shorter distance between ball traces. As a result, the workpiece surface is subjected to greater amount of plastic deformation and residual stresses due to more repetitive compression by the ball tool.

Figure 6-6(a) shows the distributions of the axial residual stress after roller burnishing predicted by 2D FEM simulations. It should be noted that as burnishing feed was increased, the magnitude of compressive residual stresses beneath the machined surface slightly decreased. This trend can be observed

also for experimental values shown in the same figure since residual stresses for f_b=0.02 mm/rev are more compressive than those measured for f_b=0.05 mm/rev. Magnitudes of FEM predictions for axial residual stress were in good agreement with experimental measurements, especially for depths greater than 0.05 mm but not at smaller depth values or at the workpiece surface (see Figure 6-7 which shows the deviation of FEM predicted residual stresses from experimental values).

The inconsistency before mentioned could be due to a combination of several factors as those discussed in Section 6.2.1 for surface roughness. Additionally, experimental axial residual stresses produced by hard turning (see Figure 4-4) were not considered for 2D FEM simulations because they were initially unknown (all X-ray diffraction measurements were conducted after machined surfaces were burnished). The inclusion of this data into the workpiece mesh before running roller burnishing simulations could lead to an increase of accuracy for the FEM simulation model as discussed in [Zhuang, 2004].

Figure 6-6(b) shows the distribution of the tangential residual stress after roller burnishing. A similar trend with the axial residual stress results was observed, where the magnitude of tangential compressive stress decreases for increasing burnishing feed. Simulations show greater influence of burnishing feed on tangential residual stresses (i.e. more variation of residual stresses in tangential direction due to change in burnishing feed). The feed effects on residual stresses are consistent with experimental observations except at the surface as in the case of axial residual stresses. However, FEM predictions for tangential residual stress presented more accuracy than those obtained for axial stress compared to experimental values (see Figure 6-6(b) and Figure 6-7).

(a)

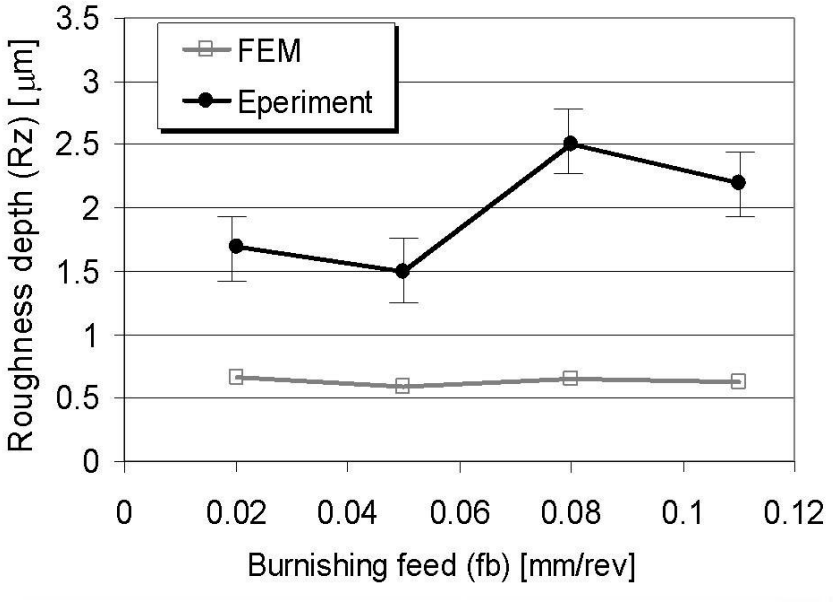

(b)

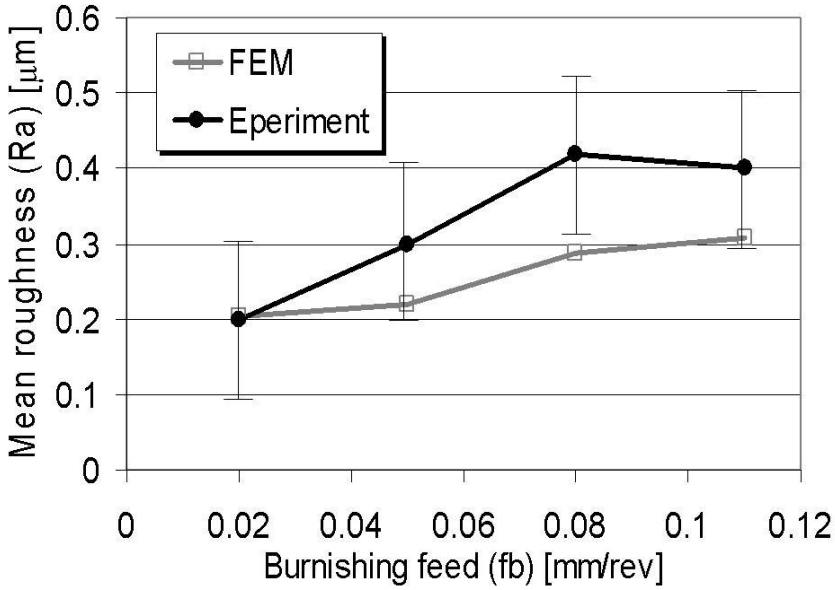

Figure 6-5: Effect of the burnishing feed on surface roughness. A comparison between experimental measurements and FEM predicted results using the 2D simplified model is shown. **(a)** Roughness depth (R_z). **(b)** Mean roughness (R_a).

(a)

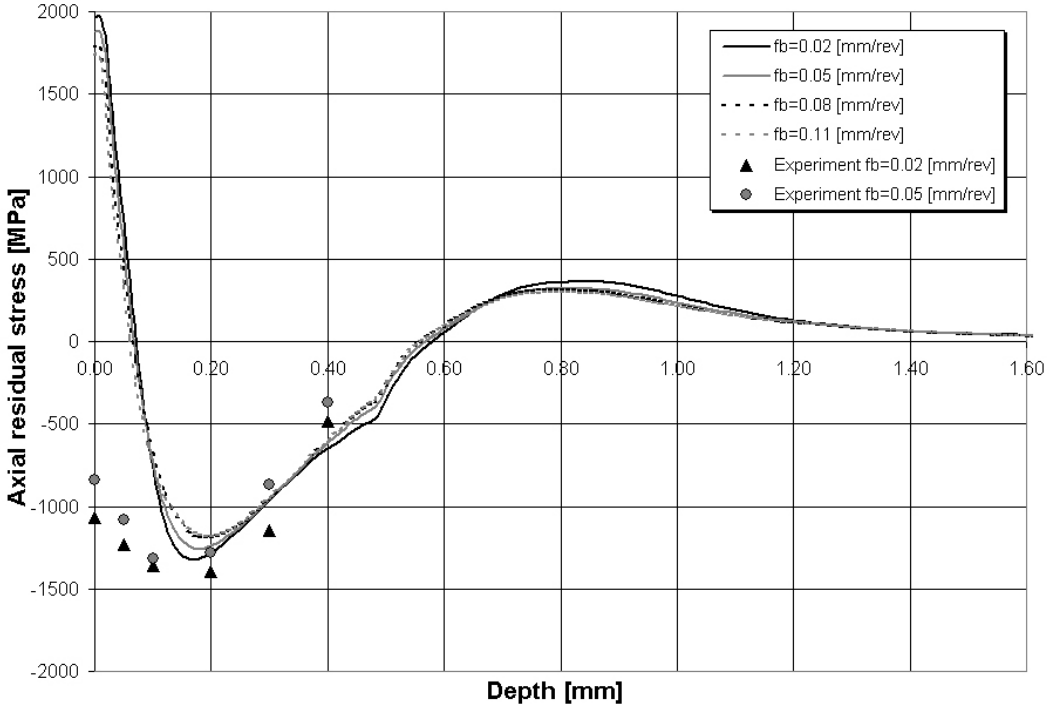

(b)

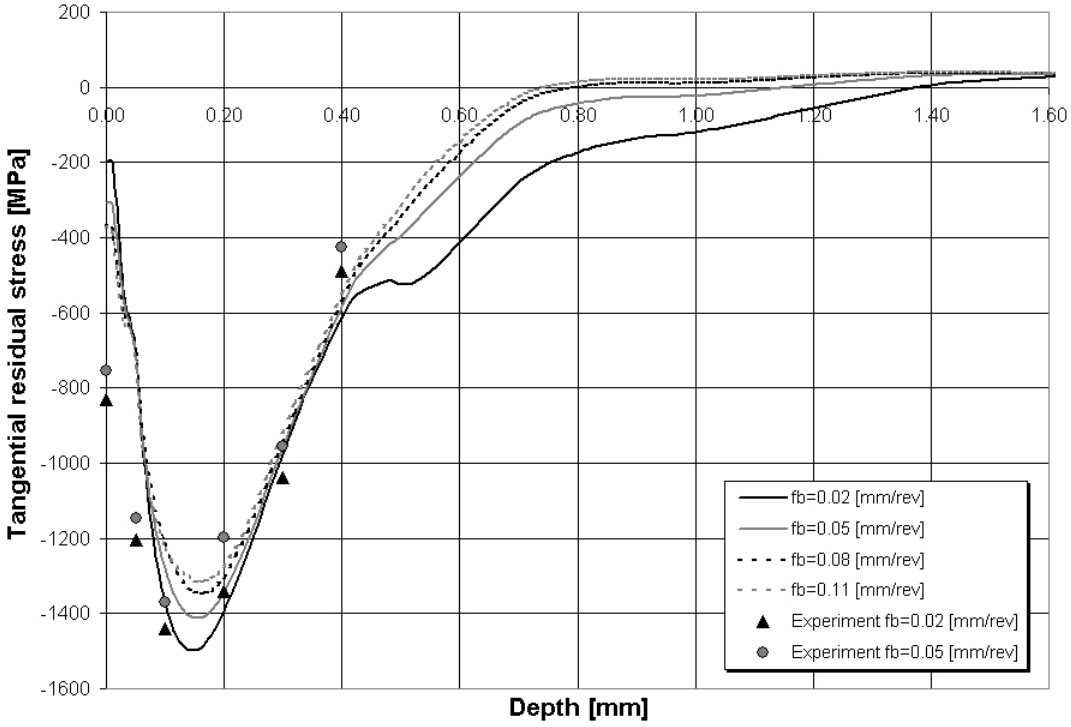

Figure 6-6: Effects of the burnishing feeds (f_b) on the residual stress distributions beneath the burnished surfaces. **(a)** Axial stresses and **(b)** Tangential stresses.

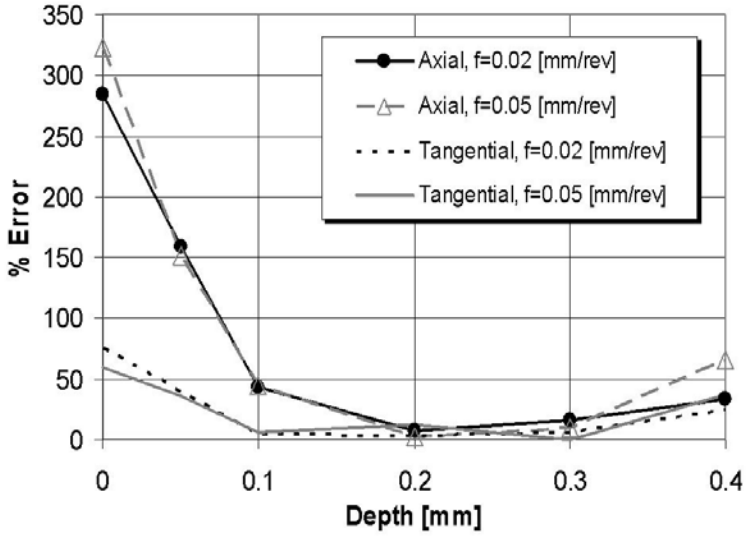

Figure 6-7: Deviation of FEM predicted residual stresses from experimental measurements values. Error is more significative at the surface in the case of axial residual stress.

6.3 Effects of Burnishing Pressure (P_b) on Surface Properties

It was observed in Section 6.2 that the effects of burnishing feed (f_b) upon surface qualities are very small, especially for residual stresses (see Figure 6-6). On the other hand, several studies showed that burnishing pressure (P_b) has the most significant effect on the burnished surface [Röttger, 2002 and Luca, 2005]. The effects of burnishing pressures were analyzed by conducting 2D simulations that assume fixed burnishing feed of 0.05 mm/rev and change only the burnishing pressures (i.e. 32, 36 and 40 MPa).

6.3.1 Surface Roughness

The effects of burnishing pressure on surface roughness are shown in Figure 6-8. The value of roughness depth (R_z) predicted by FEM simulation decreases as the burnishing pressure increases from 32 to 36 MPa. However, further increase in the burnishing pressure up to 40 MPa produces a higher roughness depth which means that the optimum pressure value for the best surface finish is

between 32 and 40 MPa (see Figure 6-8(a)). Surface finish predictions by FEM simulations have the same trend over different burnishing pressure as those of experiments in [Sartkulvanich, 2004b] but show difference in the values of surface roughness parameters. Only qualitative results can be provided by FEM simulations. The quantitative differences between FEM simulation and experimental surface roughness are due to the combination of several factors as those discussed on Section 6.2.1.

The values of mean roughness (R_a) predicted by FEM simulations reasonably agreed with the experimental results. FEM simulations showed that the mean roughness decreased when higher burnishing pressure was used. However, unlike the experimental observations, FEM simulations did not show the trend that there was almost no improvement of surface finish when using burnishing pressure higher than 36 MPa.

6.3.2 Residual stresses

Figure 6-9 shows the distribution of the residual stresses when using the same burnishing feed and increasing the value of the burnishing pressure. The increase of burnishing force (or pressure) leads to an increase in the amount of plastic deformation and to more roughness voids being filled during the process. This leads to an increase in the compressive stresses applied to the surface, which in turn increase the surface hardness and compressive residual stresses as observed in [Némat, 2000 and Sartkulvanich, 2004b]. In addition, higher applied burnishing pressure tended to move the location of maximum compressive residual stresses deeper into the surface (at about 0.12 mm for P_b = 32 MPa and at 0.2 mm for P_b = 36 MPa in Figure 6-9(a)).

FEM predictions for axial and tangential residual stresses are in reasonable agreement with experimental measurements at different depth values beneath the burnished surface (see Figure 6-9) but not at the surface (see Figure 6-10). It is necessary to modify the proposed simulation model so that experimental

measurements of residual stresses produced during hard turning could be attached into the workpiece mesh before running a burnishing simulation. As mentioned before, this could lead to an increase in accuracy for the FEM simulation model and this approach should be investigated [Zhuang, 2004].

(a)

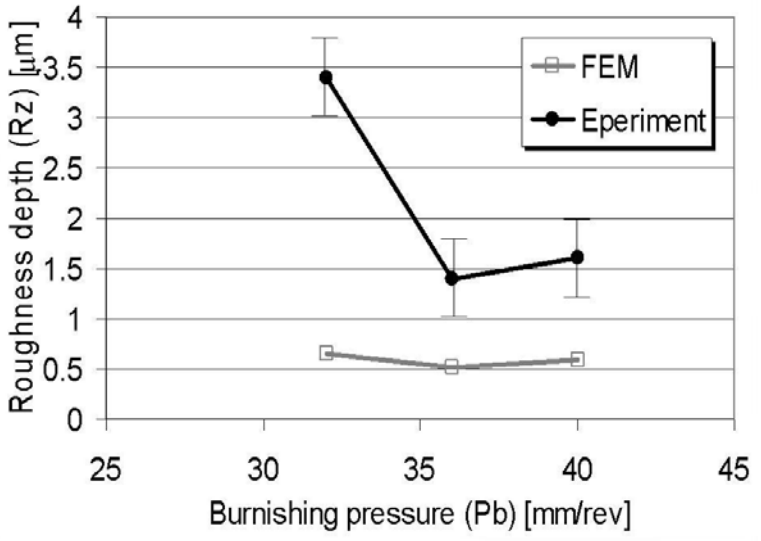

(b)

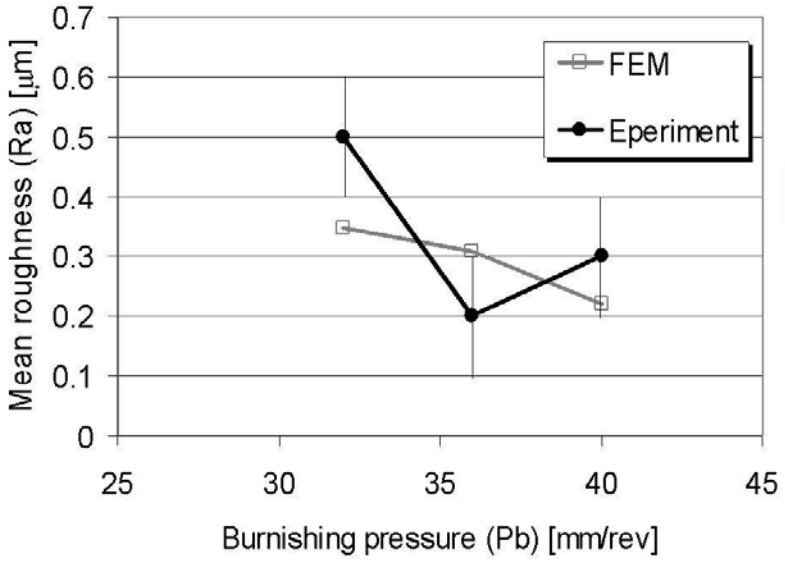

Figure 6-8: Effects of the burnishing pressures on surface roughness. A comparison between experimental measurements and FEM predicted results by using the 2D simplified model. **(a)** Roughness depth (R_z). **(b)** Mean roughness (R_a).

(a)

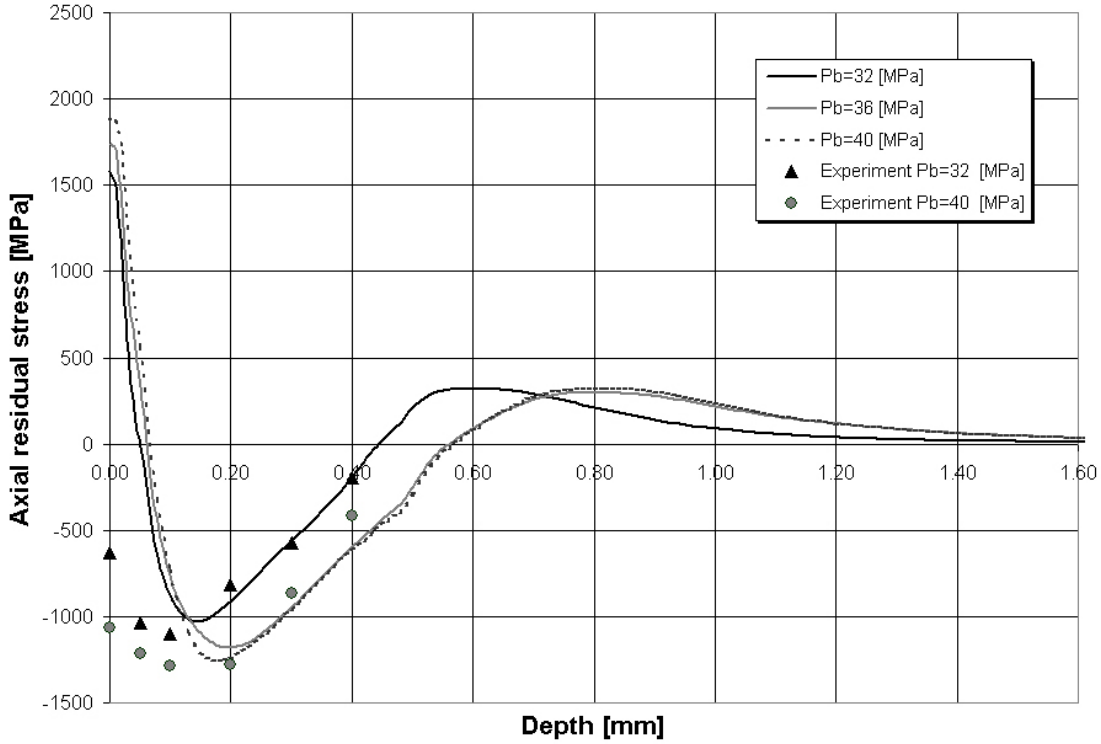

(b)

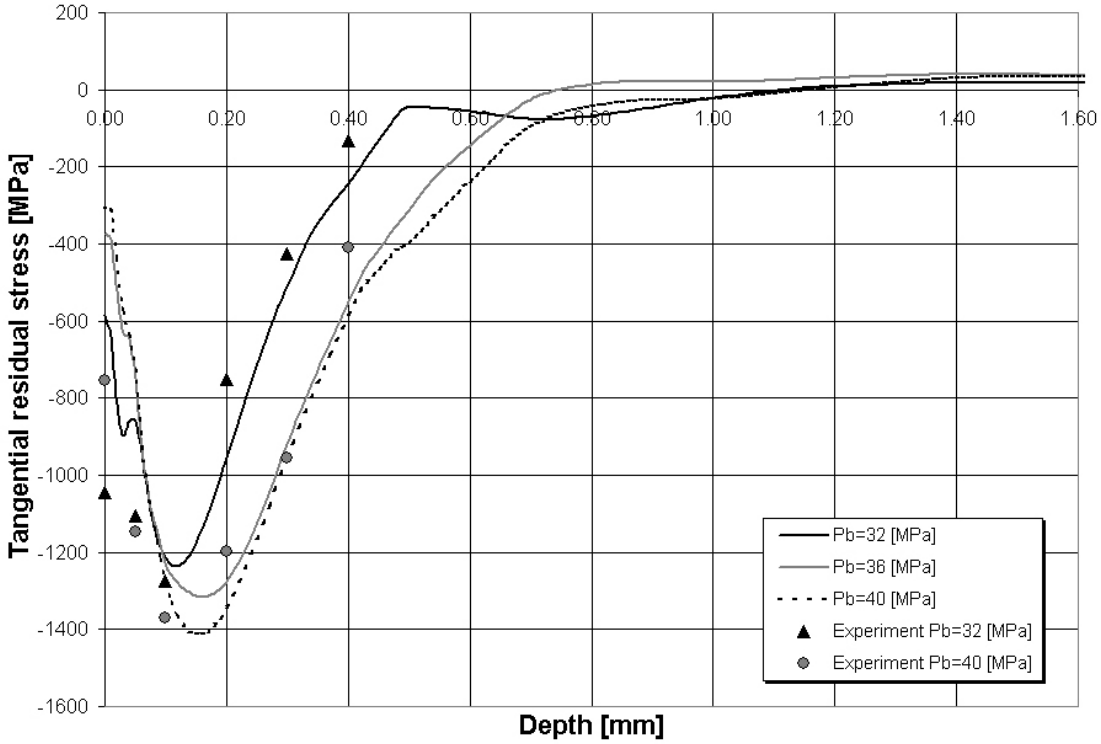

Figure 6-9: Effects of the burnishing pressures (P_b) on the residual stress distribution beneath the burnished surface. **(a)** Axial stress. **(b)** Tangential stress.

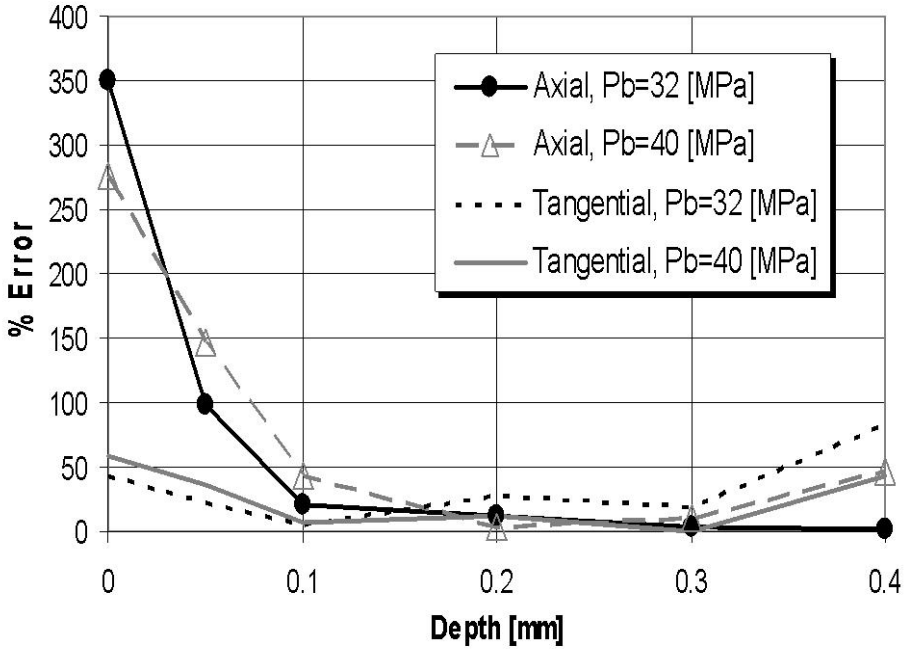

Figure 6-10: Deviation of FEM predicted residual stresses from experimental measurements values. Error is more significative at the surface in the case of axial residual stress.

CHAPTER 7
CONCLUSIONS, FUTURE WORK AND CONTRIBUTIONS

7.1 Conclusions

The conclusions of this research can be summarized as follows:

7.1.1 Surface roughness

1) As burnishing feed (f_b) increases, surface roughness will also increase (see Figure 6-5). If a very high feed value is used, the tool has less chance to flatten the roughness peaks as observed for the feed of 0.11 mm/rev. In this case, the burnishing feed is almost "parallel" to the turning feed (f_c=0.1 mm/rev) and most likely not rolls on the roughness ridges.

2) FEM simulations and experimental measurements for roughness depth (R_z) and mean roughness (R_a) showed the same trend but difference in magnitudes. This is due to numerical errors, the assumptions 2D plane strain, the fact that FEM simulation cannot consider the dynamic of machine tool and workpiece interaction (possible chatter), and the defined element size of the workpiece surface that is relatively larger than the original roughness surface.

3) Burnishing pressure has the most important effect in surface roughness. Both FEM and experiments show the same trend that the higher burnishing pressure produces better surface finish. However, FEM cannot observe the limit at which surface roughness did not decrease after increasing burnishing pressure to a certain value (as shown in Figure 6-8). Similar reasons to those of 2) may explain this inconsistency.

7.1.2 Residual stresses

1) Residual stresses are slightly influenced by the burnishing feed at very high pressures of 40 MPa (see Figure 6-6). Increasing burnishing feed causes slight decrease in residual stresses. Experimental residual stresses at a depth greater than 0.05 mm beneath the burnished surface were in good agreement with FEM simulation predictions; however, residual stresses at the surface or depths lower than 0.05 were not in agreement with experiments, especially for the axial residual stress (see Figure 6-7 and Figure 6-10). Axial residual stress is supposed to be compressive as the trends shown in Figure 6-6 and Figure 6-9 for experimental measurements.

2) Burnishing pressure is the process parameter that has the most important influence on residual stresses. As burnishing pressure increases, the amount of plastic deformation in the workpiece increases and hence the magnitude of compressive residual stresses. Experimental results and FEM predictions for the residual stresses at different burnishing pressures were also in agreement for the depths greater than 0.05 mm beneath the workpiece surface (see Figure 6-9). However, as discussed before, residual stresses at the surface are not accurate enough when compared to experimental measurements (see Figure 6-10).

7.2 Contributions

The main contributions that result from this research are listed below:

1) Improvement of an existing 2D FEM simulation model for roller burnishing developed by Yen [Yen, 2004]. This modifies model is able to predict the surface properties of burnished components with a reasonable accuracy (as discussed in CHAPTER 6). Moreover, this tool was found to be not only reliable but also efficient in terms of the computational resources

needed for its use (2D roller burnishing simulations required only some computation hours instead of days, which are required for 3D roller burnishing simulations).

2) As a consequence of 1), it was possible to have a *virtual manufacturing laboratory* which allowed an analysis on the effect of process parameters (i.e., burnishing feed and pressure) upon surface properties (i.e., surface roughness and residual stresses). To date, there is not any published study based on FEM simulations in which the effect of roller burnishing parameters on surface properties is investigated. As a result, 2D simulation model used throughout this research can provide an advancement in the fundamental understanding of the roller burnishing mechanics since it was observed to have a good agreement with experimental results published in literature [Klocke, 1998; Röttger, 2002 and Sartkulvanich, 2004b].

3) Development of a methodology to consider the effect of residual stresses produced during hard turning on the results predicted by the 2D FEM simulation model. This methodology is based in the attachment of the experimental residual stress values into the workpiece mesh before running a roller burnishing simulation (See APPENDIX D for details).

The achievement of general contributions discussed above was possible by performing the following tasks:

- The existing 2D FEM model (developed at the ERC/NSM by Yen [Yen, 2004]) was modified as discussed in CHAPTER 5. Major changes include:

  1) The use of the constitutive equation (for AISI 52100 hard turned surface) obtained from ball indentation tests presented in [Morris, 2005]. This approach made possible to consider the difference between the bulk material condition and the condition after hard turning. The reasons for such a difference are related mainly to large plastic deformations and possible phase transformations (due to the

high temperatures reached because of the chip/tool friction) generated during hard turning as observed by several researchers [Thiele, 1999; Liu, 2004; Dahlman, 2004; Ramesh, 2004 and Morris, 2005].

2) The consideration of pressure loss during roller burnishing operations also influenced the FEM predicted results (as discussed in CHAPTER 6).

- It was proposed a methodology for finding the optimum workpiece size for roller burnishing simulations in order to minimize the effects of the boundary constraints on the predicted surface roughness and residual stresses. For the material studied (AISI 52100 bearing steel) and process parameters selected in this research (especially the maximum burnishing pressure value of 40 MPa), it was found that a workpiece size of 5 x 4.5 mm^2 should be used in the FEM model since the predicted surface properties are not strongly affected by the displacement boundary constraints (as discussed in CHAPTER 5).

- An exhaustive analysis was conducted in order to determine the most reliable method for the estimation of the maximum ball penetration depth during roller burnishing (*D*) (discussed in CHAPTER 5 and APPENDIX B). The calculation of this value was a very important issue since it was used as input for the 2D roller burnishing simulation with a *displacement control* for tool movement (as in [Yen, 2004]). As a result from that analysis, it was decided to use Yen's 3D roller burnishing model [Yen, 2004] to calculate the maximum ball penetration depth (see Figure 5-12). This was due to more reliable surface properties predictions obtained with this approach and to more realistic tool/workpiece contact conditions considered with this model (roller burnishing is a 3D process in nature).

7.3 Perspectives for Application of Roller Burnishing Technology in Mexican Industry

Although this research was focused on the study of roller burnishing on hardened cylindrical workpieces, application of this process is not restricted to axisymmetric components and hardened materials. Free-shaped surfaces as those obtained from milling can be burnished by using CNC milling centers and especial roller burnishing tooling (i.e., spring or hydrostatically loaded) for surface enhancement purposes as in [Shiou, 2003 and López, 2005]. On the other hand, roller burnishing has been successfully applied in a wide variety of components made of different metals such as titanium alloys [Prévey, 2000], aluminum alloys [Hassan, 1997; Némat, 2000 and Prévey, 2004], soft steels [El-Axir, 2000; Némat, 2000 and Bouzid, 2004] and brass [Hassan, 1998b].

Roller burnishing is a surface finish/enhancement process (as discussed in CHAPTER 3) and has as major improvements: 1) an increase in strength and performance of components under cyclic loads (more fatigue life), 2) an increase in corrosion resistance, 3) an increase in wear resistance and 4) it is possible to achieve good dimensional accuracy. As a result of those roller burnishing finish/enhancement capabilities, this process along with the FEM predictive tools provided in this work can be applied by Mexican companies in different fields such as: 1) aerospace industry, 2) automotive/bearing industry, 3) tube/pipe industry, 5) mould/die industry, etc. APPENDIX C provides some examples for possible roller burnishing applications for different kinds of industries.

7.4 Future Work

Suggestions for further research on the application of hard turning and roller burnishing technology can be summarized as follows:

1) Technical and economical feasibility studies should be conducted in order to show advantages in the use of hard turning and roller burnishing for surface finish/enhancement purposes. In order to

achieve this goal, application of both processes should be compared to commonly used abrasion-based techniques for surface finish (i.e. grinding, honing and lapping) and other thermal/mechanical surface enhancement processes (i.e. nitriding, case hardening, induction hardening, hammering, autofrettage and shot peening).

2) Additional to 1), it is necessary to establish of a methodology to model and evaluate hard turning and roller burnishing processes. Both tasks 1) and 2) are recently being developed at ITESM as complementary work of this thesis [Jasso et. al, 2005b]. The approach proposed implies the use of FEM simulation models for hard turning and roller burnishing processes as well as the development of experimental procedures to validate FEM simulations.

3) Prediction of surface roughness parameters after hard turning by means of FEM simulations is not possible. It is necessary to conduct some hard turning experiments in order to generate data to be used as input for predictive models based on artificial neural networks or statistical approaches so that surface roughness parameters R_a and R_z can be estimated after hard turning.

4) Prediction of residual stresses after hard turning is possible by means of FEM simulations when using elastic-plastic workpiece formulation; however, DEFORM^{TM}-2D V8.0 can not handle elastic-plastic analysis under non-isothermal conditions (which is the case of metal cutting). The use of FEM-based software other than DEFORM^{TM}-2D or a Mesh Free-based code should be considered to perform numerical simulations of hard turning and roller burnishing.

5) It is necessary to run more 2D roller burnishing simulations in order to analyze the effect of using different burnishing ball diameters on surface roughness and residual stresses.

6) FEM simulation model can be improved by mesh refinement (reduction of the element size in the vicinity of the tool/workpiece contact zone) in order to increase the accuracy of predicted results for surface roughness parameters R_a and R_z.

7) Surface roughness parameters may be highly influenced by tool/workpiece stiffness and vibration. If the accuracy of the 2D FEM model cannot be increased by means of mesh refinement, it would be necessary to use statistical approaches to model the surface roughness parameters (R_a and R_z). This can be done by fitting a response surface model for the given experimental measurements of surface roughness parameters R_z and R_a from [Sartkulvanich, 2004b] for different combinations of process parameters.

8) Error in FEM predictions for residual stresses at the workpiece surface can be due to the combination of factors discussed in CHAPTER 6 and other possible sources of error:

   a. The proposed model does not consider the axial length of the workpiece. Elastic deflections of loaded workpiece during roller burnishing may become a significant source of errors because an unbalanced body is rotating in the lathe.
   b. Elastic deflections of the burnishing tool are neglected in this thesis. The assumption of the ball as a rigid object with a rigid mounting is not totally realistic. In order to avoid this possible source of error, simulation model should be improved by adding an elastic mounting for the tool, specially to achieve a more realistic and accurate estimation of the maximum ball penetration depth (D) into the workpiece surface layer.
   c. The process modeling considered burnishing fluid as lubricant/coolant. This assumption was based on several experimental and modeling literature publications for roller burnishing[Klocke, 1998; Ecoroll, 2004; Zhuang, 2004 and Luca,

2005]. This means that friction-induced temperature rises are neglected. A further research in lubrication theory is suggested in order to validate the non friction assumption of this thesis.

d. Roller burnishing FEM simulations were conducted under isothermal conditions because the burnishing fluid was considered as coolant and also because DEFORM^{TM}-2D was not able to handle elastic-plastic analysis under non isothermal conditions. Another FEM software should be used in order to include the thermal effect related to workpiece plastic deformation in simulations.

9) The development of a design of experiments (DOE) and statistical analysis to optimize the burnishing process parameters upon surface finish and residual stresses from a series of 2D FEM roller burnishing simulations can be performed.

REFERENCES

[Al-Zkeri, 2005] Al-Zkeri, I., Altan, T., "State of The Technology in Hard Turning –Prediction and Measurement of Residual Stress–". *ERC Report No. HPM/ERC/NSM-05-R-31*, 2005, The Ohio State University.

[Bouzid, 2004] Bouzid, W., Tsoumarev, O., Saï, K. "An Investigation of Surface Roughness of Burnished AISI 1042 Steel". *International Journal of Advanced Manufacturing Technology*. Vol. 24 (2004), pp. 120-125.

[Bouzid, 2005] Bouzid, W., Saï, K. "Finite Element Modeling of Burnishing of AISI 1042 Steel". *International Journal of Manufacturing Technology*. Vol. 25 (2005), pp. 460-465.

[Dahlman, 2004] Dahlman, P., Gunnberg, F. and Jacobson, M., "The Influence of Rake Angle, Cutting Feed and Cutting Depth on Residual Stresses in Hard Turning", *Journal of Materials Processing Technology*, Vol. 147 (2004), pp. 181-184.

[Ecoroll, 2001] ECOROLL AG Werkzeugtechnik. "Application Description: Hard Roller Burnishing Status of Research and Application". *ECOROLL AG Werkzeugtechnik Research Report No.5593E* (2001) pp.1-11.

[Ecoroll, 2004] ECOROLL AG Werkzeugtechnik. "Lecture 6090e: Deep Rolling Process and its Applications". *ECOROLL AG Werkzeugtechnik Lecture No.6090E* (2004) pp.1-9.

[El-Axir, 2000] El-Axir, M.H., "An Investigation into Roller Burnishing", *International Journal of Machine Tools & Manufacture*, Vol. 40, (2000) pp. 1603-1617

[Emmer, 1992] Emmer, T. and Popke, H. "Hartglattwalzen - eine Verfahrensalternative zum Rundschleifen", *Wissenschaft-liche Zeitschrift der technischen Universität Magdeburg*, Vol. 36 (1992) Heft 2/3

[Hassan, 1996] Hassan, A.M., Al-Bsharat, A.S. "Influence of Burnishing Process on Surface Roughness, Hardness, and Microstructure of some Non-Ferrous Metals". *Wear.* Vol. 199, pp. 1-8.

[Hassan, 1997] Hassan, A. M., "An Investigation into the Surface Characteristics of Burnished Cast AlCu Alloys", *International Journal of Machine Tools and Manufacture*, Vol. 37, No. 6 (1997), pp. 813-821.

[Hassan, 1998] Hassan, A.M., Al-Jalil, H.F., Ebied, A.A. "Burnishing Force and Number of Ball Passes for the Optimum Surface Finish of Brass Components". *Journal of Materials Technology*. Vol. 83 (1998), pp. 176-179.

[Hassan, 2000] Hassan, A.M., Maqableh, A. M. "The Effects of Initial Burnishing Parameters on Non-Ferrous Components". *Journal of Materials Processing Technology*. Vol. 102 (2000), pp. 115-121.

[Hughes, 2000] Hughes, T.J.R., "The Finite Element Method: Linear Static and Dynamic Finite Element Analysis". *Dover Publications*, USA, 2000.

[Jasso et. al, 2005a] Jasso, F., Sartkulvanich, P., Altan, T., "The Effects of Roller Burnishing Parameters upon Surface Properties of AISI 52100 Bearing Steel (60 HRC) –A Finite Element Analysis–". *ERC Report No. HPM/ERC/NSM-05-R39*, 2005, The Ohio State University.

[Jasso et. al, 2005b] Jasso, F., Martínez, A., Pacheco, J., Medrano, F., Vizcaya, B., Farías, G., Viesca, J., and Rodríguez, C. "Evaluation and Modeling of Hard Turning and Roller Burnishing –A Progress Report–". *Technical Report: CIMEC-2005-02*, 2005, ITESM Campus Monterrey.

[Klocke, 1998] Klocke, F. and Liermann, J., "Ball Burnishing of Hard Turned Surfaces", *International Journal of Machine Tools and Manufacture*, Vol. 38, 5-6 (1998), pp.419-423

[Liu, 2004] Liu, M., Takagi, J., Tsukuda, A. "Effect of Tool Nose Radius and Tool Wear on Residual Stress Distribution in Hard Turning of Bearing Steel". *Journal of Materials Processing Technology*, Vol. 150 (2004) pp. 234-241

[López, 2005] López, L.N., Lamikiz, A., Muñoa, J. "Surface Enhancement of Large Dies and Moulds by Ball Burnishing". *Proceedings from IMECE 2005*. November 5-11, ASME (2005), Orlando, FL, USA.

[Luca, 2002] Luca, L., "Investigation into the Use of Ball Burnishing of Hardened Steel Components as a Finishing Process", *PhD Dissertation* 2002, University of Toledo (2002).

[Luca, 2005] Luca, L., Neagu-Ventzel, S., Marinescu, I. "Effects of Working Parameters on Surface Finish in Ball-Burnishing of Hardened Steels". *Precision Engineering*. Vol. 29 (2005), pp. 253-256.

[Morris, 2005] Morris, E., Cho, H., Sartkulvanich, P., Altan, T., "Determining the Flow Stress at the Surface of Materials using Indentation Testing with Conical or Spherical Indenters". *ERC Report No. HPM/ERC/NSM-05-R-25*, 2005, The Ohio State University.

[Némat, 2000] Némat, M., Lyons, A.C. "An Investigation of the Surface Topography of Ball Burnished Mild Steel and Aluminum". *The International Journal of Advanced Manufacturing Technology.* (2000)16: pp.469-473.

[Poulachon, 2004] Poulachon, G., Bandyopadhyay, B. P., Jawahir, I. S., Pheulpin, S. and Seguin, E., "Wear Behavior of CBS Tools while Turning Various Hardened Steels", *Wear*, Vol. 256 (2004) pp. 302-310

[Prevéy, 2000] Prevéy, P. S., "The Effect of Cold Work on the Thermal Stability of Residual Compression in Surface Enhanced IN718", *Proceedings of 20th ASM Materials Solutions Conference & Exposition*, St. Louis, Missouri, October 10-12 (2000) pp. 1-9.

[Prévey, 2004] Prévey, P., and Cammett, J. "The Influence of Surface Enhancement by Low Plasticity Burnishing on the Corrosion Fatigue Performance of AA7075-T6". *International Journal of Fatigue*. Vol.26 (2004), pp.975-982.

[Ramesh, 2005] Ramesh, A., Melkote, S.N., Allard, L.F., Riester, L., Watkins, T.R. "Analysis of White Layers Formed in Hard Turning of AISI 52100 Steel". *Materials Science & Engineering A*. Vol. 390 (2005), pp. 88-97.

[Röttger, 2002] Röttger, K., "Walzen Hartgedrehter Oberflaechen", *PhD Dissertation* (2002), WZL, RWTH-Aachen, Germany.

[Sartkulvanich, 2004a] Sartkulvanich, P., Altan, T., "State of the Art on Ball Burnishing Process", *ERC Report No. HPM/ERC/NSM-04-R-22*, 2004, Ohio State University

[Sartkulvanich, 2004b] Sartkulvanich, P., Moradi, C., Altan, T. "Hard turning and Hard Roller Burnishing Experiments on AISI 52100 Steel (60 HRC)". *ERC Report No. HPM/ERC/NSM-04-R-39,* 2004, The Ohio State University.

[SFTC, 2004] DEFORM™-2D Version 8.1 User Manual, 2004, *Scientific Forming Technologies Company* (SFTC), Columbus, Ohio, USA.

[Shiou, 2003] Shiou, F.-J., Chen, C.-H. "Determination of Optimal Ball-Burnishing Parameters for Plastic Injection Moulding Steel". *International Journal of Advanced Manufacturing Technology*. Vol. 3 (2003), pp. 177-186.

[Sugino, 2004] Sugino Corp. "Roller Burnishing Tooling and Applications". Sugino Corp. http://www.suginocorp.com

[Thiele, 1999] Thiele, J. D., Melkote, S. N., "Effect of Cutting Edge Geometry and Workpiece Hardness on Surface Generation in the Finish Hard Turning of AISI 52100 Steel", *Journal of Material Processing Technology*, Vol. 94 (1999) pp. 216-226

[Yen, 2004] Yen, Y.-C. "Modeling of Metal Cutting and Ball Burnishing –Prediction of Tool Wear and Surface Properties–", *Ph. D Dissertation* (2004), The Ohio State University.

[Zhuang, 2004] Zhuang, W., Wicks, B. "Multipass Low-Plasticity Burnishing Induced Residual Stresses: Three-Dimensional Elastic-Plastic Finite Element Modeling", *Proceedings of the Institution of Mechanical Engineers*. Vol. 218 (2004), pp.663-668.

APPENDIX A

CHARATERIZATION OF SURFACE TOPOGRAPHY

R_a, R_q Mean roughness

DIN 4762, DIN 4768, ISO 4287/1

Arithmetical mean deviation R_a is the arithmetical mean of the areas of all profile values of the roughness profile.

$$R_a = \frac{1}{l} \int_0^l |y(x)|dx$$

Root-mean-square deviation R_q is the root-mean-square calculation of all profile values of the roughness profile.

$$R_q = \sqrt{\frac{1}{l} \int_0^l y^2(x)\,dx}$$

y (x) = profile values of the roughness profile.

R_a is also called AA and CLA, R_q also RMS.

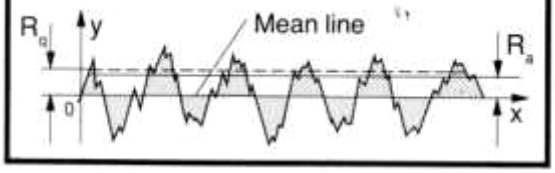

R_z, R_{max} Roughness depth

DIN 4768

Single roughness depth Z_i is the vertical distance of the highest to the deepest profile point (= R_y).

Mean roughness depth R_z is the mean value of the single roughness depths Z_i of consecutive sampling lengths:

$$R_z = R_{zDIN} = \frac{1}{n}(Z_1 + Z_2 + \ldots + Z_n).$$

R_{zDIN} is equal to the R_y mean value of several sampling lengths as per DIN 4762.

Maximum roughness depth R_{max} is the largest single roughness depth within the evaluation length.

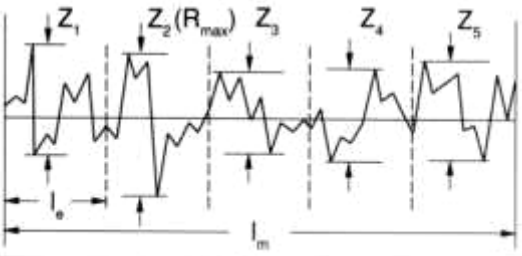

Selection of cut-off λ_c

DIN 4768, ISO 4288

Periodic profiles	Non-periodic profiles		Cut-off	Sampling/ evaluation length
Spacing of prof. irregularities S_m (mm)	R_z (µm)	R_a (µm)	λ_c (mm)	l_e / l_m (mm)
>0.01 up to 0.04	up to 0.1	up to 0.02	0.08	0.08 / 0.4
>0.04 up to 0.13	>0.1 up to 0.5	>0.02 up to 0.1	0.25	0.25 / 1.25
>0.13 up to 0.4	>0.5 up to 10	>0.1 up to 2	0.8	0.8 / 4
>0.4 up to 1.3	>10 up to 50	>2 up to 10	2.5	2.5 / 12.5
>1.3 up to 4	>50	>10	8	8 / 40

R_p Levelling depth, R_m, R_y

DIN 4762

R_p is the distance between the highest profile peak and the reference line (levelling depth).
According to an older definition the R_p mean value is called R_{pm}. In this case, R_p is the maximum levelling depth of several sampling lengths.

R_m is the distance between the deepest profile valley and the reference line. R_m is also called R_v (profile valley depth).

R_y is the vertical distance between the highest peak and the deepest valley: $R_y = R_p + R_m$.

R_y corresponds to the definition of a single roughness depth Z_i as per DIN 4768, i.e. the R_y mean value of several sampling lengths is identical to $R_{z\,DIN}$.

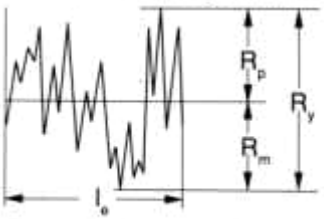

Roughness depth R_t as per DIN 4762 (1960) corresponds to the R_y definition.
R_t was withdrawn in 1978.

Figure A-1: Characterization of surface topography [Ecoroll, 2001].

Below are the codes, written in MAPLE software to calculate for the mean roughness (R_a) of the FEM simulation's predicted burnished surface.

```
> restart:
> with (CurveFitting):
> xydata:=readdata("p36f005roughness.txt",2):
  l:=500:
  a:=-500:
  b:=-0:
> g:=Spline(xydata, x, degree=3):
> plot(g,x=a..b);
```

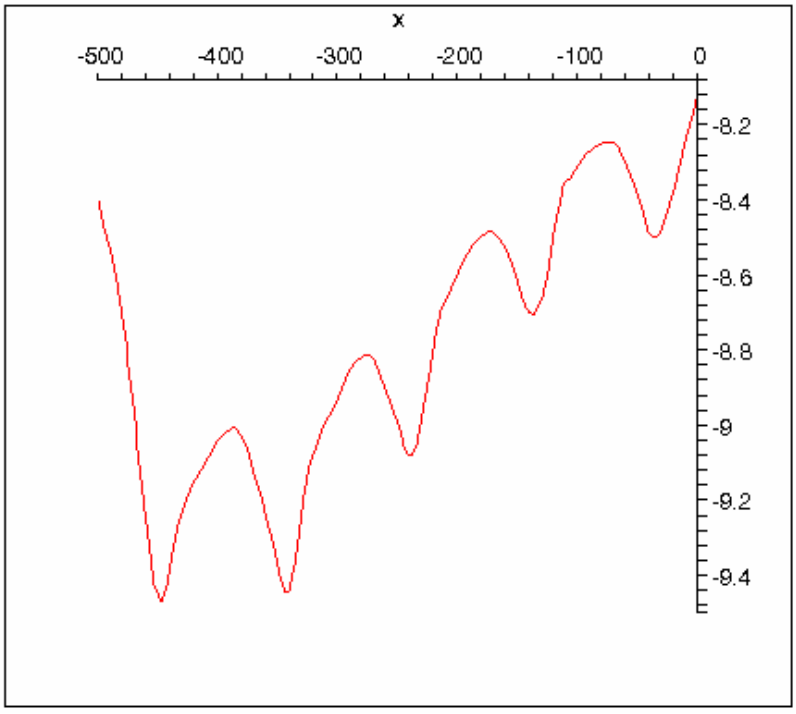


```
> shift:=evalf((1/l)*int(g,x=a..b));
                                  shift := -8.762671392
> Area:=evalf(int(abs(g-shift),x=a..b));
                                  Area := 161.8956575
> Ra:=Area/l;
                                  Ra := 0.3237913150
```

```
> plot(g-shift,x=a..b);
```

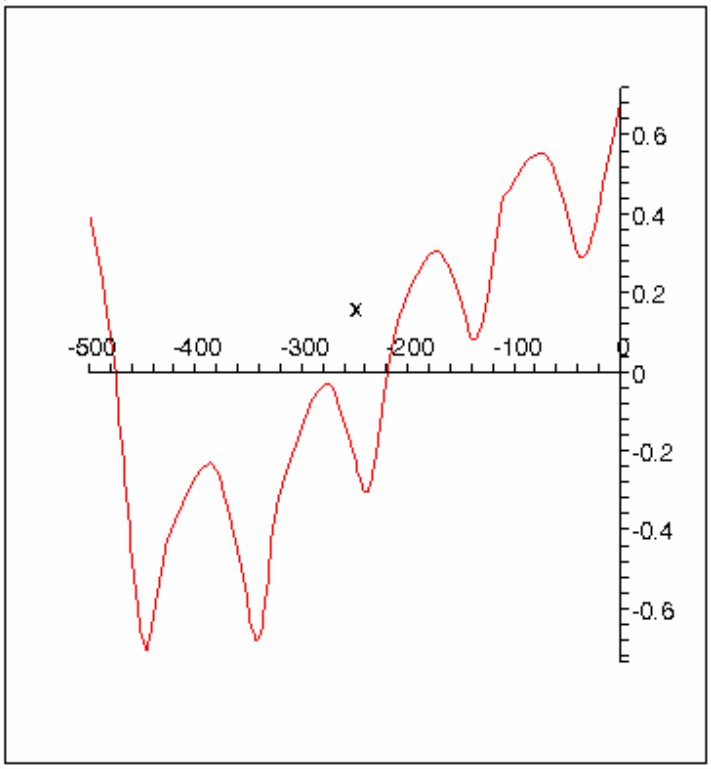

APPENDIX B
DETERMINATION OF BALL PENETRATION DEPTH IN THE WORKPIECE SURFACE BY USING DIFFERENT METHODS

B.1 Elastic Theory of Contact

The maximum ball penetration depth (δ in Figure B-1) can be estimated by using Hertz theory for normal contact of two elastic bodies [Bouzid, 2004]. Workpiece and tool can be considered to have cylindrical and spherical geometries respectively. The diameter of the contact area between these two bodies is obtained using the expression

$$d_c = m\left(\frac{3\pi\left(K_1+K_2\right)F}{2\left(C_1+C_1^{'}+C_2+C_2^{'}\right)}\right)^{\frac{1}{3}} \tag{B.1}$$

where

F is the burnishing force [N]

d_c is the diameter of the contact surface [mm]

C_1, C_1' are the maximum and the minimum curvature of the workpiece

C_2, C_2' are the maximum and the minimum curvature of the ball

K_1, K_2 are material properties defined by the workpiece's/tool's modulus of elasticity (*E*) and Poisson ratio (ν) (see Eq. (B.2)).

$$K_1 = \frac{1-\nu_1}{\pi E_1} \qquad K_2 = \frac{1-\nu_2}{\pi E_2} \tag{B.2}$$

The ball penetration in the workpiece surface layer is given (in μm) by

$$\delta = \frac{3(10)^3 \pi}{4 d_c} r \left(K_1 + K_2 \right) F \tag{B.3}$$

Parameters *m* and *r* in Eqs. (B.1) and (B.3) depend on the angle φ as in Figure B-2. This angle is calculated with the equation

$$\cos(\varphi) = \frac{\sqrt{\left(C_1 - C_1^{'}\right)^2 + \left(C_2 - C_2^{'}\right)^2 + 2\left(C_1 - C_1^{'}\right)\left(C_2 - C_2^{'}\right)\cos\theta}}{C_1 + C_1^{'} + C_2 + C_2^{'}} \tag{B.4}$$

Because workpiece is cylindrical and burnishing ball is spherical, the expression of different curvatures is as follows

$$C_2 = C_2^{'} = \frac{1}{R_2} \tag{B.5}$$

$$C_1 = \frac{1}{R_1} \quad \text{and} \quad C_1^{'} = 0$$

Finally, Eq. (B.4) can be simplified to calculate the angle φ

$$\cos(\varphi) = \frac{R_2}{2R_1 + R_2} \tag{B.6}$$

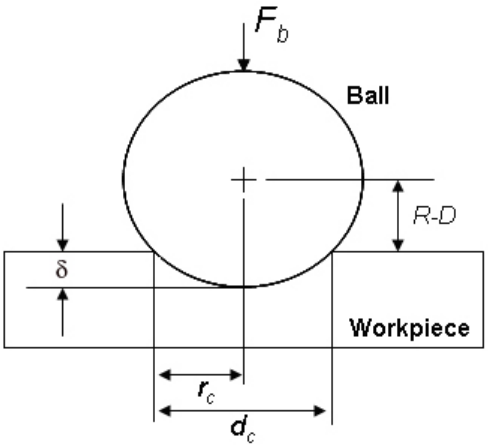

Figure B-1: Tool's displacement normal to the workpiece surface (δ) and diameter of contact area (d_c).

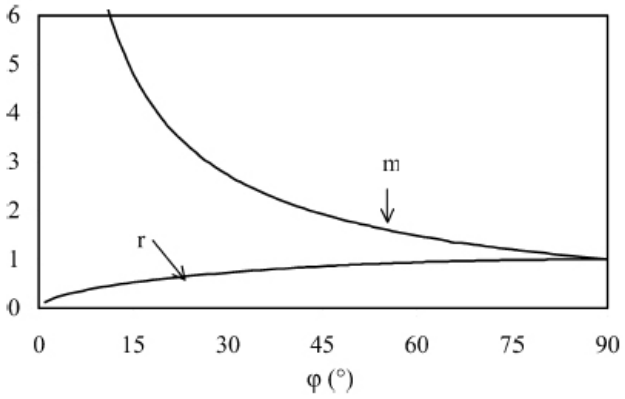

Figure B-2: Evolution of parameters *m* and *r* with angle φ [Bouzid, 2004].

B.2 2D Axis-symmetric Simulation of Ball Indentation in a Flat Elastic and Elastic-plastic Surfaces

Ball indentation in a flat surface simulation was conducted by using the same axis-symmetric FEM model proposed by Morris to perform FEM inverse analysis (see Figure 5-3) [Morris, 2005]. Simulation was conducted using DEFORM^{TM}-2D considering elastic and elastic-plastic workpieces for two simulations. In both cases, the rigid ball was pressed against the workpiece surface with a very low speed until the burnishing force was reached (considering the pressure loss discussed in 5.3.1). Simulation was stopped and the maximum ball penetration depth was obtained from the load-stroke curve of each simulation, which was very similar to that shown in Figure 5-2.

B.3 2D Plane Strain Roller Burnishing Simulation

2D plane strain simulation for one indentation cycle was conducted by using Yen's model with no feed effect as discussed in Section 5.3.3. The applied force during simulation was measured at different ball penetration depths by using the load vs. stroke curve shown in Figure B-3. After determining the applied force, the contact diameter between the two bodies was manually measured in the DEFORM^{TM}-2D post-processor as shown in Figure B-4 for the different

penetration depths. Finally, since force calculated in 2D FEM plane strain model considers the width of 1 mm (normal to plane direction), force were calculated assuming the area of contact (from position of contact nodes between ball and workpiece) is circular (the values of d_c at different depths were used to calculate this new force). The result of this approach was a burnishing force (F_b) - ball penetration depth (D) curve, as shown in Figure B-5.

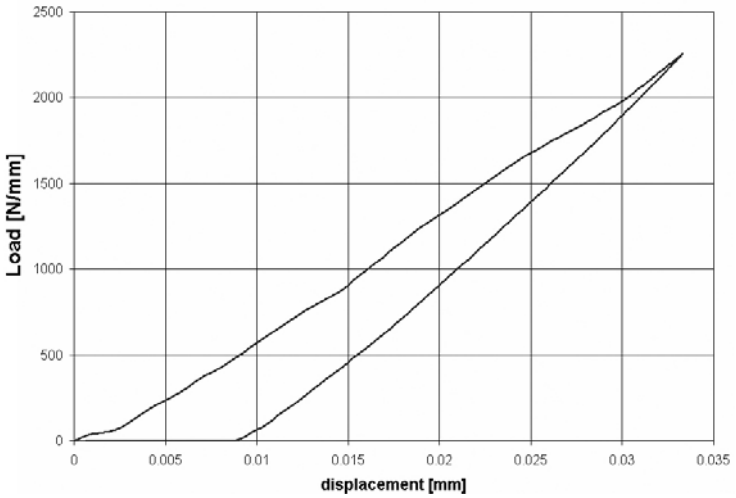

Figure B-3: Load (per 1 mm depth) vs. stroke curve obtained from 2D plane strain simulation for a single indentation cycle.

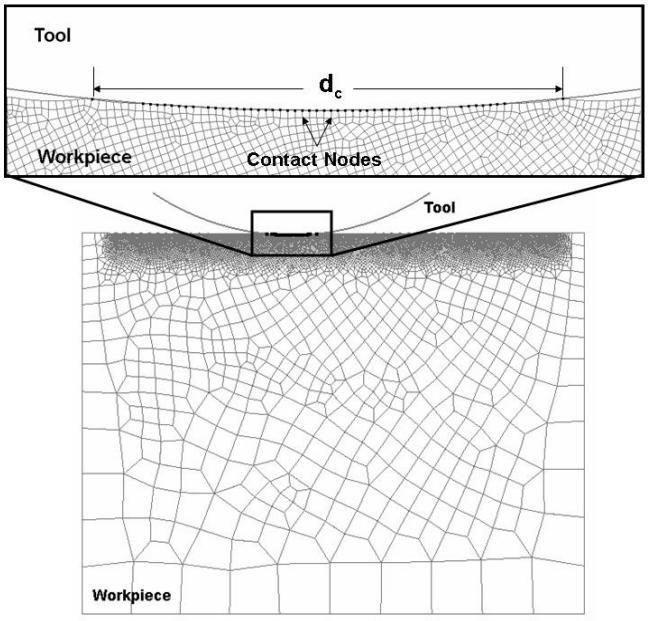

Figure B-4: Determination of the contact diameter (d_c) at different penetration depths using 2D plane strain simulations.

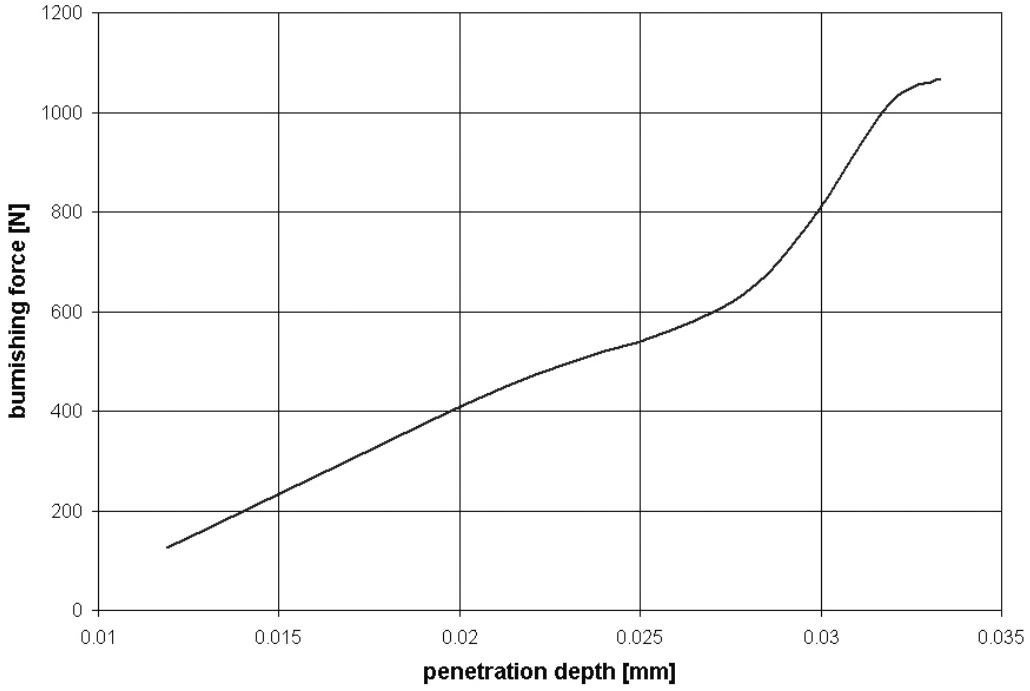

Figure B-5: Force vs. ball penetration depth curve obtained from 2D simulations for one indentation cycle.

B.4 3D Roller Burnishing Simulation

Although roller burnishing is in nature a three-dimensional process, the use of 3D FEM simulations is not practical since they are very time consuming when considering the effect of burnishing feed (f_b). The 3D nature of this process was considered in the same way as Yen [Yen, 2004]. A 3D simulation model as that shown in Figure B-6 was defined in the DEFORM^{TM}-3D environment and simulations for one burnishing path were conducted by assuming different ball penetration depths until the burnishing force measured in simulations matched the known burnishing force (decreased by pressure loss). As in the case of 2D plane strain simulations, a characteristic curve was obtained in which the known burnishing force and the corresponding ball penetration depth were related (see Figure B-7).

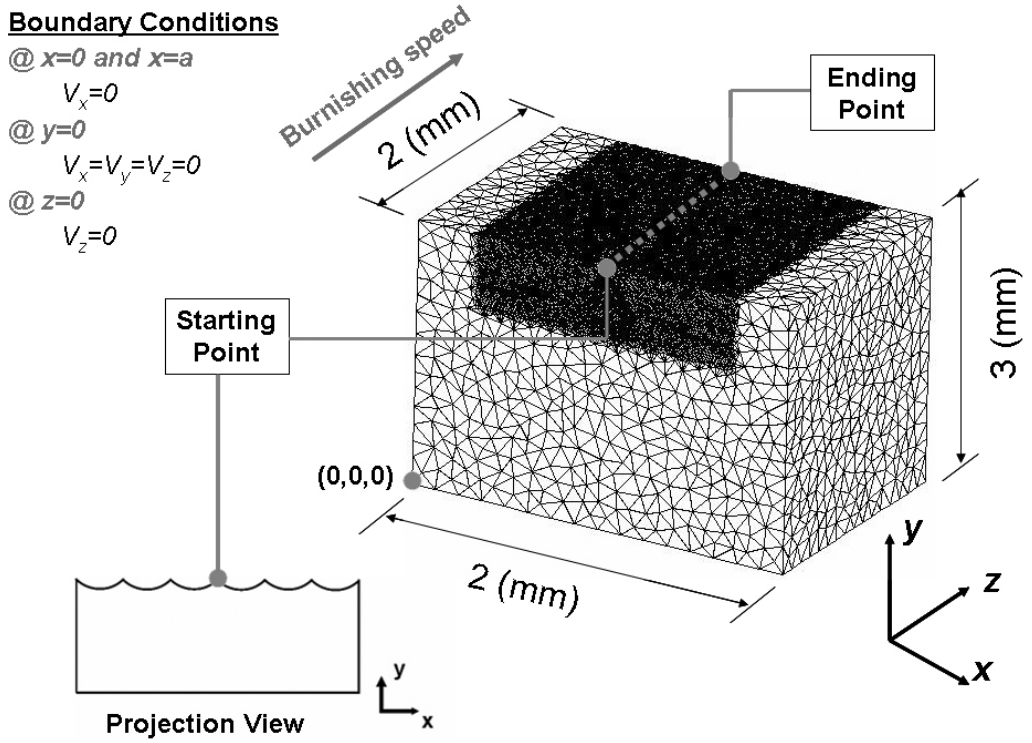

Figure B-6: 3D FEM simulation model for one burnishing path.

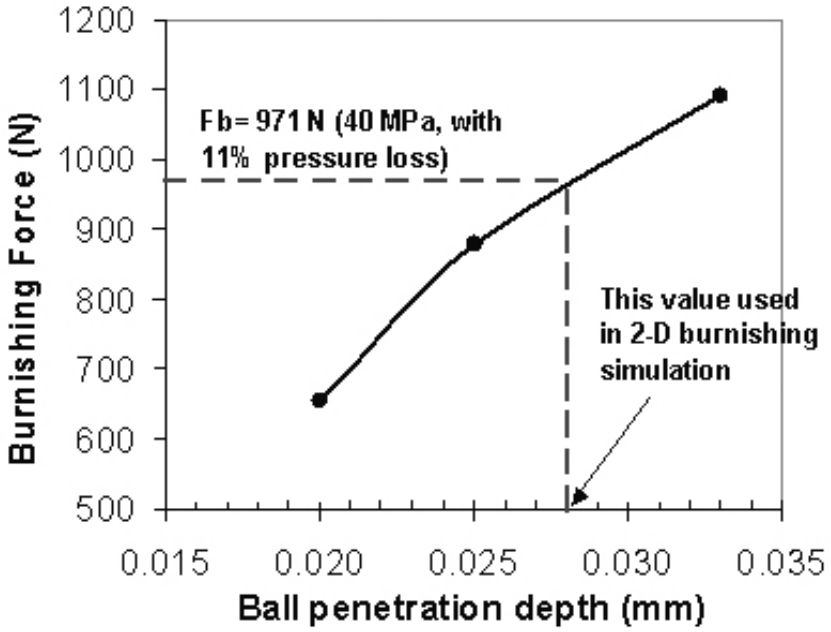

Figure B-7: Relationship between the burnishing force and maximum penetration depth *D* predicted by 3D roller burnishing simulations.

APPENDIX C
ROLLER BURNISHING APPLICATIONS THAT CAN BE USED IN MEXICAN INDUSTRY

Figure C-1 and Figure C-2 show some examples of industrial applications for roller burnishing. It should be noted that figures show spring-loaded and hydrostatically-loaded tools respectively. These tools can be used for processing axisymmetric and free-form components.

Figure C-1: Spring-loaded roller burnishing tools and some industrial applications [Sugino, 2004].

Burnishing of valves for diesel engines

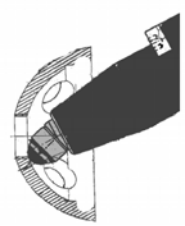

Burnishing of shell shaped components

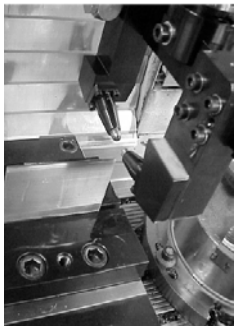

Burnishing of turbine blades

Burnishing of turbine blades

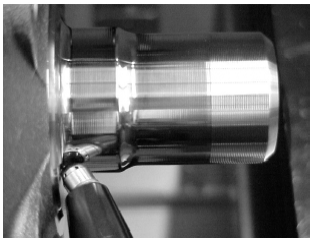

Burnishing of hubs

Burnishing of welded joints

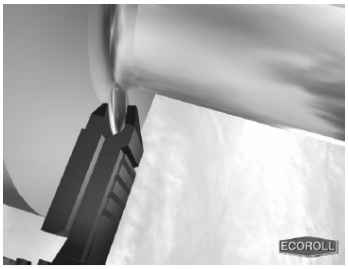

Burnishing of turbine shafts

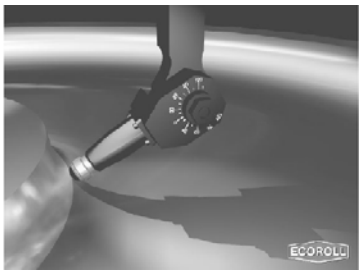

Turbine wheel

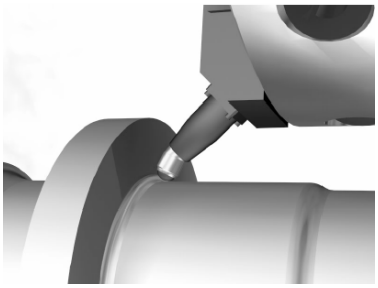

Burnishing of automobile shafts

Tool for screw thread undercuts burnishing

Figure C-2: Hydrostatically-loaded roller burnishing tools and some industrial applications [Ecorrol, 2004].

APPENDIX D
IMPLEMENTATION OF SURFACE RESIDUAL STRESSES GENERATED BY HARD TURNING INTO THE 2D SIMULATION MODEL FOR ROLLER BURNISHING

As discussed in CHAPTER 5, flow stress model for hard turned surface obtained from ball indentation tests and FEM inverse analysis was designed to consider possible changes in workpiece plastic behavior produced by hard turning [Morris, 2005]. Simulation results shown in CHAPTER 6 were observed to be in good agreement with experimental measurements of axial and tangential residual stresses; however, FEM predicted results were not close to experimental measurements obtained at the workpiece surface, especially for the axial stresses. The reason of this lack of accuracy at the workpiece surface could be due to the same combination of factors discussed in Section 6.2.1 and to the fact that Eq. (5.4) does not consider the residual stresses produced during hard turning. As suggested in [Zhuang, 2004], inclusion of X-ray measured residual stress data can lead to an improvement of the FEM simulation model. In this appendix, a procedure to consider the cutting-induced residual stresses is presented.

D.1 Attachment of Cutting-Induced Residual Stress data into the Workpiece Surface Layer for Roller Burnishing Simulations

Figure D-1 shows a flowchart for the procedure proposed to include the X-ray measured residual stress data produced by hard turning (see Section 4.4.2) into the roller burnishing simulation model. This methodology is described in five steps.

1) The simulation keyword file for roller burnishing simulations which contains the specifications of process parameters (i.e. maximum penetration depth, burnishing feed, workpiece flow stress data, etc.) is used as input for a MATLAB program named **keymod.m** (i.e. FILE.KEY in Figure D-1). Program code is provided in Section D.2.

2) Program **keymod.m** opens the keyword file (i.e., FILE.KEY) and extracts the (*x,y*) coordinates of the four nodes that belong to each element in the workpiece mesh.

3) Once the nodes coordinates are known for each element, the program uses finite element shape functions for bilinear four node square element (see Figure D-2) to calculate the element's depth beneath the workpiece surface. According to this, the position of a material point in the real space can be approximated by the equation

$$\{\mathbf{x}\} = \sum_{a=1}^{4} N_a(\xi,\eta)\{\mathbf{x}_a\}^e \tag{D.1}$$

where N_a are the shape functions for the bilinear four node square element, which are given by [Hughes, 2000]

$$N_a = \frac{1}{4}(1+\xi_a\xi)(1+\eta_a\eta) \tag{D.2}$$

ξ_a, η_a are the node coordinates in the natural space (see Figure D-2)

The element depth value calculated by this approach for each mesh element corresponds to the location of the point necessary to evaluate a one-point Gaussian quadrature rule for numerical integration (i.e. center of the element in the natural space), since DEFORM^{TM}-2D evaluates stresses at the center of finite elements.

4) Program **keymod.m** opens a text file in which the experimental measurements of residual stresses are defined and calculates the axial and tangential residual stresses for each element according to its

depth value calculated in 3) (see Figure D-3). **Note**: data must be included as shown in Table D-1 so that program can run successfully. Additionally, program was written considering that the *y*-coordinate origin is located at the top of the workpiece (at the roughness peaks as shown in Figure D-3).

5) After the residual stresses are assigned for each element, residual stress data is written together with the original information provided in FILE.KEY into another keyword file (i.e. FILEMOD.KEY in Figure D-1). Figure D-4 shows a contour line diagram of the workpiece for FILEMOD.M. Experimental residual stresses have been attached into the roller burnishing simulation model.

.

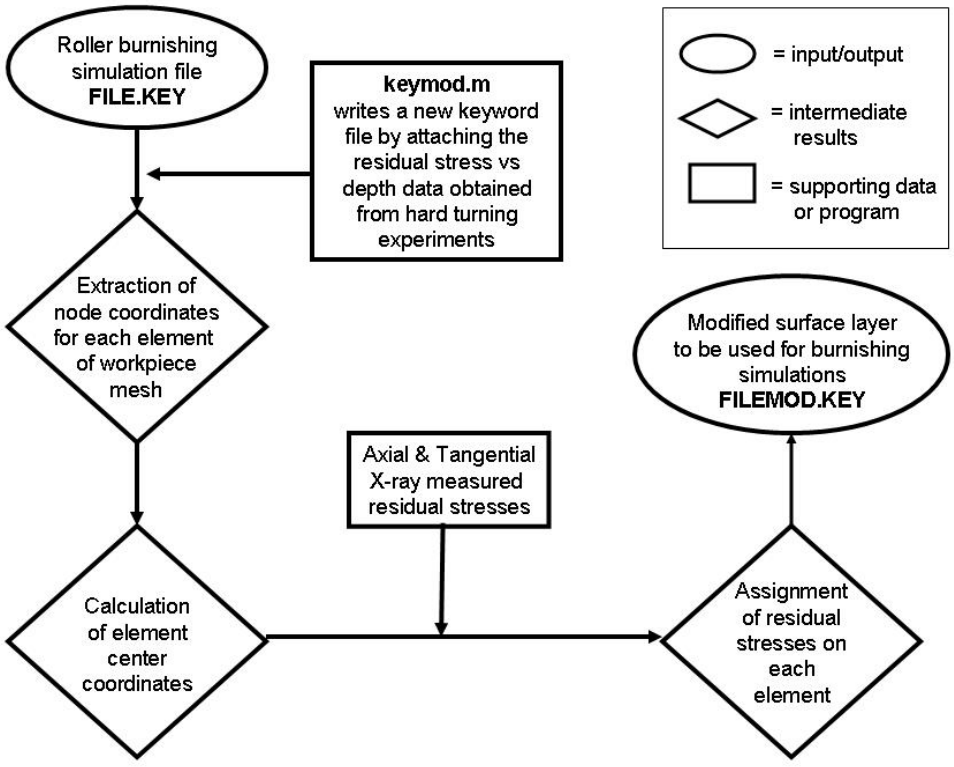

Figure D-1: Flow chart for the procedure of including the variation of cutting-induced residual stresses with depth in the surface layer to be burnished.

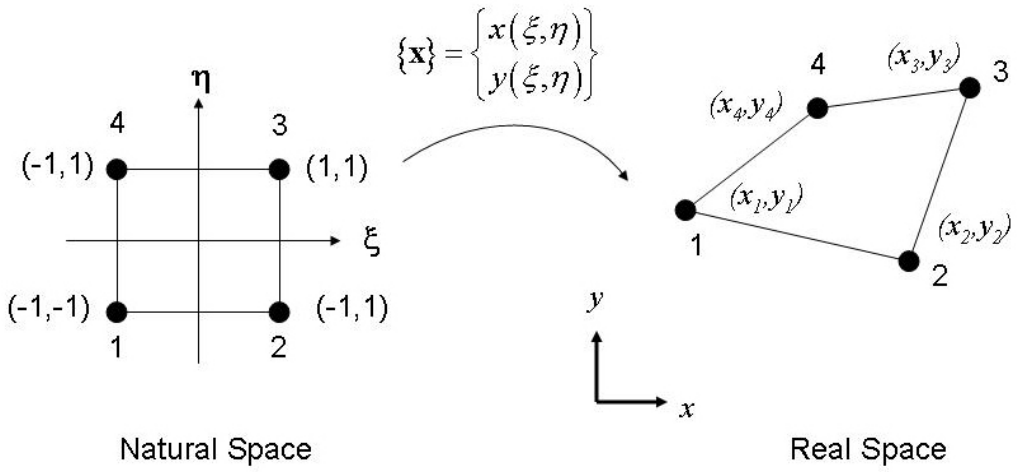

Figure D-2: Mapping function from natural to real space for a four-node bilinear finite element [Hughes, 2000].

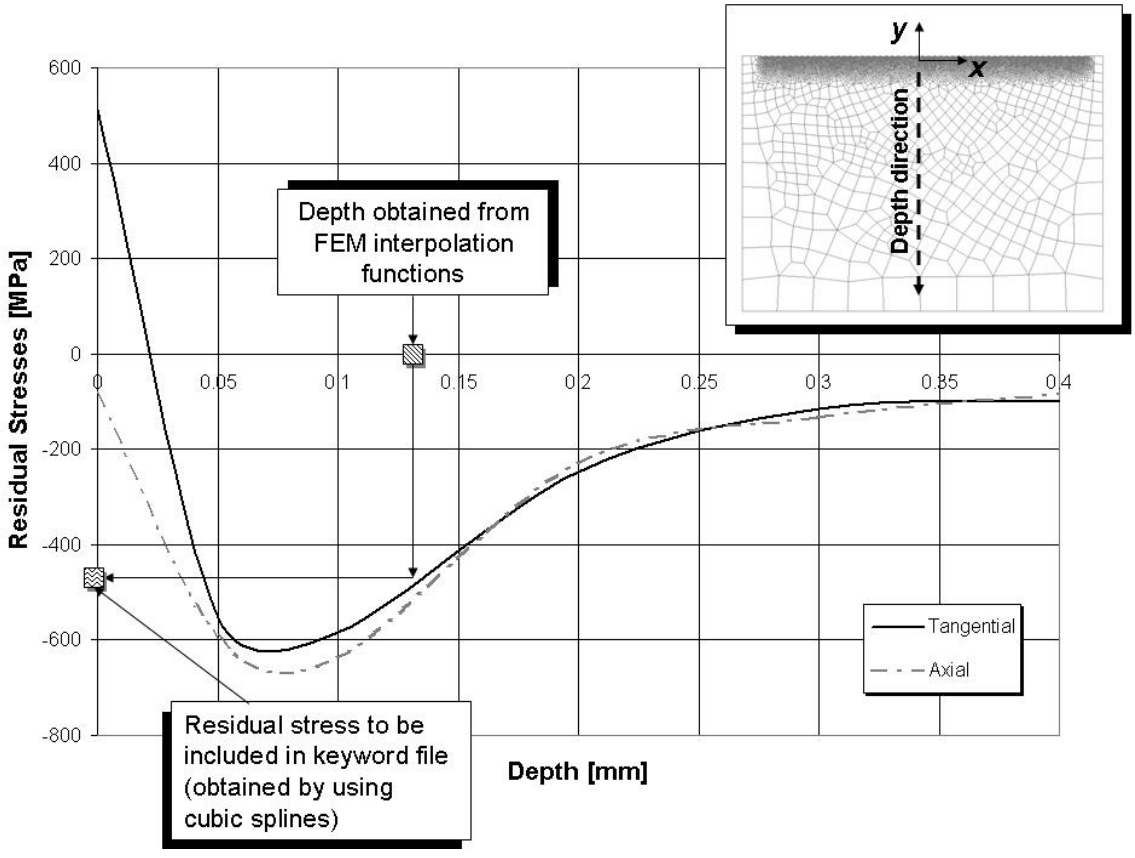

Figure D-3: Estimation of the residual stress value (axial or tangential) by means of cubic splines performed by MATLAB program keymod.m.

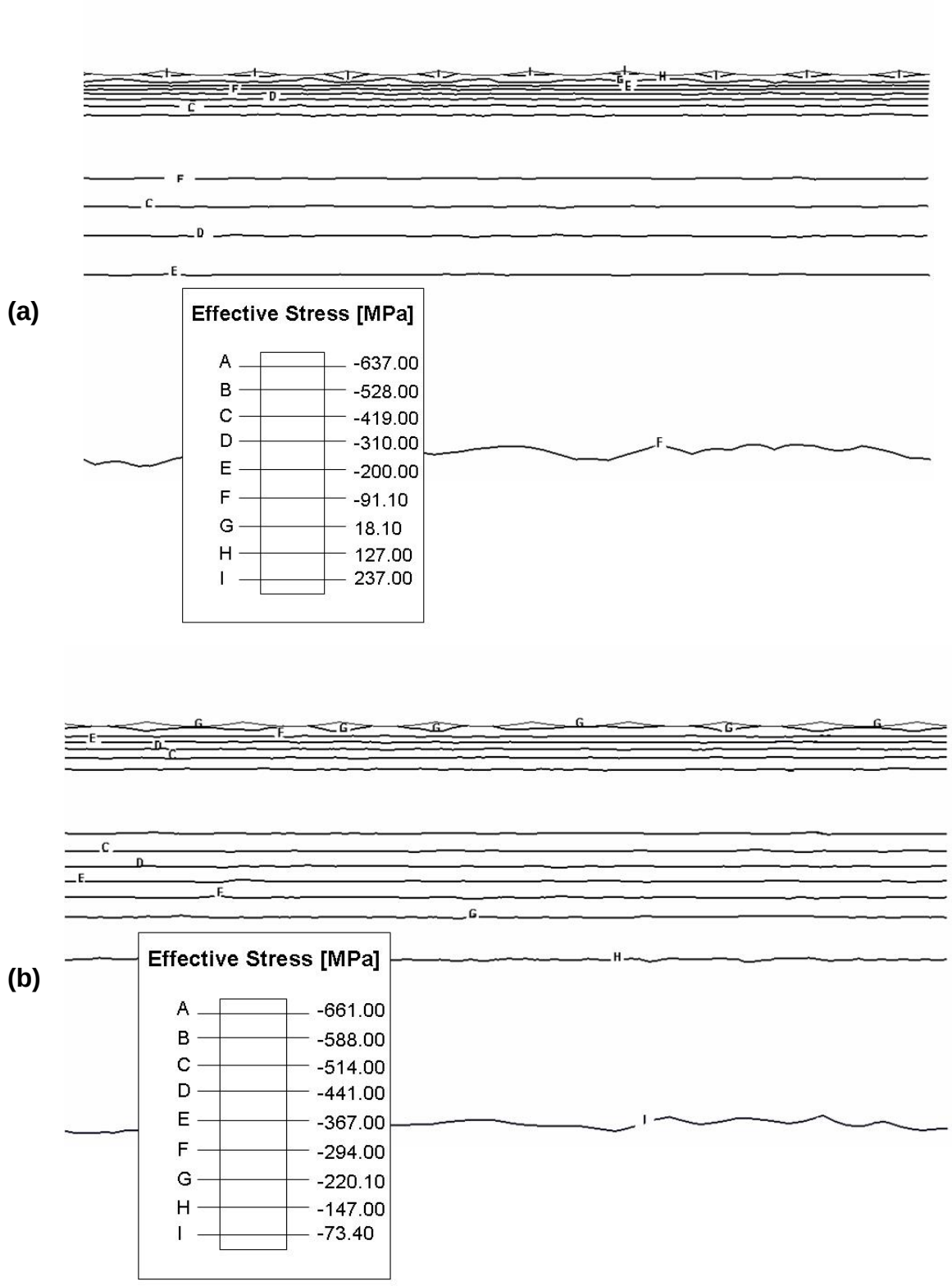

Figure D-4: Result of the inclusion of cutting-induced experimental residual stresses into 2D roller burnishing simulation model. **(a)** Axial residual stresses. **(b)** Tangential residual stresses.

X-ray measured residual stress data			
Point	Depth [mm]	σ_x [MPa]	σ_z [MPa]
1	0.00	-81.7	513
2	-0.05	-593.1	-553.4
3	-0.10	-638.1	-584.4
4	-0.20	-230.7	-247.1
5	-0.30	-133.6	-114.9
6	-0.40	-84.9	-96.9

Table D-1: A text file containing the experimental measurements of residual stress at different depths must be created as shown in order to use MATLAB program **keymod.m**.

D.2 MATLAB Program Code

Program **keymod.m** was divided into subroutines (functions in MATLAB code). Each subroutine has a specific task to perform in order to modify the original keyword file generated in the DEFORM^{TM}-2D pre-processor for roller burnishing simulations so that residual stress/strain can be attached to the workpiece mesh.

D.2.1 keymod.m

```
%%%%%%%%%%%%%%%%%%%%%%%%%%%%%%%%%%%%%%%%%%%%%%%%%%%%%%%%%%%%%%%%
% KEYMOD.M
%%%%%%%%%%%%%%%%%%%%%%%%%%%%%%%%%%%%%%%%%%%%%%%%%%%%%%%%%%%%%%%%
%
% RECORD OF REVISIONS
%     Date       Programmer      Description of change
%     ======     ============    =======================
%     04/12/2005     F. Jasso        Original code
% ----------------------------------------------------------------------------------------------------------------------------------------
 clear;
fprintf ('\t%s','********************************************************************************************');
fprintf ('\n\t%c \t\t\t\t\t\t\t\t\t%s \t\t\t\t\t\t\t\t\t\t%c\n', '*','KEYMOD.M','*');
fprintf ('\t%c\t %s \t%c\n','*','This program introduces the pre strain/stress information on a .KEY file generated','*');
fprintf ('\t%c\t %s \t%c\n','*','using DEFORM-2D. The user must select the type of input data (e, s or both) in or-','*');
fprintf ('\t%c\t %s \t%c\n','*','der to generate the KEYOUT.KEY file to be used as input for burnishing simulations','*');
fprintf ('\t%c\t \t\t\t\t\t%s \t\t\t\t%c\n','*','Program developed by: P. Sartkulvanich and F. Jasso','*');
fprintf ('\t%s\n','********************************************************************************************');
fprintf ('\t%c\t \t%s \t\t%c\n','*','WARNING: The origin of the workpiece must be located on the contact surface','*');
fprintf ('\t%s\n\n','*******************************************************************************************');

% The user is asked to select the type of data to add on .KEY file
option=input('Please select the input data (1)Strain, (2)Stress, (3)Both >');
if option==1;
      rstrains=input('Type the experimental residual strains data file (ex: data.txt) >','s');
   elseif option==2;
      rstresses=input('Type the experimental residual stresses data file (ex: data.txt) >','s');
```

```
    elseif option==3;
        rstrains=input('Type the experimental residual strains data file (ex: data.txt) >','s');
        rstresses=input('Type the experimental residual stresses data file (ex: data.txt) >','s');
    else
        fprintf ('Option NOT VALID, please run program again and type (1),(2) or (3)');
        break;
end;

% File name of .KEY file to modify is requested
keyname=input('Type the keyfile name for wich data will be attached (ex: XX.key) >','s'); % .KEY file name is introduced

% Depth for stress/strain zero
if option==1;
    dpstr=input('Type the depth for which residual strain=0 [mm] >');
elseif option==2;
    dpstrss=input('Type the depth for which residual stress=0 [mm] >');
elseif option==3;
    dpstr=input('Type the depth for which residual strain=0 [mm] >');
    dpstrss=input('Type the depth for which residual stress=0 [mm] >');
end;

% Radial and shear stresses are setted as zero
srd=0; %Workpiece radial stress is zero
tau=0; %Workpiece shear stress is zero
if option==1;
    ystrain=-1*dpstr; % Depth where residual strain is zero
elseif option==2;
    ystress=-1*dpstrss;% Depth where residual stress is zero
elseif option==3;
    ystrain=-1*dpstr; % Depth where residual strain is zero
    ystress=-1*dpstrss;% Depth where residual stress is zero
end;

% Node position, no. of elements and element connectivity is read from .KEY file
[alltxt, RZ, n, ELMCON, strainpos, stresspos]= textinfo(keyname);

% Matrix containing the center points of mesh elements is initialized
cne=zeros(n,2);

% The center position of each element is calculated using FE interpolation
% for 4 node bilinear elements
for k=1:n
    cne(k,1)=cne(k,1)+ecenter(RZ(ELMCON(k,2),2),RZ(ELMCON(k,3),2),RZ(ELMCON(k,4),2),RZ(ELMCON(k,5),2));
    cne(k,2)=cne(k,2)+ecenter(RZ(ELMCON(k,2),3),RZ(ELMCON(k,3),3),RZ(ELMCON(k,4),3),RZ(ELMCON(k,5),3));
end;

% The number of elements to modify is counted
if option==1;
    nstrain=counter(cne,ystrain); % Elements affected by residual strain data
elseif option==2;
    nstress=counter(cne,ystress); % Elements affected by residual stress data
elseif option==3;
    nstrain=counter(cne,ystrain); % Elements affected by residual strain data
    nstress=counter(cne,ystress); % Elements affected by residual stress data
end;

%%%%%%%%%%%%%%%%%%%%%%%%%%%%%%%%%%%%%%%%%%%%%%%%%%%%%%%%%%%%%%%%%%%%%%%%%%%%
if option==1;
    % Information of residual strains is read from .TXT file
    [depepsilon,repsilon]=readstrain(rstrains);

    % Matrix containing the residual strains is initialized
    lstrain=zeros(n,1);

    % The residual strain is calculated for each element
    for k=1:n
        if cne(k,2)<ystrain;
            epin=0;
        else
            epin=spline(depepsilon, repsilon, cne(k,2)); % Initial residual strain
        end;
        lstrain(k,1)=lstrain(k,1)+epin; % Strain-effective
```

```
    end;

    % New keyword file is generated
    opt=fopen('keyout.key','wt');
    for i=1:(strainpos-2)
        fprintf (opt,'%s \n',alltxt{i});
    end;
    fclose(opt);

    % strain data is attached to keyout.key
    opt=fopen('keyout.key','at');
    fprintf (opt,'%s\t %s\t %f\t %s\n', 'STRAIN', '1', nstrain, '0.000E+00');
    for i=1:n
        if cne(i,2)<ystrain;
            i=i+1;
        else
        fprintf(opt,'\t%d\t %E\n', i, lstrain(i,1));
        end;
    end;

    %Data after word STRAIN to final of .KEY file is written on KEYOUT.KEY
    m=strainpos;
    for i=m:length(alltxt);
        fprintf (opt,'%s \n',alltxt{i});
    end;
    fclose(opt);

%%%%%%%%%%%%%%%%%%%%%%%%%%%%%%%%%%%%%%%%%%%%%%%%%%%%%%%%%%%%%%%%e
lseif option==2;
    % Information of residual stresses is read from .TXT file
    [depsigma, sigmat, sigmax]=readstress(rstresses);

    % Matrix containing the residual stresses is initialized
    lstress=zeros(n,2);

    % The residual stress is calculated for each element
    for k=1:n
        if cne(k,2)<ystress;
            sax=0;
            stn=0;
        else
            sax=spline(depsigma, sigmax, cne(k,2)); % Axial stress
            stn=spline(depsigma, sigmat, cne(k,2)); % Tangential stress
        end;
        lstress(k,1)=lstress(k,1)+sax; % Axial stress
        lstress(k,2)=lstress(k,2)+stn; % Tangential stress

    end;

    % New keyword file is generated
    opt=fopen('keyout.key','wt');
    for i=1:(stresspos-2)
        fprintf (opt,'%s \n',alltxt{i});
    end;
    fclose(opt);

    % stress data is attached to keyout.key
    opt=fopen('keyout.key','at');
    fprintf (opt,'%s\t %s\t %f\t %s\n', 'STRESS', '1', nstress, '0.000E+00');
    for i=1:n
        if cne(i,2)<ystress;
            i=i+1;
        else
            fprintf(opt,'\t%d\t %E\t %E\t %E\t %E\n', i, lstress(i,1),srd,lstress(i,2),tau);
        end;
    end;

    %Data after the STRESS word to end of .KEY file
    m=stresspos;
    for i=m:length(alltxt);
        fprintf (opt,'%s\n',alltxt{i});
    end;
```

```
    fclose(opt);

%%%%%%%%%%%%%%%%%%%%%%%%%%%%%%%%%%%%%%%%%%%%%%%%%%%%%%%%%%%%%%%%%%%%%%%%%%%%%%%%
elseif option==3;
    % Information of residual stresses/strains is read from .TXT files
    [depsigma, sigmat, sigmax]=readstress(rstresses);
    [depepsilon,repsilon]=readstrain(rstrains);

    % Matrix containing the residual strains and stresses are initialized
    lstrain=zeros(n,1);
    lstress=zeros(n,2);

    % The residual strain/stress is calculated for each element
    for k=1:n
        if cne(k,2)<ystrain;
            epin=0;
        else
            epin=spline(depepsilon, repsilon, cne(k,2)); % Initial residual strain
        end;
        lstrain(k,1)=lstrain(k,1)+epin; % Strain-effective

        if cne(k,2)<ystress;
            sax=0;
            stn=0;
        else
            sax=spline(depsigma, sigmax, cne(k,2)); % Axial stress
            stn=spline(depsigma, sigmat, cne(k,2)); % Tangential stress
        end;
        lstress(k,1)=lstress(k,1)+sax; % Axial stress
        lstress(k,2)=lstress(k,2)+stn; % Tangential stress
    end;

    % New keyword file is generated
    opt=fopen('keyout.key','wt');
    for i=1:(strainpos-2)
        fprintf (opt,'%s \n',alltxt{i});
    end;
    fclose(opt);

    % strain data is attached to keyout.key
    opt=fopen('keyout.key','at');
    fprintf (opt,'%s\t %s\t %f\t %s\n', 'STRAIN', '1', nstrain, '0.000E+00');
    for i=1:n
        if cne(i,2)<ystrain;
            i=i+1;
        else
        fprintf(opt,'\t%d\t %E\n', i, lstrain(i,1));
        end;
    end;

    %Data between STRAIN and STRESS words
    m=strainpos;
    for i=m:(m+1);
        fprintf (opt,'%s \n',alltxt{i});
    end;

    % stress data is attached to keyout.key
    fprintf (opt,'%s\t %s\t %f\t %s\n', 'STRESS', '1', nstress, '0.000E+00');
    for i=1:n
        if cne(i,2)<ystress;
            i=i+1;
        else
            fprintf(opt,'\t%d\t %E\t %E\t %E\t %E\n', i, lstress(i,1),srd,lstress(i,2),tau);
        end;
    end;

    %Data after the STRESS word to end of .KEY file
    m=stresspos;
    for i=m:length(alltxt);
        fprintf (opt,'%s\n',alltxt{i});
    end;
    fclose(opt);
```

```
end; % End of program
```

D.2.2 textinfo.m

```
function [alltxt, RZ, nel, ELMCON, pstrain, pstress]= textinfo(filename)
%%%%%%%%%%%%%%%%%%%%%%%%%%%%%%%%%%%%%%%%%%%%%%%%%%%%%%%%%%%%%%%%
% TEXTINFO.M
% -----------------------------------------------------------------------------------------------------------------------------------------
% PURPOSE
% THIS FUNCTION READS THE ORIGINAL KEYWORD FILE AND FINDS THE LOCATION
% OF THE MESH INFORMATION
% -----------------------------------------------------------------------------------------------------------------------------------------
% RECORD OF REVISIONS
%      Date          Programmer                    Description of change
%      ======        ================         =======================
%    04/12/05        F. JASSO                      Original code
% -----------------------------------------------------------------------------------------------------------------------------------------

alltxt = textread(filename, '%s', 'delimiter', '\n', 'whitespace',' ');

for k=1:length(alltxt);

   aaa=alltxt(k);
   bbb=strmatch('RZ',alltxt(k));
   if bbb==1 %detect RZ matrix
      matnum=sscanf(char(aaa),'RZ %u  %u');
      nrz=matnum(2);
      for kk=1:nrz
         RZ(kk,:)=str2num(char(alltxt(k+kk)));
      end
   end

   ccc=strmatch('ELMCON',alltxt(k));
   if ccc==1 %detect connectivity matrix
      elnum=sscanf(char(aaa),'ELMCON %u  %u');
      nel=elnum(2);;
      for kk=1:nel
         ELMCON(kk,:)=str2num(char(alltxt(k+kk)));
      end
   end

   if strmatch('STRAIN',alltxt(k))==1
      pstrain=k+1; % line to insert for initial strain data
   end
   if strmatch('STRESS',alltxt(k))==1
      pstress=k+1; % line to insert for initial stress data
   end
end
```

D.2.3 counter.m

```
function [n] = counter(X, depth)
n=0;
   for i=1:length(X)
      if X(i,2)<depth;
         i=i+1;
      else
         n=n+1;
      end;
   end;
```

D.2.4 readstress.m

```
function [depth, sigtan, sigax]=readstress(filedata)
[depth, sigtan, sigax]=textread(filedata, '%*f %f %f %f');
```

D.2.5 readstrain.m

```
function [depth, rstrain]=readstrain(filedata)
[depth, rstrain]=textread(filedata, '%*f %f %f');
```

D.2.6 ecenter.m

```
function [position]=ecenter(n1,n2,n3,n4)
   position=(1/4)*n1+(1/4)*n2+(1/4)*n3+(1/4)*n4;
```